SPONTANEOUS ACOUSTIC OSCILLATIONS OF HELIUM GAS IN TUBES WITH STEEP TEMPERATURE GRADIENT

by

Taichi Yazaki

Dissertation submitted to the Faculty of the Graduate School
of the University of Tsukuba in partial fulfilment
of the requirements for the degree of
Doctor of Science
December 1980

TABLE OF CONTENTS

		Page
ABSTRACT OF THE DISSERTATION		iv
Chapter		Page
1.	INTRODUCTION	1
2.	THEORETICAL	7
2.1	ENERGY CONSIDERATION	9
2.2	DERIVATION OF HYDRODYNAMIC EQUATIONS	12
2.3	RADIAL AVERAGE OF T_1 AND u	14
2.4	MOMENTUM AND ENERGY EQUATION	17
2.5	BEHAVIOR OF F AND F*	20
2.6	SUMMARY OF FUNDAMENTAL EQUATIONS	21
2.7	CALCULATION OF $\partial \langle p_1 u \rangle / \partial x$	25
2.8	SECOND-ORDER HEAT FLUX	30
2.9	STABILITY LIMITS	35
3.	EXPERIMANTAL	41
3.1	CAVITY	42
3.2	PRESSURE MEASUREMENTS	47
3.3	APPARATUS	51
3.4	MEASUREMENTS OF LIQUID HELIUM EVAPORATION RATE	58
4.	RESULTS AND DISCUSSIONS	61
4.1	STABILITY LIMITS	62
4.2	STABILITY CURVES	66
4.3	FREQUENCY OF THE ACOUSTIC	90
4.4	STABILITY LIMITS FOR TUBES WITH VARIABLE CROSS-SECTION	99
4.5	SECOND-HARMONIC	105
4.6	SECOND-ORDER HEAT FLUX	115

	Page
APPENDIX	124
REFERENCES	134
SUMMARY AND CONCLUSIONS	137
PERSONAL HISTORY	139
ACKNOWLEDGMENTS	140

ABSTRACT OF THE DISSERTATION

The present investigation is an experimental study of the acoustic oscillations of a gas column("Taconis oscillations") spontaneously generated in tube or pipe with steep temperature gradient. Spontaneous acoustic oscillations occur in tubes which are warm at their closed end and cold at their open end. In this thesis, some properties of such oscillations, the stability, the frequency, higher harmonics and the effective thermal conductivity are experimentally studied.

The stability curves for helium gas between oscillations and no oscillations are determined under a nearly step-functional temperature distribution, which is established by a continuous flow of liquid or gaseous helium as coolant. They are discussed on the plane of the dimensionless variables, the temperature ratio α between warm and cold parts versus the ratio of a tube inner radius to the Stokes boundary layer thickness formed on the tube wall for the ratio ξ (=0.3, 0.5, 1, 2, 5, and 10)of warm length of the tube to cold length as a parameter. Measurments are performed below $\alpha \simeq 70$. Frequency of the acoustic oscillations is also determined corresponding to the stability curves. For small ξ(=0.3), we find new phenomena, which are the transitions from the fundamental to a second-harmonic and from the second-harmonic to a third-harmonic. These transitions occur at $\alpha \simeq 15$ and $\alpha \simeq 60$ at one hand branch of the stability curve. The unstable region is experimentally and numerically determined for the fundamental and higher harmonic in order to explain such transitions.

Results obtained in our experiments for the fundamental are compared with the theory of Rott. In order to qualitatively explain the results, stability curves and appearences of higher harmonics, we roughly make some suggestions.

The effective thermal conductivity of the oscillations is estimated from the evaporation of liquid helium. Experimental results are made a rough comparison with the theory of the second-order heat flux taking into account a finite boundary layer thickness.

CHAPTER I

INTRODUCTION

Spontaneous acoustic oscillations of a gas column may be generated in a long cylindrical tube or pipe with non-uniform temperature distribution along its axis. This oscillating instability can be induced, as well-known, when the open end of the tube is cold and the closed end is warm. In low temperature system such oscillations have often been observed, in particular, in a transfer line of liquid helium and in the pumping line from liquid helium reservoir to room temperature system, along which a steep temperature gradient is maintained. The acoustic pressure amplitudes are sometimes surprisingly high; 10^4pa or more. They are accompanied by a considerable heat flux to liquid helium reservoir; the attainable evaporation rate under the oscillations is empirically more than three orders of magnitude larger than that without them. Thus the problems of the oscillations become of great importance for developements of cryogenics. Although the phenomenon has been one of a good many years standings in low temperature system since helium gas was liquified very little was systematically performed by experimental studies.

We have been interested in this phenomenon occured in liquid helium reservoir for some years. A deeper understanding of

1. the stability and the frequency of the oscillations.
2. excitation of higher harmonic(second and third).

3. thermal effects accompanied by the oscillations. has been acquired by experiments. Our experimental results are supported by the theory of Rott(summarized in 1980)or expansion of it.

This phenomenon was already known before the beginning of the studies in cryogenics by more than a century at higher temperature systems. We refer to the phenomena associated with the name of "Sondhauss(1850)"; when a glass bulb attached to a piece of a narrow tube, such as a flask, is heated by a burner, audible sounds are spontaneously produced, as glass-blowers sometimes experience. In his paper the earlier observation by Pinaud(1837)and Marx(1841)are quoted. Sondhauss's experiments and other topics related to thermally driven acoustic oscillations have been described in the text book "The Theory of Sound" by Lord Rayleigh(1945).

In cryogenics, spontaneous oscillations of helium gas columns were observed by Keesom(1945) and Taconis et al.(1949) at the Kamerlingh Onnes Laboratory at Leiden where helium gas was first liquified The oscillating instability is called "Taconis Oscillations" in cryogenics. On several occasions in the Leiden experiments a disturbing phenomenon occured; a column of helium gas in cryostat began to oscillate. When these oscillations appear, considerable heat transport takes place, which gives rise to abnormal evaporation of liquid helium for several experiments under cryogenic condition. Clement and Gaffney(1954)or Gaffney and Clement(1956) applied

them to a liquid helium level finder based on the discontinuous change of the frequency and the amplitudes of the oscillations that occur when the open end of a tube reaches the liquid helium surface. Twenty years later, this phenomenon is theoretically explained by Zouzoulas and Rott(1976). A considerable heat flux along the tube, which is paid to maintain the oscillations, has been measured by Banister(1966). Although several experimental studies were performed, these works were not essential to characterize the Taconis oscillations. Such delay of experiment to find the stability of the oscillations would be due to the lack of the theoretical investigation.

The first theoretical studies of the stability problems of thermally driven acoustic oscillations were carried by Kramers(1949)using the boundary layer approximation that the boundary layer thickness(Stokes layer)formed on the tube wall is sufficiently small compared with the tube inner radius. His theory has not been sufficient to interpret the experiments. It took twenty years until the comparable theory with experiments was considered. The theoretical approaches that follow has been developed by Rott(1969), who has discussed the stability limits of the oscillations using a long tube approximation, where a finite boundary layer thickness neglected by Kramers is taken into account. The temperature distribution along a tube is assumed to be piecewise constant with a steep change at a given location. The stability curves

between oscillation and no-oscillation have been theoretically predicted for helium gas by Rott(1973), which consists of two branches: at one hand branch the boundary layer fills a tube at warm part, and at another limit it is sufficiently samll compared with the tube radius. Such two branches predicted by the theory were first recognized by Hoffman et al.(1973) roughly. Experiments heretofore have been rough or qualitative because no experiments has been carried out under a given temperature distribution along a tube, especially in the cold part.

In our experiments, two developements are performed: one is the establishment of temperature distribution and another is the continuous variation of the boundary layer thickness. A U-shaped tube instead of a half open tube employed in previous works enables us to perform such developements. The stability curve for helium gas was first determined by Yazaki et al.(1979)or Tominaga et al.(1979), where a comparison between the theory and experiments was directly performed. The frequency diagrams and more detailed stability curves were experimentally determined by Yazaki et al.(1980)or Narahara et al(1980). Our experimental data will be, in future, useful when one designs apparatuses for low temperature systems avoiding the Taconis oscillations.

In studies up to present only the fundamental mode of oscillations was discussed or observed. At one-hand branch on the stability curve we found the transitions from the

fundamental to a second-harmonic and from the second--harmonic to the third harmonic[Yazaki et al.(to be published in 1980)]. These transitions occur on account of the intersection between the stability curves.

Melkli and Thomann(1975)have studied the thermal effects (second-order heat flux) produced by the standing acoustic waves in the tube with uniform temperature distribution, executed by harmonic oscillation of a piston. More general theory taking into account a non-uniform temperature distribution, which is interestedhere, has been discussed by Rott (1975). The effective thermal conductivity of the oscillations was measured by Yazaki et al.(to be submitted). They indicated that the abnormal evaporation of liquid helium, as above stated, is due to the second-order heat flux including the temperature gradient.

In this thesis, I will summarize the experimental results and its analysis performed in the works up to present. In chapter II , qualitative explanations for the occurrence of the spontaneous oscillations are suggested instead of the theory of Rott. They are too rough to give the stability curves but are useful to give a qualitative interpretation of our experimental results. The experimental apparatus in cryogenics is described in chapter III including the pressure measurement system, by which a step-functional temperature distribution is able to be established. In chapter IV I will give the experimental results and discussion of, mainly the stability

curves and the frequency diagrams of the acoustic oscillations, the transition from the fundamental to the second-harmonic and from the second-harmonic to the third-harmonic, and the effective thermal conductivity comparing with the theory of Rott or our rough explanations.

CHAPTER II

THORETICAL

Theoretical investigations on the stability problem for thermally driven acoustic oscillations of gaseous helium have been performed by Kramers(1949)and Rott(1969-1980)using linearized hydrodynamic equations. A series of the studies by Rott, et al. has predicted the stability curves between oscillation and no-oscillation, taking into account a finite thickness of boundary layer formed on a tube wall neglected by Kramers. Their studies enable us to make a complete comparison with our experimental results for the stability curves of helium gas.

We think that their theoretical treatments of the stability problem are correct, but are too mathematical for us to qualitatively understand this type of thermally driven acoustic oscillations; namely we feel it is not clear what role the temperature gradient plays to maintain the oscillations. Then the quantitative treatments for deriving the stability curves depend on the theory of Rott. We will give, in this chapter, the quantitative explanation for the occurrence of the spontaneous oscillations induced by a finite temperature gradient. It is too qualitative to give the stability curve numerically, but is useful to give a qualitative interpretation to our experimental results in chapter IV, and throw light on the distinct difference from a normal case(uniform temperature).

We start from a intuitive model simplified a motion of a fluid in a pipe instead of exact treatment performed by Rott,

and hydrodynamic equations and acoustic variables are obtained under the model. So as to examine the role of shear viscosity and thermal conductivity of gas to sustain the oscillations, firstly we consider the case including only thermal conductivity and then introduce the effect of the viscosity. The energy considerations are performed for such two case.

We will also study thermal effect(second-order heat flux) produced by the standing acoustic waves. The most drastic phenomenon, a large amount of evaporation of liquid helium, is able to be interpreted by the second-order heat flux, which has been theoretically derived by Merkli and thomann(1975) or Rott(1975)with slight different approach. The results are used to explain our experiments.

At last section we roughly review the outline of the theory of Rott predicted the stability curves for the fundamental.

Let's consider briefly the mechanism for the spontaneous acoustic oscillations, which is shown to be compatible with many features of the experimental data. An essential quastion is " what is the energy source to maintain the oscillations with finite amplitudes in the system without the mechanical energy source such as an oscillating piston or speaker"? In a pipe with a steep temperature gradient along its axis, the heat(thermal energy)acquired from the tube wall should possibly become the driving energy for the oscillations. Recalling the first law of thermodynamics, such an idea is realistic; a part of the thermal energy is transformed to the internal energy of the oscillating gas

and the rest is transformed to the mechanical energy, which is interested here. An inflow of heat is not a sufficient condition to induce the mechanical energy, but the suitable phase differences between the acoustic pressure and the displacement of the particles(or velosity) is needed. When the driving energy overcomes all dissipative energy due to the shear viscosity and thermal conductivity of gas, it will be possible that the acoustic oscillations are spontaneously induced and sustained with finite amplitudes. Thus we will call this type of the oscillations "thermally driven acoustic oscillations" or "netsu-shindo" in Japanese, corresponding to "piston-driven acoustic oscillations". In the section 2.6, we will give the increment of the mechanical (acoustic)energy under above intuition before we quantitatively caluculate it with hydrodynamic equations.

2.1 ENERGY CONSIDERATION

There are two means to sustain the acoustic oscillation of a gas colum in a cyrindrical cavity. One of them is a piston-driven oscillation and another is thermally driven oscillation. The energy source in the former method is the moving piston executed by external means; the pressure against the piston varies in such a way that energy is transmitted to a gas, whose average power delivered per unit piston area is given by the time average of the product of the acoustic pressure and the velocity at the piston, as investigated by Temkin(1967, 1968)and other authors. In the latter case

(we consider the "Taconis oscillation"), where only a finite temperature gradient instead of a piston exists along a tube axis and which is intersted here, we will discuss whether a temperature gradient plays a role of the energy source to induce sound in a tube, comparing with the uniform temperature case.

Let's consider the acoustic oscillations transmitted in a long cylindrical cavity as a plane waves. As shown in fig. 2.1, we consider a volume element enclosed by a tube wall and two cross-sections normal to the tube axis(x-axis), whose location is situated in x and $x+\Delta x$. The work done on the "slab of ring" at x by the pressure P in time δt, as stated in the text book "The Theory of Sound" by Lord Rayleigh, is given by

$$\frac{\delta W}{\delta t} = P(x)\ \dot{\xi}(x,r)\ 2\pi r\ dr = (p_m + p_1)u\ 2\pi r\ dr \quad (2.1.1)$$

where $\dot{\xi}$ (=u) denotes the x-component of the velocity of a particle, and p_m and p_1 show the static and acoustic pressure respectively. If the investigation with respect to time extends over any number of complete periods, or whenever its range is sufficiently long, the periodic term(the first order), the product of the static pressure and the velocity in eq.(2.1.1) should not contribute to the work. Taking into account

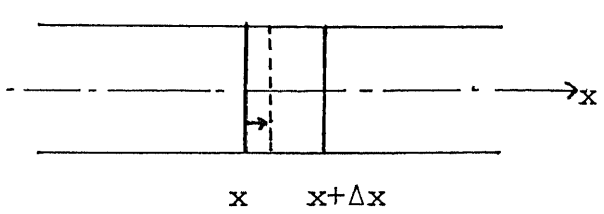

fig.2.1 Volume element sorrounded by two "slabs" in cylindrical cavity.

the dissipative terms of shear viscosity and thermal conductivity of gas, the velocity depends on the distance from the tube wall. Thus after taking the time average of eq.(2.1.1), the work done on the slab at x per unit time is written as

$$\bar{Q}(x) = \int_0^{r_0} \overline{p_1(x)\ u(x,r)}\ 2\pi r\ dr \qquad (2.1.2)$$

r_0 inner tube radius of pipe

where the bar indicates the time average. The quantity $\overline{p_1 u}$ is called the acoustic energy density flux or sound intensity (refer to text book, Itoh;1979 or Kohashi;1978). The net work ΔQ which the volume element $\Delta x \pi r_0^2$ does to the external system is, taking into consideration the contribution from the slab at $x+\Delta x$

$$\Delta\bar{Q}(x) = \bar{Q}(x+X) - \bar{Q}(x) = \Delta x \frac{\partial}{\partial x}\bar{Q}(x) \qquad (2.1.3)$$

The radial average of a value X(abbreviation $< X >$)is given by

$$< X > = \frac{1}{\pi r_0^2} \int_0^{r_0} X\ 2\pi r\ dr \qquad (2.1.4)$$

Using the definition (2.1.4), eq.(2.1.3)can be expressed as

$$\Delta\bar{Q} = \Delta x \pi r_0^2 \left\{ \overline{< p \frac{\partial u}{\partial x} >} + \overline{< u \frac{\partial p}{\partial x} >} \right\} \qquad (2.1.5)$$

Negative value of $\Delta\bar{Q}$ means the damping of the acoustic wave in the volume element $\Delta x \pi r_0^2$, as discussed later. Positive value of $\Delta\bar{Q}$ means that the energy to sustain the oscillations is supplied there. For example, let's imagine such a system,

progressive harmonic wave, that the pressure and the velocity are given by $p=A\sin(\hat{k}x-\omega t)$ and $u=B\sin(\hat{k}x-\omega t)$, where A and B are constants everywhere. In this case $\Delta\overline{Q}$ is vanished. Therefore the sound is not excited and not damped. Taking into account the dissipative effects, A and B depend on x and decrease with x, so that the value $\Delta\overline{Q}$ is negative. The sound is damped. Thus in the normal system(uniform temperature), there exists no system that $\Delta\overline{Q}$ takes positive value.

Nextly we will consider a system in which a finite temperature gradient is established along a tube axis. It is expected that the important value $\Delta\overline{Q}$ may be able to take a positive value. In order to discuss a sign of $\Delta\overline{Q}$, $\langle u\frac{\partial p_1}{\partial x}\rangle$ and $\langle p_1\frac{\partial u}{\partial x}\rangle$ will be calculated from a set of the fundamental hydrodynamic equations with non-uniform temperature distribution.

2.2 DERIVATION OF HYDRODYNAMIC EQUATION

The fundamental equations(the axial and radial momentum equations, the continuity equation, the energy equation and the equation of state)governing a oscillatory motion of a fluid in a long cylindrical pipe with non-uniform temperature distribution have been given by Rott(1968)with a long tube approximation in cylindrical coordinates.* The following assumptions were performed through his theory;

1. a strict linearization of all hydrodynamic equations.

* In the case of uniform temperature the acoustic solutions of the basic differential equation were given by Bergh and Tijdeman(1965).

2. as a radial momentum conservation, the radial gradient of the acoustic pressure p_1 is neglected through a pipe;

$$\frac{\partial p_1}{\partial r} = 0 \qquad (2.2.1)$$

3. the radial gradient of the mean temperature T_m is neglected;

$$\frac{\partial T_m}{\partial r} = 0 \qquad (2.2.2)$$

4. The dissipative terms(viscosity and thermal conductivity)in the basic equation which contain the axial gradient are neglected.

Assumption 1 may be accepted, because the main purpose of this investigation is the determination of the critical points (stability limits)between damped and excited oscillations with small amplitudes. Next simplification is also accepted for reason that when the radial averages are carried out in the following section, the term containing the radial component of of the velocity are vanished, and moreover the radial velocity is sufficiently small compared with the axial one. Rott pointed out that the above assumptions are sufficiently satisfied, if the tube inner radius r_0 is much smaller than the whole length L(long tube approximation). After all, his theory takes into account the full and unrestricted range of the boundary layer thickness neglected by Kramers under the boundary layer approximation.

The mean value of pressure, temperature and density will be indicated by the subscription m, so that the mean pressure

$p_m = R\, T_m \rho_m$ (R; gas constant and ρ_m; mean density). The time-variation of the acoustic variables is assumed to be given by the factor $\exp(i\omega t)$. In acoustics, where only small variations of the flow properties about a basic state occur, a following perturbation calculation can be emloyed;

$$\begin{aligned} p &= p_m + p_1(x)\exp(i\omega t) \\ T &= T_m + T_1(x,r)\exp(i\omega t) \\ \rho &= \rho_m + \rho_1(x,r)\exp(i\omega t) \\ u &= \quad u(x,r)\exp(i\omega t) \\ &\cdots\cdots\cdots\cdots\cdots\cdots \end{aligned} \qquad (2.2.3)$$

It is sufficient, in acoustics, to consider terms up to first order only.

In Appendix(1), we will give only an outline of a slight different derivation of the basic equations comparing with that of Rott. Of course results are in agreement together. Intuitive derivation of them is presented in the next section.

2.3 RADIAL AVERAGES OF T_1 AND u UNDER SIMPLE MODEL

As given in Appendix(2), the velocity and the temperature distribution near the tube wall are strongly dependent of the distance from the wall on account of viscosity and thermal conductivity. In the place sufficiently far from the wall, they are independent of the distance from the wall. The behaviors of r-dependence for oscillatory viscous fluid(Poiseuille flow or Couette flow)are discussed in several text books(Imai 1978 and Landau and Lifshitz 1950). The distribution

of them over the cross-section may be able to be classified into two region; one of them in "boundary layer" where the fluctuations are neglected and another is the "core" where the amplitudes of them are not dependent of the distance from the tube wall.

RADIAL AVERAGE OF u The distribution of the velocity in a pipe is classified into two parts as shown in Fig.2.3.(a). One of them is velocity core indicated by u_c and another is the velocity boundary layer indicated by u_b which is practical equal to zero. The region occupied by the respective velocity should be dependent of the viscous effect. Therefore in order to introduce such a effect, we impose on the normalized "weight" F and (1-F) to the boundary layer and the core respectively. The values F and (1-F) may physically show the occupation rates of the respective area to the whole cross-section, and generally are complex. In the following section, the quantitative formulation of F will becomes to be clearer.

Using the above idea, the radial average of the velocity is simply given by the equation

$$\langle u \rangle = F\, u_b + (1-F)\, u_c \qquad (2.3.1)$$

This equation suggests that F approaches to unity or zero, according as viscous boundary layer becomes sufficiently thick or thin.

RADIAL AVERAGE OF T_1 In the same way as the velocity distribution, the temperature fluctuation(refer to Appendix 2)

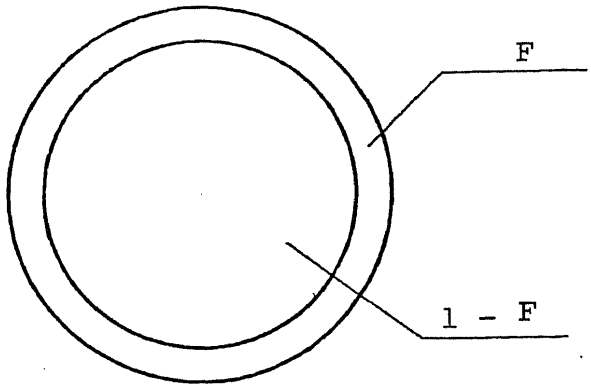

(a)

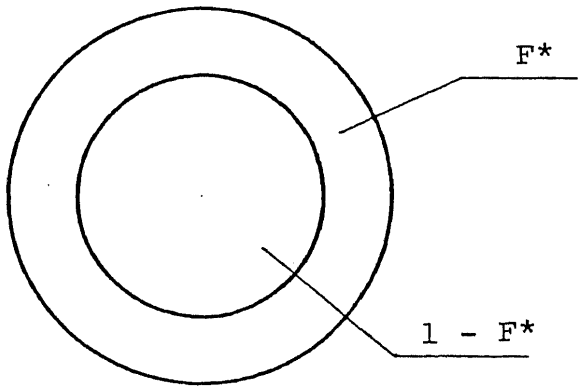

(b)

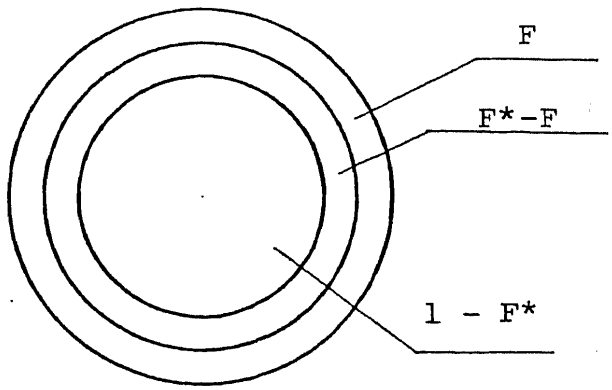

(C)

Figure 2.3 The simple model for the mothion of a fluid in a pipe. (a), the velocity distribution is classified into two region; the velocity core imposed by the weight F and the boundary layer (1-F). (b), temperature distribution is classified as same as (a). (c), the case taking into account both of (a) and (b).

is simplified into the model which is shown in Fig.2.3.(b). In the core region where the "weight" (1-F*) is imposed, the motion of fluid is isentropic. On the other hand, in the thermal boundary layer region imposed F*, the motion is isothermal (T_b=0). Thus the radial average of temperature fluctuation is given be

$$\langle T_1 \rangle = F^* T_b + (1-F^*) T_c \qquad (2.3.2)$$

where T_c and T_b are temperature fluctuation in the core and the boundary layer. According as the thermal boundary layer thickness is sufficiently large or small compared with the tube radius, F* will become unity or zero.

After the cross-section of a tube may be classified into three region as shown in Fig.2.3.(c); the first region imposed by (1-F*) is the velocity core and moreover the temperature core, second region imposed by (F*-F), which may be important for Taconis oscillation to be induced is the velocity core and temperature boundary layer where a gas is able to move freely and isothermal, and last region imposed by F, where a gas is too viscous to move, so to speak, has same effects as the wall of a pipe.

2.4 MOMENTUM AND ENERGY EQUATION UNDER SIMPLE MODEL

Under the model which is considered in the previous section the hydrodynamic basic equations, in particular, the momentum equation and the energy equation, are derived. The derivation taking into account the temperature distribution have been

performed by Rott(1969), and reviewed in Appendix 1 in order to compare with the results in this section.

One dimensional momentum equation is written as

$$\rho_m \frac{\partial u}{\partial t} + \frac{\partial P}{\partial x} = 0 \qquad (2.4.1)$$

where the second order terms are neglected. The core velocity u_c in eq.(2.3.1) should correspond to the velocity in eq.(2.4.1). If so, u in eq.(2.4.1) is able to be substituted to u_c and we simply obtain the momentum equation for viscous fluid;

$$\rho_m \frac{\partial}{\partial t} \frac{\langle u \rangle}{1-F} + \frac{\partial P}{\partial x} = 0 \qquad (2.4.2)$$

which coincides with eq.(A.1.14) if F is assumed to be a suitable form. Let's consider the asymptotoc behavior of F. In the case that the boundary layer fills up the entire tube the fluid in a tube will become viscous due to the kinematic viscosity and the axial velocity distribution becomes parabolic. Thus a fluid has to be, in a moment, associated with the law of Poiseuille;

$$\pi h_0^2 \langle u \rangle = 2\pi \int_0^{h_0} u\, r\, dr = -\frac{dP}{dx} \frac{\pi h_0^4}{\mu} \qquad (2.4.4)$$

Comparing eq.(2.4.4) and eq.(2.4.2), we obtain the asymptote of F to be $(1 - \eta_0^2/8)$, $\eta_0 \equiv h_0\sqrt{i\omega/\nu}$.

The energy equation corresponding to the adiabatic motion of fluid is given by, using the Lagragian differential formulation,

$$\rho T \frac{DS_c}{Dt} = 0 \qquad (2.4.5)$$

S_c; entropy of core

where S_c means the total entropy. Equation.(2.4.5) is expressed in the Eular formulation. Moreover from thermodynamic identical equation $dH=TdS+\frac{1}{\rho}dp$ (H; enthalpy), we obtain

$$\frac{\partial S_c}{\partial t} = \frac{1}{T}\left\{\frac{\partial H}{\partial t} - \frac{1}{\rho}\frac{\partial P}{\partial t}\right\}$$
$$\frac{\partial S_c}{\partial x} = \frac{1}{T}\left\{\frac{\partial H}{\partial x} - \frac{1}{\rho}\frac{\partial P}{\partial x}\right\} \qquad (2.4.6)$$

Thus a combination of eqs.(2.4.5)and(2.4.6)leads to one dimensional adiavatic equation;

$$i\omega(\rho_m c_p T_c - P_1) + c_p u \rho_m \frac{\partial T_m}{\partial x} = 0 \qquad (2.4.7)$$

where we employ the relation $\frac{\partial H}{\partial t} = i\omega c_p T$, and again neglect the terms more than second order. By the way remember the geometric model presented in the previous section, and we will recognize that the motion in the temperature core must be satisfied by eq.(2.4.7), so that T_1 and u will able to be changed to $T_c=\langle T_1\rangle/1-F^*$ and u_c^t(the velocity in the temperature core). Thus the energy equation taking account of the dissipative terms and the variable temperature distribution is written as

$$i\omega\left\{\rho_m c_p \langle T_1\rangle - (1-F^*)P_1\right\} + (1-F^*)c_p u_c^t \rho_m \theta T_m = 0 \qquad (2.4.8)$$
$$\theta \equiv \frac{1}{T_m}\frac{dT_m}{dx}$$

By the help of results of Rott, we find that u_c^t should be assumed to be

$$u_c^t = \frac{\langle u\rangle}{1-F^*}\left\{1 - \frac{F^*-F}{(1-\sigma)(1-F)}\right\} \qquad (2.4.9)$$

σ ; Prandtl number.

This formulation may be reasonable, because for vanishing case

of shear viscosity(σ=0 and F=0), u_c^t becomes equivalent to the velocity in the core in eq.(2.3.1). Equation.(2.4.8) is change to, using eq.(2.4.9)

$$i\omega\left\{\rho_m c_p \langle T_1\rangle - (1-F^*)P_1\right\} + \rho_m c_p T_m \theta \langle u\rangle\left\{1 - \frac{F^*-F}{(1-\sigma)(1-F)}\right\} = 0 \qquad (2.4.10)$$

which is also given from a combination of eqs.(A.1.12) and (A.1.13), if the formulation of F and F* is suitably determined.

2.5 BEHAVIOR OF F AND F*

The fundamental equation derived in the previous section are equivalent to those given in the Appendix 2, if the following expressions for F and F* are imposed by

$$F = \left\langle J_0(i\eta) \Big/ J_0(i\eta_0) \right\rangle \qquad (2.5.1)$$

$$F^* = \left\langle J_0(i\eta^*) \Big/ J_0(i\eta_0^*) \right\rangle \qquad (2.5.2)$$

with $\eta_0 = r\sqrt{\frac{i\omega}{\nu}}$, $\eta = r\sqrt{\frac{i\omega}{\nu}}$ and $\eta^* = \sqrt{\sigma}\,\eta$

where ν ($= \mu/\rho_m$) and σ is kinematic viscosity and Plandtl number respectively. In Fig.2.5, the numerical data calculated by a computer about imaginary and real parts of F are illustrated. It is reasonable that the weight F and F* tend to zero for non-dissipative case, when we remember the physical meaning of F suggested in section 2.3. The asymptotic behavior of F is given by the following;

$$F = 1 + \frac{1}{2}\left(\frac{i\eta_0}{2}\right)^2 + \frac{1}{3}\left(\frac{i\eta_0}{2}\right)^4 \cdots \qquad \text{for } |\eta_0| \ll 1 \quad (2.5.3)$$

and

$$F = \frac{2}{\eta_0} - \frac{1}{4}\left(\frac{2}{\eta_0}\right)^2 - \frac{1}{32}\left(\frac{2}{\eta_0}\right)^3 \cdots \qquad \text{for } |\eta_0| \gg 1 \quad (2.5.4)$$

As suggested below eq.(2.4.5), the value F approaches to $(1 - \eta_0^2/8)$ for $|\eta_0| \ll 1$.

2.6 SUMMARY OF FUNDAMENTAL EQUATION

In order to discuss,in following section, the effects of the thermal boundary layer and the viscous boundary layer to characterize the thermally driven acoustic oscillations we present here the basic equation where the effect of viscosity is not taken into account but the effect of thermal conductivity only is taken into account or where the both effects are taken into consideration. For the first case, since F and σ is vanished, we obtain from eqs.(2.4.2)and(2.4.10)as momentum and energy equation;

$$i\omega \rho_m u + \frac{\partial p_1}{\partial x} = 0 \qquad (2.6.1)$$

$$i\omega\left\{\rho_m c_p \langle T_1 \rangle - (1 - F^*) p_1\right\} + \rho_m c_p T_m \theta \langle u \rangle (1 - F^*) = 0 \qquad (2.6.2)$$

On the other hand, the equationstaking into acount the viscosity are;

$$i\omega \rho_m u + (1 - F)\frac{\partial p_1}{\partial x} = 0 \qquad (2.6.1')$$

$$i\omega\left\{\rho_m c_p \langle T_1 \rangle - (1 - F^*) p_1\right\} + \rho_m c_p T_m \theta \langle u \rangle \left\{1 - \frac{F^* - F}{(1-\sigma)(1-F)}\right\} = 0 \qquad (2.6.2')$$

Other basic equation, the continuity equation and the equation of state for ideal gas are not varied for above two cases;

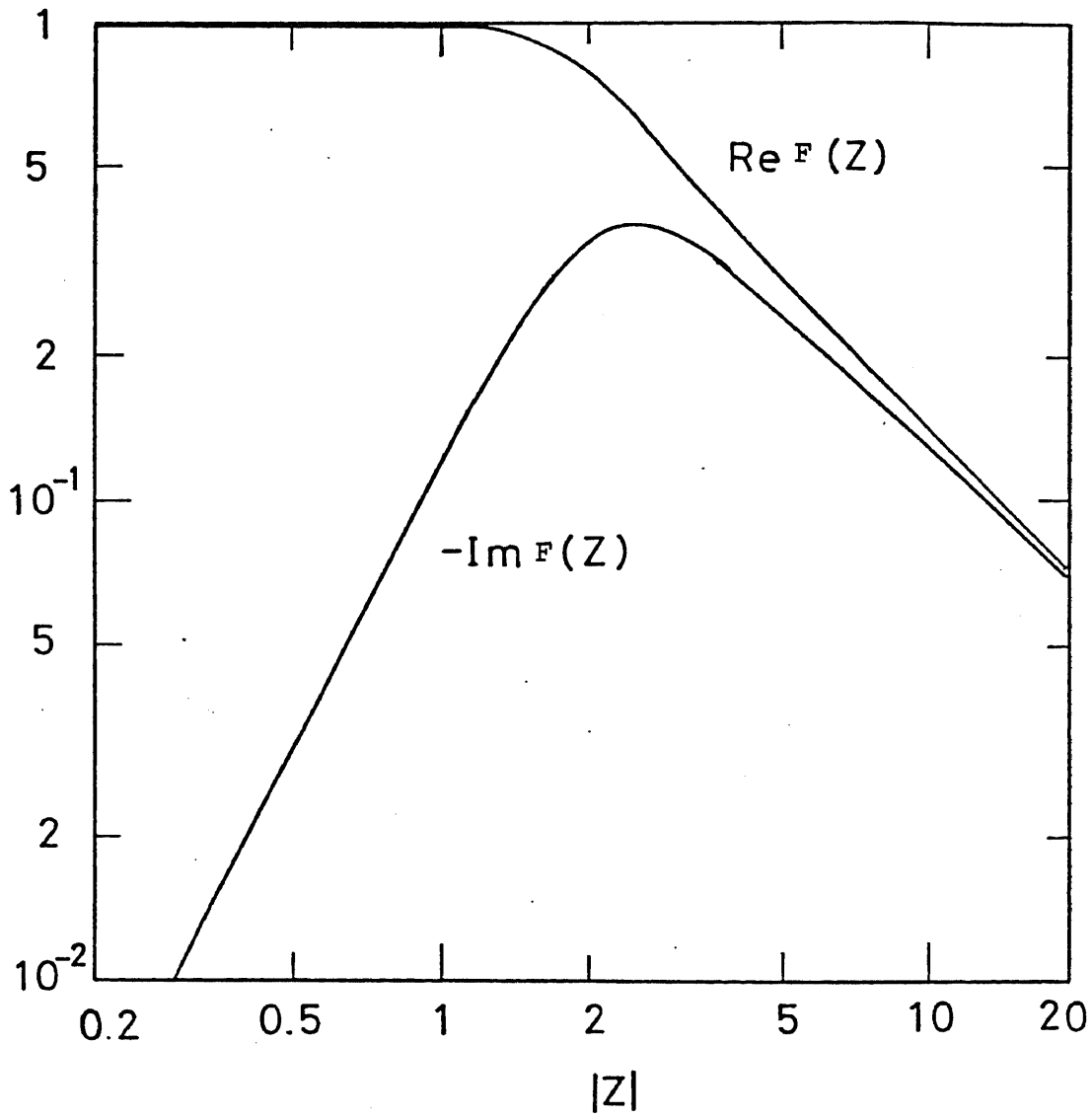

Figure 2.5 Behavior of real and imaginary parts of F(Z). Real part and imaginary part of F are always positive and negative respectively.

namely

$$i\omega\langle\rho_1\rangle + \rho_m \partial\langle u\rangle/\partial x + \langle u\rangle \partial\rho_m/\partial x = 0 \qquad (2.6.3)$$

$$p_1/p_m = \langle\rho_1\rangle/\rho_m + \langle T_1\rangle/T_m \qquad (2.6.4)$$

Before we calculate the increment of the mechanical energy $\Delta\bar{Q}$ on the basis of these fundamental equations, we will intuitivelly derive it as indicated in introduction in this chapter. For the simplicity, the effect of the viscosity of gas is neglected($F=0$), so that the axial velocity u is independent of radial coordinate. Only the effect of the thermal conductivity($F^*\neq 0$) is considered. As shown in fig.2.6 let's imagine the periodical disturbance of displacement of particles along the tube axis with finite temperature gradient. Since enthalpy and internal energy of ideal gas depend on temperature only, they are written as $H=C_pT_m$+constant and $U=C_vT_m$+constant respectively. Thus the increase of enthalpy and internal energy per unit mass for such disturbance is $C_p\Delta T_m$ and $C_v\Delta T_m$ respectively[$\Delta T_m = T_m(x+\Delta x)-T_m(x)$]. By the way the particles in the region of temperature core is not able to acquire the heat from the external(tube wall), but only those in the region of temperature boundary layer can acquire the heat; the particles occupied in $\pi r_0^2 F^*$ shown in fig.2.6 can acquire or give off the heat. Taking into account the total mass passed per unit time, the first law of thermodynamics shows that the increment of the mechanical energy $\Delta\bar{Q}$ is given by

$$\overline{(C_p - C_v)(dT_m/dx)\rho\, u\, F^*\, \Delta V}$$

$$\Delta V = \pi r_0^2 \Delta x$$

where we take the time average on account of the priodic motion of the particle (the first order term is vanished) Using the first order of the state equation for ideal gas and the momentum equation;

$$\rho_1 = p_1/RT_m$$

$$i\omega\rho_1 u + dp_1/dx = 0$$

where T_1 is neglected since we consider the thermal boundary layer only, we will obtain the equation related with acoustic pressure, which accords with eq.(2.7.4) shown later. When we take into account the effect of the viscosity of gas, F*-F may be adopted instead of F* as studied in the section 2.3. The quantity F* is closely related with the phase differences between the radial average of T_1 and T_c(temperature in core) and plays an important role for the increment of the mechanical energy. As indicated in eq.(A.1.16), F* is also

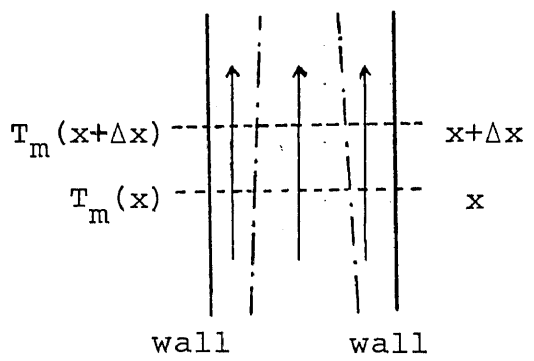

fig. 2.6

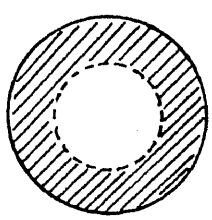

thermal boundary layer

$\kappa\pi r_0^2$ F*

related with phase differences between the acoustic pressure and the velocity. When the phase differences are 90 degrees the time average of the product between the acoustic pressure and the velocity is zero. The phase of F* shifts such phase differences from 90 degrees For $r_0/\delta >> 1$, the argument of F* approaches to $\pi/4$ and for $r_0/\delta << 1$ to zero.

2.7 CALCULATION OF $\frac{\partial}{\partial x}\overline{\langle p_1 u\rangle}$

The main purpose in this section is to calculate the quantities $\frac{\partial}{\partial x}\langle \overline{P_1 u}\rangle$ which is considered in section 2.1 and to discuss the possibilityof spontaneous oscillations. The quantity $P_1 \frac{d}{dx}\langle u\rangle$ is reduced to ordinary differential equation for the acoustic pressure p_1, using the basic equations presented for two cases in previous section, results are, for the first case,

$$\overline{P_1 \frac{\partial \langle u\rangle}{\partial x}} \simeq \omega \frac{|P_1|^2}{2\gamma P_m}(\gamma-1)\, I_m F^* - \frac{R}{2\omega M P_m}\frac{dT_m}{dx}\frac{\partial |P_1|^2}{\partial x} I_m F^* \qquad (2.7.1)^*$$

where M is molar mass of gas(4 for helium gas).
And for other case

$$\overline{P_1 \frac{\partial \langle u\rangle}{\partial x}} \simeq \omega \frac{|P_1|^2}{2\gamma P_m}(\gamma-1)\, I_m F^* - \frac{R}{2\omega M P_m}\frac{dT_m}{dx}\, I_m \frac{F^*-F}{1-\sigma} \qquad (2.7.2)^*$$

Substitution of eqs.(2.7.1),(2.7.2)and(2.6.1')yields the final results;

$$\Delta \overline{Q} = \Delta x\, \pi r_0^2 \left(\Delta \overline{Q_1} + \Delta \overline{Q_2} + \Delta \overline{Q_3}\right) \qquad (2.7.3)$$

where for the first case

$$\Delta\bar{Q}_1 = -\frac{R}{2\omega M P_m}\frac{dT_m}{dx}\frac{\partial |P_1|^2}{\partial x}\,\mathrm{Im}\,F^* \qquad (2.7.4)$$

$$\Delta\bar{Q}_2 = \frac{\omega |P_1|^2}{2\gamma P_m}(\gamma-1)\,\mathrm{Im}\,F^* \qquad (2.7.5)$$

and for other case

$$\Delta\bar{Q}_1 = -\frac{R}{2\omega M P_m}\frac{dT_m}{dx}\frac{\partial |P_1|^2}{\partial x}\,\mathrm{Im}\left(\frac{F^*-F}{1-\sigma}\right) \qquad (2.7.6)$$

$$\Delta\bar{Q}_2 = \frac{\omega |P_1|^2}{2\gamma P_m}(\gamma-1)\,\mathrm{Im}\,F^* \qquad (2.7.7)$$

$$\Delta\bar{Q}_3 = \frac{\omega P_m}{2}\left|\frac{\langle u\rangle}{1-F}\right|^2 \mathrm{Im}\,F \qquad (2.7.8)$$

These equations give us several important information to discriminate the possibitity of the maintenance of the acoustic wave.

At first let's consider the case for a pipe with constant temperature distribution, where $\Delta\bar{Q}$ is associated with $\Delta\bar{Q}_2$ and $\Delta\bar{Q}_3$. Since imaginary part of F and F* is always negative as shown in Fig.2.5, $\Delta\bar{Q}_2$ and $\Delta\bar{Q}_3$ never take positive value. Therefore in such a tube only damping of oscillation is, of course, possible and spontaneous oscillation is never induced. Qualitatively $\Delta\bar{Q}_2$ and $\Delta\bar{Q}_3$ show parts of potential and kinetic energy dissipated by thermal conductivity and viscosity respectively, whose rates is shown by imaginary parts of F* and F respectively.

* The apprximation is performed for second term in the right-hand side of eqs.(2.7.1) and (2.7.3); that is we employ $d|P_1|^2/dx$ instead of the exact form $P_1\, dP_1/dx$. For stationary wave, the acoustic pressure p_1 can be written as $P_1(x)\exp(i\omega t)$ including time factor. For $\mu=0$ and $R=0$ or for $\mu=0$ and $R=\infty$, the imaginary part of $p_1(x)$ is vanished, so that eqs.(2.7.1) and (2.7.2) are exact. But for practical case the problem of phase

Nextly let's imagine a pipe with temperature gradient, which is interested here. In this case it is possible that $\Delta\bar{Q}$ takes positive value, because $\Delta\bar{Q}_1$ can take large enough positive value to make good the loss of $\Delta\bar{Q}_2$ and $\Delta\bar{Q}_3$. Thus in a pipe with suitable temperature distribution to make positive value $\Delta\bar{Q}_1$, net acoustic energy is supplied to gas, and enables a gas to sustain the oscillations. A finite temperature gradient plays the same role of energy source as piston, which is employed in piston-driven oscillations(refer to Betchove 1958).

The driving term $\Delta\bar{Q}_1$ is proportional to the inverse of M, so that the light gases as helium, hydrogen and neon is too easy to be unstable. This is confirmed in Introduction. Members of cryogenics well-know that the oscillations are occured when the closed end of a pipe is at warm part and the open end is at cold as shown in Fig.2.7.a. This is able to be explained from above discussion. In this situation the product of dT_m/dx and $d|P_1|^2/dx$ are positive(see Fig.2.7.a), moreover imaginary part of F* is always negative, so that $\Delta\bar{Q}_1$ can take positive value! In the tube with configuration such as Fig.2.7.a, only the damping occurs at the warm and cold parts. However near middle location with a steep temperature gradient $\frac{dT_m}{dx} \neq 0$, $\Delta\bar{Q}$ is possible to be positive. Thus when $\Delta\bar{Q}$

shifts is produced, as indicated by Merkli and Thomann(1975). This problem is very difficult. However the approximation is sufficient to give a qualitative explanation of our experimental results. Of course, in order to give more detailed discussion, the solution of $p_1(x)$ must be solved for non-uniform temperature case. But this will be very difficult. A calculation including the imaginary part of p_1 has to be performed by a computer.

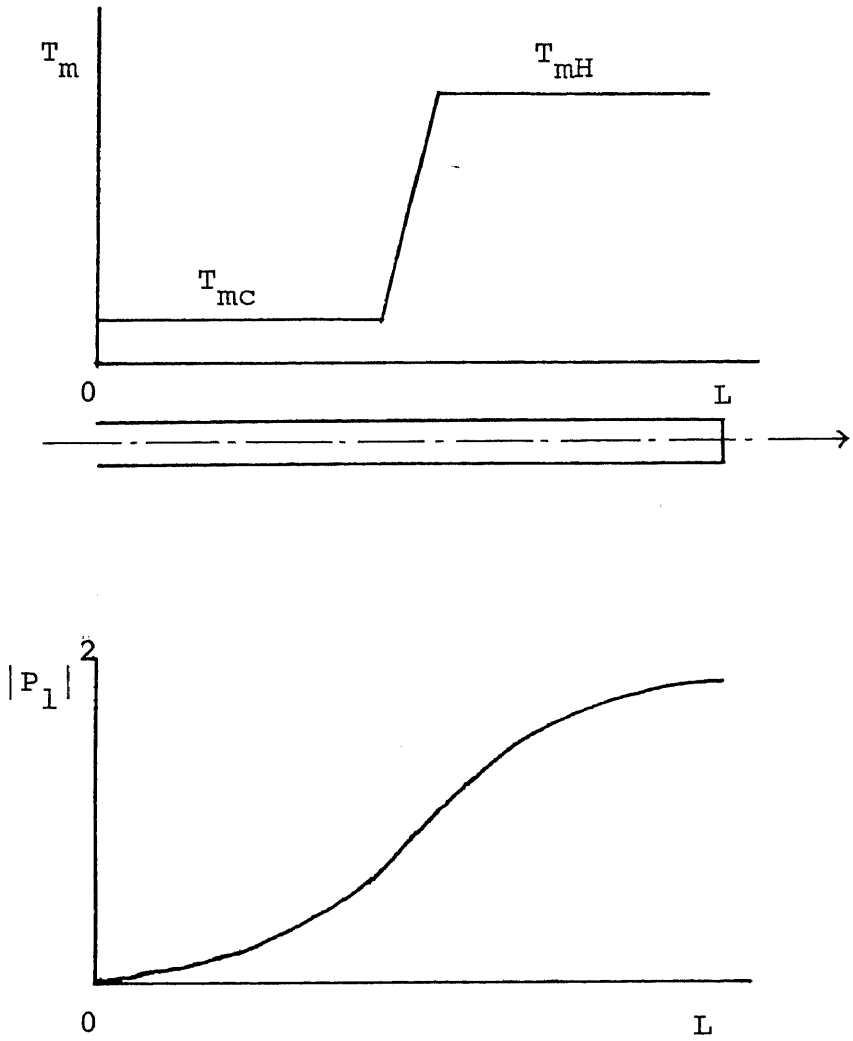

Figure 2.7.(a) A half open tube with a temperature gradient along it's axis. And the distribution of the square of the pressure amplitudes for constant temperature case and wide tube limit.

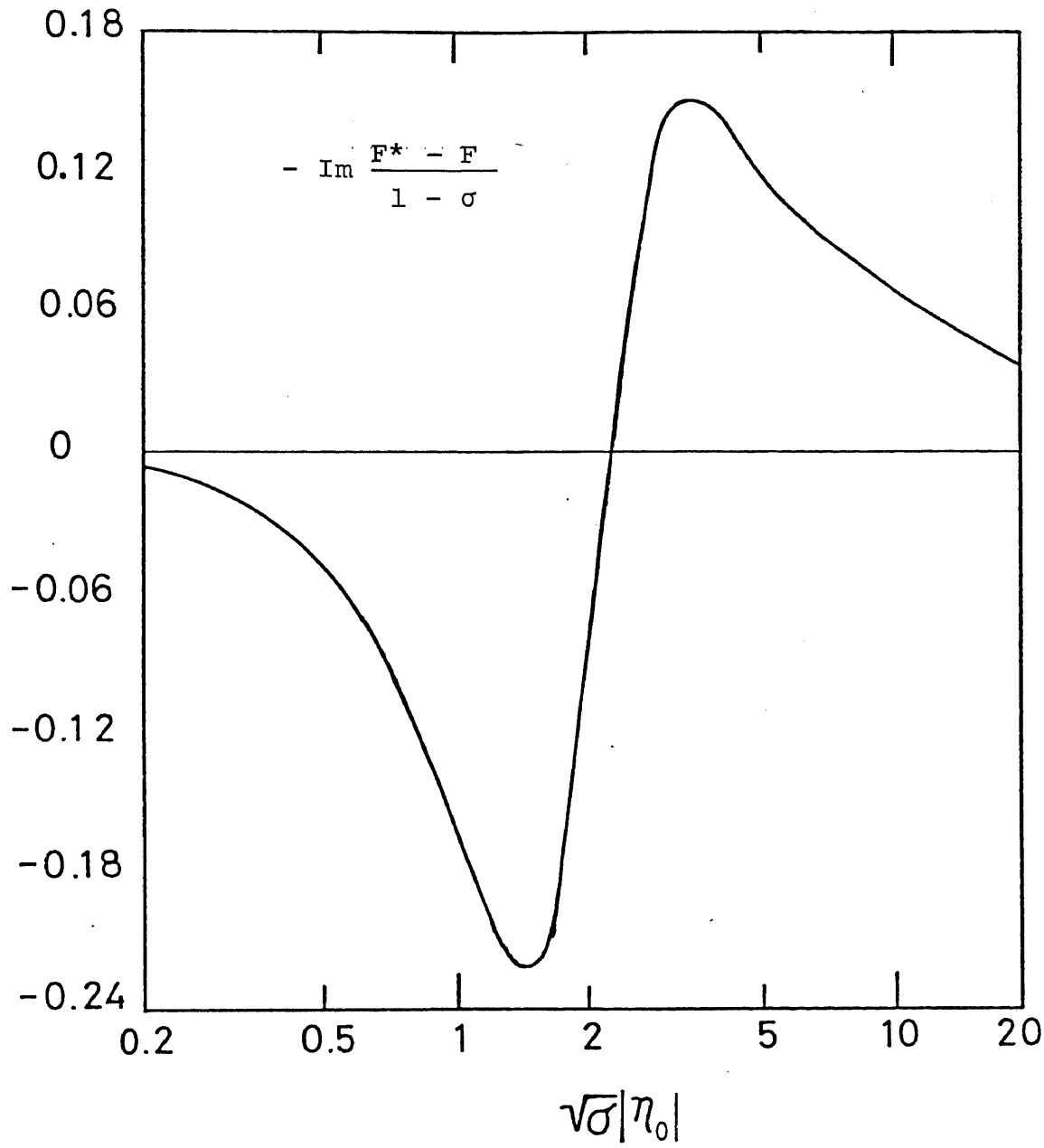

Figure 2.7.b Behavior of - Im $\frac{F^*-F}{1-\sigma}$ for helium gas ($\sigma=2/3$). The sign of it is varied from negative to positive at $\sqrt{\sigma}|\eta_0| \simeq 2.3$

becomes positive through the whole tube, the acoustic wave are able to be sustained. Taking into account the effect of viscosity(refer to eq.2.7.6), we can understand that since the effect of it F makes $\Delta\bar{Q}_1$ negative at samller $|\eta_0|$ as shown in Fig.2.7.b, the unstable region is reduced. These show a good correspondence with our experimental results as shown in the next chapter. Equation.(2.7.6) suggests the following Phenomena:

1. the existence of two branches on the stability curves.
2. the possibility of the oscillations in the cavity closed both ends.
3. the appearence of the second-harmonic instead of the fundamental.

These will be discussed in the next chapter as compared with several experimental data.

2.8 SECOND-ORDER HEAT FLUX

The second-order heat flux is important to interprete the thermal effect produced by "Taconis oscillation". This consists of two parts. One of them which exists in a pipe with constant temperature distribution has been theoretically given by Merkli and Thomann(1975)and experimentally confirmed in a pipe where the standing acoustic wave executed by a piston at one end are induced. Another which is interested here, comes from finite temperature gradient. A large amount of heat transfer to liquid helium system is caused by the latter

of the second-heat flux.

The thermal effect(the cooling and the heating effect) observed in a experiment is time averages. Therefore only terms of second and higher order in the fundamental equations contribute to the experiments. Then we have to carry out the perturbation calculation up to the second order instead of the first order in acoustics. Thus we employ the equation simplified by setting(with $\varepsilon \ll 1$)

$$\begin{aligned} T &= T_m + \varepsilon T_1 + \varepsilon^2 T_2 \\ p &= p_m + \varepsilon p_1 + \varepsilon^2 p_2 \\ u &= \quad\ \varepsilon u_1 + \varepsilon^2 u_2 \\ k &= k_m + \varepsilon k_1 + \varepsilon^2 k_2 \\ &\cdots\cdots\cdots\cdots\cdots \end{aligned} \qquad (2.8.1)$$

where we take into account the variation of the thermal conductivity and the shear viscosity associated with temperature fluctuation. The basic energy equation containing the terms up to the second order in cylindrical co-ordinates modified by other basic equation is integrated over the cross-section of the tube and furthermore averaged by time(in detail reffer to the paper by Merkli and Thomann or Rott). Consequently the local second--order heat flux q_2 per unit area penetrating into the tube wall is obtained;

$$-q_2 \equiv k_m \left(\overline{\frac{\partial T_2}{\partial r}}\right)_{r=r_0} + \left(\overline{k_1 \frac{\partial T_1}{\partial r}}\right)_{r=r_0} = \frac{1}{2\pi r_0} \frac{\partial \overline{E_2}}{\partial x} \qquad (2.8.2)$$

$$\overline{E_2} = \rho_m \pi r_0^2 \langle \overline{h_1 u_1} \rangle \ , \quad h_1 = C_p T_1 ; \text{ first order enthalpy} \qquad (2.8.3)$$

where $\bar{E}_2$ is total axial first order enthalpy flux over the

cross-section of the tube. The angular brackets and bar show the radial and time averages. The equation.(2.8.2) is related with the heat exchange between the tube wall and the oscillating fluid. Thus $\bar{E}_2$ is able to be obtained from the product of the first order solutions u_1 and T_1. The expression of eqs.(2.8.2)and(2.8.3) have been derived by Merkli and Thomann(1975) or Rott(1975) with a slightly different approach.

We will obtain the acoustic variables u_1 and T_1 under the simple model suggested by us. From eqs.(2.6.1')and(2.6.2') the radial averaged acoustic variables are given by

$$\langle u_1 \rangle = \frac{i}{\omega \rho_m} (1 - F) \, dp_1/dx \tag{2.8.4}$$

$$\rho_m c_p \langle T_1 \rangle = \left[p_1 - \frac{\theta}{(\gamma-1)(1-\sigma)} \frac{a^2}{\omega^2} \frac{dp_1}{dx} \right](1 - F^*) + \frac{\sigma \theta}{(\gamma-1)(\sigma-1)} \frac{a^2}{\omega^2} (1-F) \frac{dp_1}{dx} \tag{2.8.5}$$

After inserting F and F* into above equations, still more taking off the angular brackets, the radial and time averages product of u_1 and T_1 is again calculated. Then we obtain the resulting equation of $\bar{E}_2$;

$$\bar{E}_2 = \pi r_0^2 \, \mathrm{Re} \left\{ \left[\frac{1}{2} u_c \tilde{p}_1 + \frac{i}{2\omega} \frac{\theta \rho_m a^2}{(\gamma-1)(1-\sigma)} u_c \tilde{u}_c \right] g \right\} \tag{2.8.6}$$

$$u_c = \frac{i}{\omega \rho_m} \frac{dp_1}{dx}$$

where

$$g = 1 - \frac{\sigma}{1+\sigma} F - \frac{1}{1+\sigma} \tilde{F}^* \tag{2.8.7}$$

The quantity $\bar{E}_2$ consists of two parts in the right-hand side of eq.(2.8.6). The first term produces the local heating and the cooling. For the standing waves, the first term

becomes

$$\overline{E_2^1} = -\frac{\pi r_0^2}{2\omega\rho_m}\frac{\partial |P_1|^2}{\partial x} \mathrm{Im}\, g \qquad (2.8.8)$$

Since imaginary part of g is everywhere positive as illustrated in Fig.2.8, this equation indicate that the derivative of $\overline{E_2^1}$ is positive(heating)at velocity node and is negative(cooling) at pressure node*. For steep temperature gradient, the second term of the inner brackets dominates over the first term. This term is purely imaginary, so that only the imaginary part of g is needed for the final results, Therefore

$$\overline{E_2^2} = \pi r_0^2 \frac{1}{2\omega} u_c \tilde{u}_c \, \mathrm{Im}\left(\frac{F^* - F\sigma}{1-\sigma^2}\right) \rho_m C_p \frac{dT_m}{dx} \qquad (2.8.9)$$

This equation can be rewritten as, using the effective heat conductivity by thermally driven acoustic oscillations produced by Rott

$$\overline{E_2^2} = -A k_{eff} \cdot \frac{dT_m}{dx} \qquad (2.8.10)$$

where A is the cross-section of area and k_{eff} is given by

$$k_{eff} = \frac{\sigma |u_c|^2}{2\omega\nu} k \, \mathrm{Im}\left(\frac{\sigma F - F^*}{1-\sigma^2}\right) \qquad (2.8.11)^{**}$$

This heat flux may contribute to a large amount of evaporation of liquid helium. Qualitatively k_{eff} is proportional to the square of the amplitudes of the oscillation.

* Mr.Haruyama and Mr.Ikeda in cryogenic center in the university of Tsukuba show that the top of liquid helium level meter becomes warm when Taconis oscillations are generated and very vigorous. This phenomenon is explained by eq.(2.8.8).

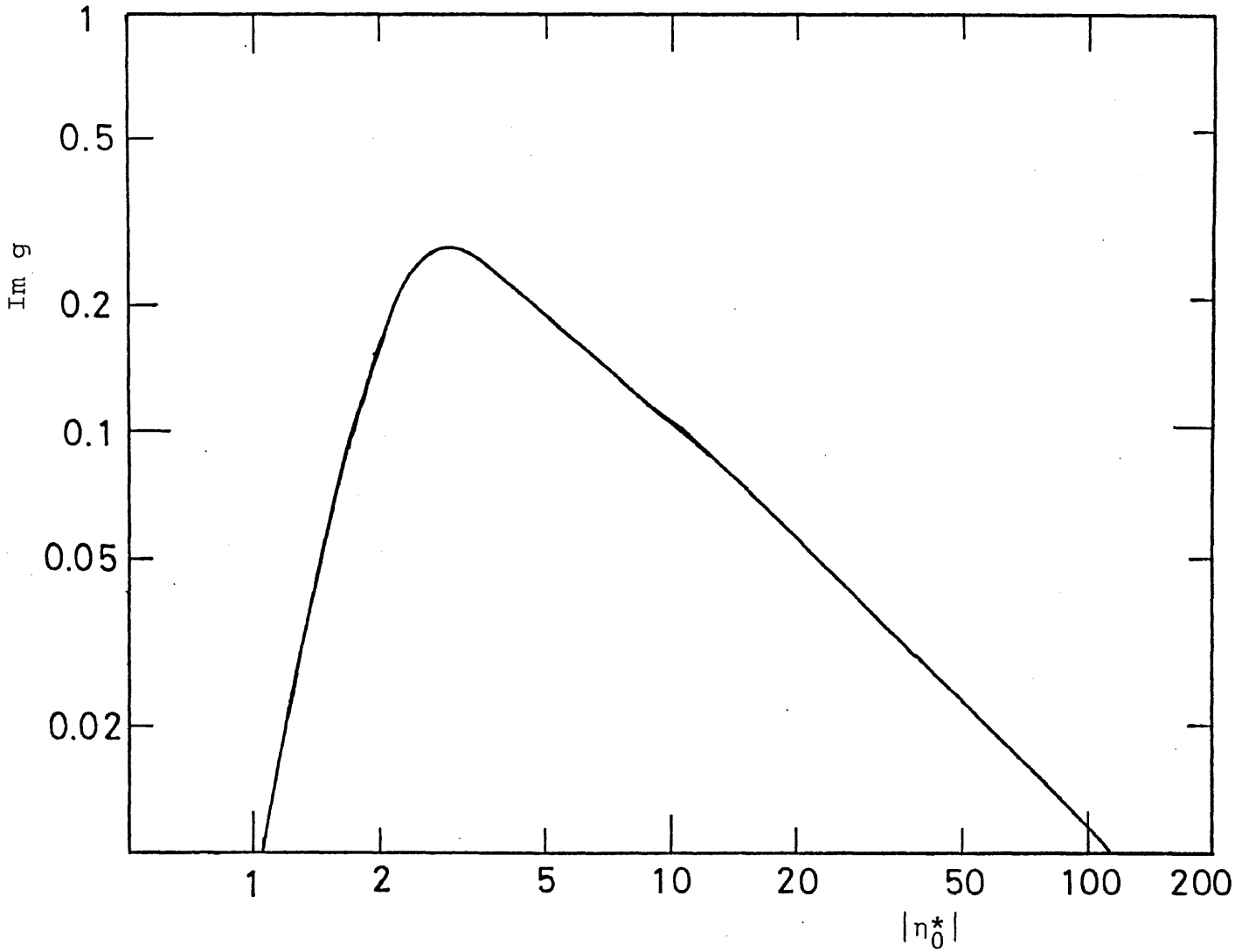

Figure 2.8 Behavior of imaginary part of g. It always takes positive values.

2.9 STABILITY LIMITS FOR THERMALLY DRIVEN OSCILLATIONS

We will roughly give the review of the theory of Rott where the stability curves for helium are numerically predicted. The stability problems are started from the differential equation(wave equation)for the acoustic pressure p_1 along the tube axis given in Appendix 1;

$$[1+(\gamma-1)F^*]+\frac{d}{dx}[\frac{a^2}{\omega^2}(1-F)\frac{dp}{dx}] - \frac{a^2}{\omega^2}\frac{F^*-F}{1-\sigma}\frac{dp}{dx}=0 \qquad (2.9.1)$$

which can be also derived from a set of equations given in section 2.6 under the simple model. This equation under the assumption"a long tube approximation" is of interst over the full and unrestricted range of the variable $|\eta_0|$, which represent the ratio of r_0 to the Stokes boundary layer thickness . The acoustic solution for $\theta=0$ was first solved by Bergh and Tijeman(1965). However as coefficients in eq. (2.9.1)depend on the temperature distribution with x for $\theta \neq 0$, the solution of p_1 appears extremely difficult.

The part except for time factor for right running plane wave is given by $\exp(-i\hat{k}x)$, where in general $\hat{k}$ is complex due to the effects of a dissipation. Thus dispersion relation for $\theta=0$ is obtained from eq.(2.9.1);

$$\hat{k} = \frac{\omega}{a}(\frac{1+(\gamma-1)F^*}{1-F})^{1/2} = \frac{\omega}{a^*}$$

$$a^* = a(\frac{1-F}{1+(\gamma-1)F^*})^{1/2} \qquad (2.9.2)$$

a; adiabatic sound velocity

where the proper sign of the root is chosen as $\hat{k}>0$ in the inviscid limit. The condition $\mathrm{Im}\,\hat{k}<0$ has to be imposed in

order to obtain the pressure amplitude converged to zero at $x=\infty$. Therefore we must select a suitable branch of η_0, which has two branches, $1\pm i$. Equation.(2.9.2) shows a good correspondence with the model given in the previous section. For simplicity the inviscid case, i.e.,F=0(but thermal conductivity is finite, i.e.,$F^*\neq 0$)is considered. Then the relation is

$$\frac{\hat{k}^2}{\omega^2} = \frac{(1-F^*)}{a_s^2} + \frac{F^*}{a_T^2} \qquad (2.9.3)$$

where

$$a_s^2 = \left(\frac{\partial P_1}{\partial \rho}\right)_S \equiv a \qquad (2.9.4)$$

$$a_T^2 = \left(\frac{\partial P_1}{\partial \rho}\right)_T = \frac{a_s^2}{\gamma}$$

a_s; adiabatic sound velocity(=a)

a_t; isothermal sound velocity

When the thermal boundary layer thickness is sufficiently small compared with the tube inner radius, the weight F* approaches to zero, so that the right-hand side of eq.(2.9.3) becomes to $1/a_s^2$. Thus for such a case, the acoustic wave is a normal adiabatic sound. On the other hand, when the thermal boundary layer thickness fills up the whole tube, F* approaches to unity, so that the sound speed becomes isothermal one. For example in narrow tube limit, the leading term of the wave

** This equation shows a good correspondence with normal thermal conductivity derived from the kinetic theory; $k=\frac{1}{3}\rho_m c_p u \ell$ where ℓ is a mean free pass. The following expression of k_{eff} in eq.(2.8.11) is convenient to compare with normal one;

$$k_{eff} = \frac{|u_c|^2}{2\omega} \rho_m c_p \, \mathrm{Im}\left(\frac{\sigma F - F^*}{1-\sigma^2}\right)$$

where the particle displacement in the core is given u_c/ω

number is written as

$$\hat{k} = \frac{2}{r_0} \frac{1}{a_T} (\upsilon \omega)^{1/2} (1 - i)$$

Thus in a capillary tube, the wave is strongly damped. As such strong damping is compensated by the driving due to the steep temperature gradient, thermally driven acoustic oscillations are sustained.

The important quantities η_0 and η_0^* are function of x in the case of a non-uniform temperatrue distribution. The assumption of a piecewise constant temperature which has a discontinuity at some situation along the tube is employed as shown in Fig.2.9, where a half open tube is cold at the open end and warm at the closed end, and temperature has a constant value T_{mc} (mean temperature at cold part) between x= 0 and x=ℓ, and T_{mH} between x= ℓ and x=L. We discuss the differential equation under such a discontinuous model for leading the stability limits of the oscillations. Equation. (2.9.1) is written as

$$[1 + (\gamma - 1) F^*] B P_1 + \frac{d}{dx} \left[\frac{a^2}{\omega^2} (1 - F) B \frac{dP_1}{dx} \right] = 0 \qquad (2.9.5)$$

with

$$\frac{\partial B}{\partial x} = - \frac{F^* - F}{(1 - F)(1 - \sigma)} \theta \qquad (2.9.6)$$

where B is so normalized that it takes unity for non-dissipative case($|\eta_0| \to \infty$). In order to discuss the boundary condition for the pressure with the temperature discontinuity at x= ℓ , the following set of equation equivalent to eq.(2.9.5)

$$P_1 = - \frac{1}{G} \frac{d\Psi}{dx} \qquad (2.9.7)$$

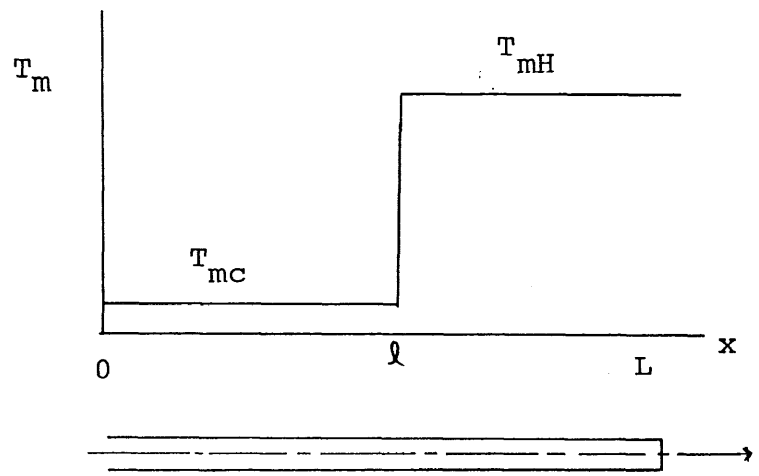

Figure 2.9 A half open tube and a step-like mean temperature distribution along the tube.

$$\Psi = \frac{G}{\hat{k}^2}\frac{dp_1}{dx} \qquad (2.9.8)$$

where $G=[1+(\gamma-1)F^*]B$ and $\hat{k}$ is wave number. The symmetry between p_1 and Ψ requires that they can not take a function such as δ-function or step-function, because Ψ will always be one degree more singular than p_1, and eq.(2.9.7) introduces a previously excluded singularity in p_1. Such demand can be recognized by analogy "the problem of well-type potential in Schrödinger equation"; the wave function can be continuous in all region. In order to avoid singularities, Ψ and p_1 should be continuous along the tube axis, even if the temperature distribution is step-functional: so that at the location $x=\ell$

$$p_1(\ell - 0) = p_1(\ell + 0) \qquad (2.9.9)$$

$$\Psi(\ell - 0) = \Psi(\ell + 0) \qquad (2.9.10)$$

The boundary conditions at the open end x=0 and at the closed end x=L are $p_1=0$ and $u=0$, i.e., $dp_1/dx=0$ respectively. The former is idealized for a half open tube, because the open end correction is not taken into account, and oscillations of the U-shaped cavity employed in our works which is closed at both ends and established a symmetrical temperature distribution satisfies $p_1=0$ exactly. Thus the following expressions for the pressure account for the above stated boundary conditions and eq.(2.9.9);

$$p_H = A_1\frac{\cos \hat{k}_H(L-x)}{\cos \hat{k}_H(L-\ell)} \quad \text{for} \quad \ell \leq x \leq L \qquad (2.9.11)$$

$$p_c = \frac{A_1 \sin \hat{k}_c x}{\sin \hat{k}_c \ell} \qquad \text{for} \quad 0 \leq x \leq \ell$$

where A_1 is the pressure amplitudes at $x=\ell$, and subscript c and H intend the cold and the warm part respectively. The final condition eq.(2.9.10) gives us the key equation for stability limits;

$$\frac{G_c}{\hat{k}_c} \cot \hat{k}_c = \frac{G_H}{\hat{k}_H} \tan \hat{k}_H (L-\ell) \qquad (2.9.12)$$

The oscillating instability is due to an amplification of the accidental and infinitesimal disturbance which is not able to be separated from any physical system. The angular frequency in eq.(2.9.12) is generally complex. According as the imaginary part of the frequency is positive, zero and negative, the system is stable, neutral(stability limits), and unstable respectively. The subsequent studies concentrate on the question of conditions for a real value of the frequency,i.e., the relations between the warm and the cold states will be sought, which give the stability limit of the oscillation(refer to the theory of Rott).

CHAPTER III

EXPERIMENTAL

There have been many experimental investigations about this type of the oscillating instability(Taconis oscillations) associated with thermally driven acoustic oscillations in cryogenic systems. They, however, are too rough or too qualitative to give sufficient understanding of this phenomenon. One reason for such failures is that the temperature distribution along a tube was not paid attentions. Another is that, in early daies, owing to a lack of theoretical investigations, it was not understood what is essential parameter to characterize the oscillating instability. The latter problem was solved through a series of the theoretical studies by Rott, et al..

In our experimental investigations, two main developements are made comparing with some previous experiments; one is the use of a U-shaped tube instead of a half open tube in previous works by other authors. Such a new type of a cavity enables us to compare our experimental results quantitatively with the theory of Rott, et al.. Another is the establishment of the temperature distribution along a tube axis, which was performed by the use of the techniques in cryogenics. High sensitivity in thermal measurements is able to be obtained there. All experiments were made over a wide range from 4.2K to about 60K as temperature at the cold part. The warm part is maintained at room temperature.

For obtaining the stability limits of the oscillations, the experimental apparatus consists of three relatively distinct parts; the cavity in which the standing acoustic waves are set up(section 3.1), the pressure measuring system(section 3.2) and the cryogenic systems for establishing a nearly step--functional temperature distribution along a tube axis(section 3.3).

Lastly we introduce a cryostat for measuring a liquid helium evaporation rates under the oscillations relating to second-order heat flux discussed in the previous section. In this cryostat, the developement of temperature distribution is also performed comparing to the earlier experiments by Banister(1966).

3.1 CAVITY

The cylindrical cavities are made of long stainless steel tubes with a wall thickness of 0.3mm, inner radius 1.2-4.7mm. The whole length of them is more than 1.5meter. Thus those tubesare sufficient for the experimental studies of plane waves in gases(when sound waves of low enough frequency are propagated in a pipe, they can be considered to be plane wave). Instead of a half open tube, which is used in the previous section and most of earlier works, a U-shaped tube is employed in our experiments. The U-tube and the symmetrical temperature distribution along it are shown in Fig.3.1.a.

In the position of x=0, two half open tubes are smoothly connected by a U-shaped brass whose length(about 3mm)is

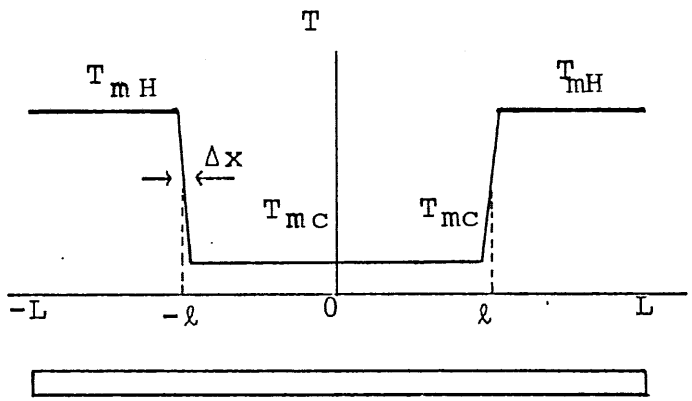

Figure. 3.1.(a) Mean temperature distribution along a U-shaped tube closed at both ends employed in our experimental studies. The part Δx is less than four percents of the whole length L.

sufficiently samll compared with wave-length. Two types of tube, a half open and U-shaped tube, are mathematically equivalent as long as the fundamental frequency mode or higher odd harmonic modes are considered. In the tube schematically shown in Fig.3.1.a, the following expressions for the pressure fluctuations corresponding to eq.(2.9.11)acount for $p_1=0$ at $x=o$, $dp_1/dx=0$ at $x=\pm L$ and the continuity of the pressure;

$$p_C = A_1 \frac{\sin \hat{k}_C x}{\sin \hat{k}_C \ell} \qquad |x| \leqq \ell$$

$$p_H = A_1 \frac{\cos \hat{k}_H (L-\ell)}{\cos \hat{k}_H (L-\ell)} \qquad \ell \leqq x \leqq L$$

$$p_{-H} = -A_1 \frac{\cos \hat{k}_H (L+x)}{\cos \hat{k}_H (L-\ell)} \qquad -L \leqq x \leqq -\ell$$

where A_1 is pressure at $x=\ell$ including the time factor. Another boundary condition as discussed in section 2.9, Ψ also has to be continuous at $x=\pm \ell$. It is understood, using above equations, that the boundary condition at $x=\ell$ is the same as that at $x=-\ell$. Thus the U-shaped tube is mathematically equivalent to a half open tube treated in chapter II, so that the theoretical results are held true for the tube employed in our experiments.

There are two experimental evidences in favor of this equivalence; one is that the acoustic pressure amplitudes are observed to be the same at two closed ends of the U-shaped tube, and another is that the phase differences between them are 180 degrees. The X-Y diagram of the pressure fluctuations observed on an oscilloscope is shown in Fig.3.1.b, whose horizonal axis is connected to the pressure at $x=L$, and

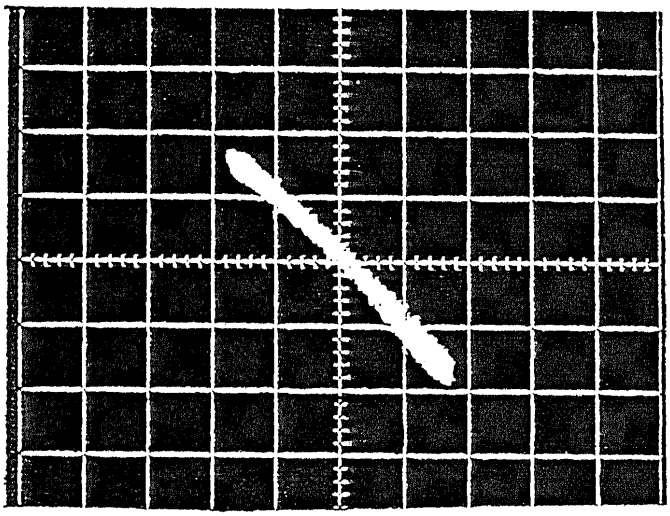

Figure 3.1.(b)

The relation between the pressure fluctuations at two closed ends in the U-shaped tube. X axis in this figure shows the pressure fluctuations at x=L and Y axis shows that at x=-L. From this photograph, two important matter are understood; one is that the phase differences between the pressure at two ends are 180 degree and another is that these amplitudes are the same. Thus it is considered that this instability is a kind of the standing waves with fundamental frequency mode.

another $x=-L$. This photograph confirms that "Taconis oscillation" is a kind of the standing acoustic waves whose pressure loops(velocity node)exist at $x=\pm L$ and pressure node (velocity loop)at $x=0$. The acoustic oscillations with the fundamental frequency mode are excited in both types of the cavities. From the symmetry between a half open and U-shaped tube the discussion and the conclusions in capter II is applied to our case. But a higher harmonic modes(as discussed in the next chapter)except for the odd harmonic(fundamental, third,...) induced in the U-tube do not satisfy the above explanation, because two types of tubes are not equivalent. In such higher harmonic mode as reported by Yazaki, et.al.(1980)the U-tube is equivalent to the closed tube at the positions $x=L$ and $x=0$, where velocity node exists.

The new type of the cavities gives us several following advantages:

1. The lowest acoustic mode excited in such a symmetric tube provides the exact boundary condition, $p_1=0$, in the middle of the tube. In a half open tube this condition is idealized, because the dynamics of the open ends are ignored, and no oscillations of a finite cavity connecting to the tube are admitted.
2. The oscillating gases can be separated from a coolant (liquid helium in our experiments), so that we can make use of several kinds of cryogenic gases* as sample.

* The oscillations have been observed for gaseous neon during the course of our stadies.

3. the mean density ρ_m can be varied through a needle valve and a capillary whose dead volume is negligible compared with that of the cavity. Therefore the boundary layer thickness δ can be continuously varied through the density of oscillating gas.

3.2 PRESSURE MEASUREMENTS

The self-sustained acoustic pressure measurements are performed at x=L, where the pressure amplitudes are maximum. Therefore, main purpose in our experimental investigations, the determination of the boundaries between oscillation and no oscillation(stability limits)will be sufficiently achieved by measurements p. At other position x=-L, the mean pressure is measured in order to determine the kinematic viscosity at the warm and cold parts. The contact between a pipe and a pressure transducers is performed using a rubber band and the leak tight is tested by a leak detector.*

PRESSURE TRANSDUCERS The pressure measurements in our experiments were carried out using the microminiature semi-conductor pressure transducers(differential types)made use of the Piezo electronic resistance effects. The pressure is determined from the voltage which is proportional to a small distortion produced on diaphragms. Such transducers have been developed in detail by members of the Toyota Ltd(1969; Tomohisa and Igarashi). Attainable pressure fluctuations are sometimes surprisingly high as 10^4 Pa or more, and their frequencies are usually below 100Hz. The transducers are able

to be employed below 10^5Pa, and their resonance frequency (diaphragm) is more than 10KHz, so that they are suitable to our experiments. The acoustic and the mean pressure are measured by type** of 1F DD102(No51) and 1F DD102(No58) respectively. The relation between the output voltage through an amplifier and pressure calibrated by a mercury manometer is shown in Fig.3.2.a for 1F DD102(No51) as an illustration, where one side of the transducer is connected to the manometer and the other side is pumped out by a rotary pump(10^{-3}torr); the calibrated line is

$$P = 155.1\ V \pm 0.2 \qquad \begin{matrix} P;\ \text{torr} \\ V;\ \text{volt} \end{matrix}$$

where the transducer resolution is below 0.2torr(27Pa), including the following electronic systems.

FOLLOWING ELECTRONIC SYSTEM A block diagram for the pressure measurement system is schematically shown in Fig.3.2.b. At first the acoustic signal came from the pressure transducer is amplified by two hundreds times using Amplifier-A.A.3000(Toyoda Koki) and their amplitudes are measured by a digital voltmeter (T.R 6858 Takeda Riken). The amplified signal by two hundreds times, stillmore, is monitored by an oscilloscope(Tectronix

* The leak tight there is very important; in our earlier experiments, on account of no leak tight the oscillations is not able to be sustained, but damped, so that the determinations of the stability limits was not able to be carried out. Stillmore the gaseous nitrogen or oxygen are solidified at cold part through the leak, and are filled up the tube cross-section. By sudden vaporization of them, a diaphragm of the pressure transducer was destroyed.

** pressure transducers

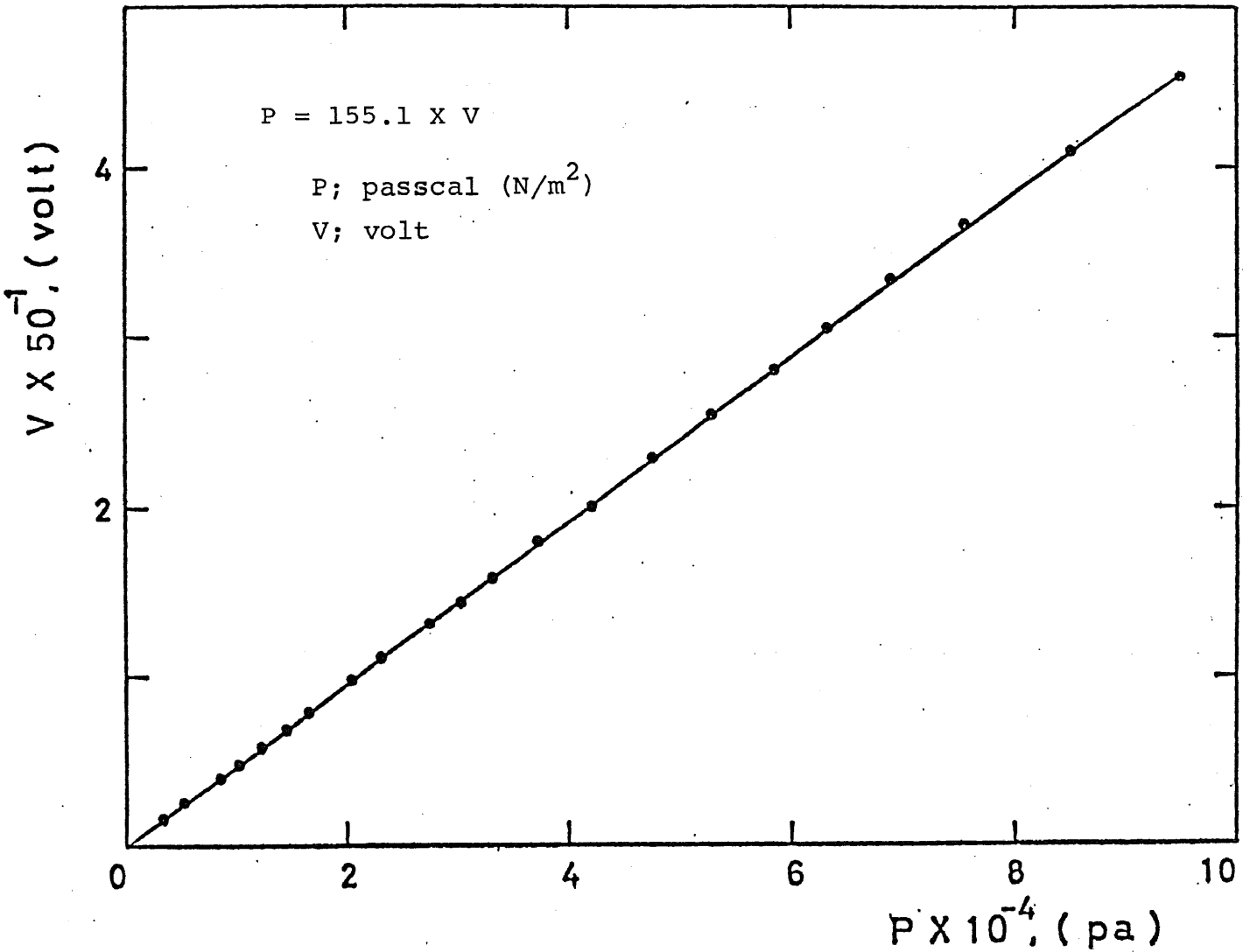

Figure 3.2 (a) The relation between the pressure and the output voltage for 1.F.DD 102(No 51)pressure transducer through amplifier(50times)

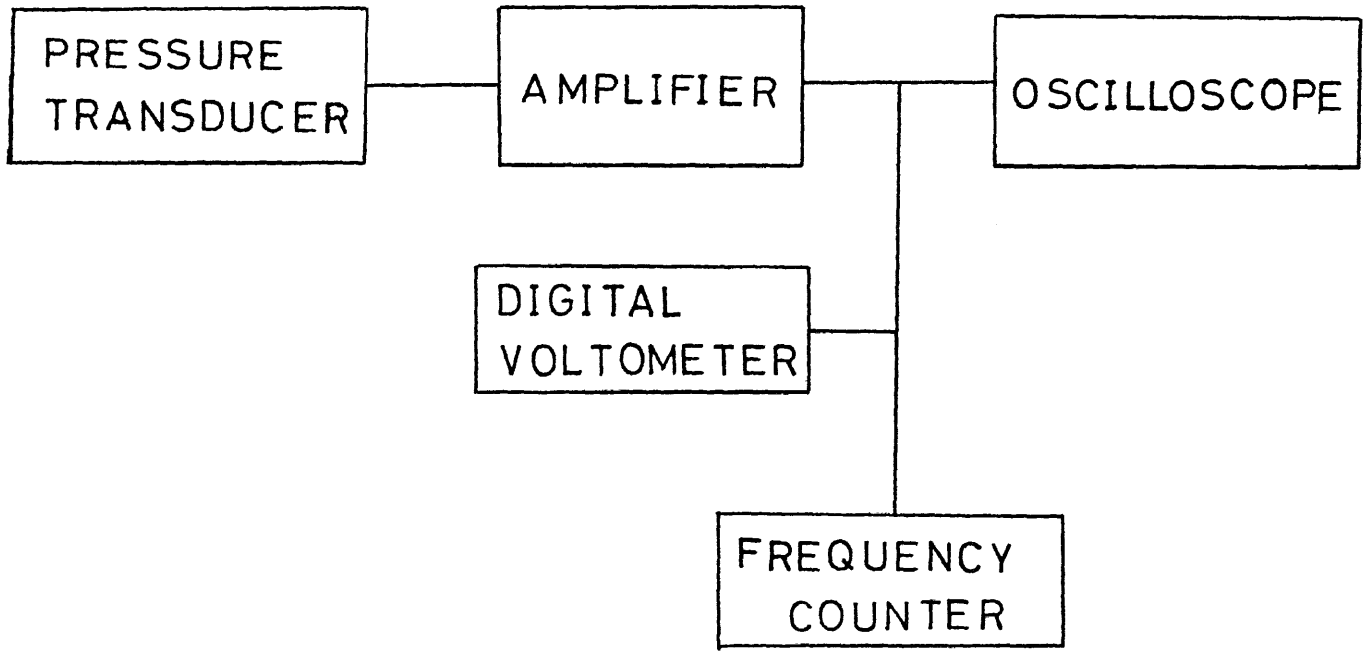

Figure. 3.2.b Schematic diagram of pressure measurements system.

7603)and whose frequencies are measured using universal counter (T.R. 5103 Takeda Riken). Secondly the voltage corresponding to the static pressure is amplified by 50 times using D.C Amplifier-A.A.3000 and measured by a digital voltometer.

The wave-forms of the pressure fluctuations are normally sinusoidal near the stability curves as long as only the fundamental or only the second harmonic is induced. According to Hoffman,et.al(1973) the wave-forms excited in a U-shaped tube become to be deviated from sinusoidal shape of the pressure-time curve for very vigorous oscillations. We also observed the same phenomenon in such a tube. Such new phenomenon may be due to the nonlinear effects or the superposition between the fundamental and the higher harmonics. Our experiments, of course, are performed within the limits of the sinusoidal pressure fromes.

3.3 APPARATUS

The cryostat consists of a three litter helium dewar made of pyrex-glass which is evacuated to 10^{-3}torr by a rotary pump and surrounded by a liquid nitrogen dewar. The experimental apparatus schematically illustrated in Fig.3.3.a, by which a nearly step-functional temperature distribution is able to be established, is consisted of a separated two reservoirs, a warm part and a cold part, and is inserted into such a double dewar. We obtained more homogeneous temperature distribution, in particular, at the cold part, using this apparatus instead of the use of an earlier cryogenic apparatus(not shown in this paper)introduced in our first paper(Yazaki, et. al. 1979).

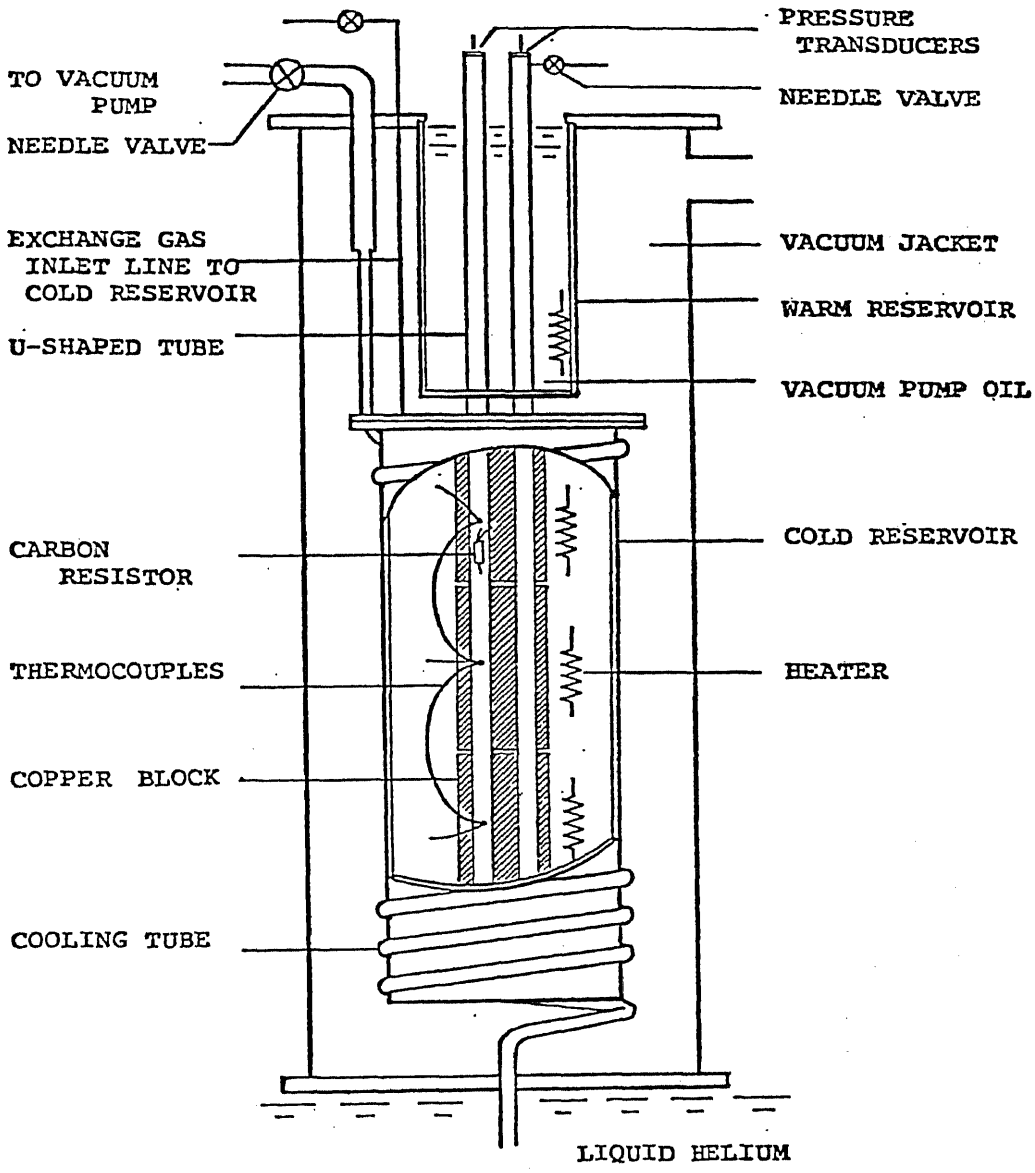

Figure 3.3.(a)

A schematical drawing of the apparatus.

Apparatus in Fig.3.3.a is employed for cooling uniformly the cold part of the U-tube with $\xi \leqq 1$. A simpler apparatus is used for $\xi \geqq 1$. As explained in chapter Ⅳ. the experimental results for $\xi = 1$ in both cryostats agree each other. Therefore in the following we introduce the former apparatus only.

WARM PART The warm part ($\ell + \frac{\Delta x}{2} \leqq x \leqq L$) is immersed into the reservoirs at liquid nitrogen (77.3K) or room temperature system made from vacuum pump oil in copper jacket (with diameter 30mm and wall thickness 2mm). Near the top end of the tube, the entrance for pouring or pumping the oscillating gases (helium gas) is connected to vacuum rotary pump through a needle valve and a capillary (0.5mm inner radius copper tubing) whose volume is negligible compared with that of the U-tubes. The cooling transmitted from the cold part (due to the heat conduction of two stainless steel tube, the second order heat flux caused by the acoustic oscillations and the radiation across the valuum space) are compensated by heaters made of constantan wire (normally less than five watt) wound around the copper jacket. A copper versus constantan thermocouple (0.2mm diameter) is used as a thermometer and we check the uniformity of the temperatrue by moving up or down it.

COLD PART The cold part ($\ell - \frac{\Delta x}{2} \geqq |x|$) is cooled by the continuous flow of cold helium gas (or liquid) as shown schematically in Fig.3.3.a. Using this cooling method, the temperature at the cold part was able to be sufficiently varied from 4.5K to

about 60K continuously. The cold reservoir is made of copper cylinder(with length 1.3m, outer diameter 30mm and 2mm wall thickness)around which a cooling tube(2mm inner diameter and 3m whole length)is wound and soft-soldered for heat exchange. Through this tube, coolant, helium gas is pumped by Kenny--pump*(KRP-3000 litter per minute). The cold part is precooled by liquid nitrogen through vacuum space and becomes about 200K, and after liquid helium is transfered, it normally takes about five houres to be cooled down to near 30K. The variation of the temperature is performed by the adjustments of a gas flow rate through a needle valve.

Even using such a way of cooling, it was not so sufficient that a long tube(~1m)was uniformly able to be cooled. Futhermore under the oscillations the thermal effect(second order heat flux)are different according to the position of the pipe. Therefore the temperature control should be demanded at the local position of the tube. Taking into account such circumstamces, we could succesfully obtain more homogeneous temperature distribution at the cold parts using the method described below.

The cold part of the U-tube is thermally kept in contact with three separated copper blocks and foils which are directly soft-soldered on the wall of the tube. This plays a role to enhance the heat capacity of the wall, so that the assumption in the theory that the wall temperature fluctuations are negligible becomes more exact.

* DAIA vacuum engineering co., LTD.

TEMPERATURE MEASUREMENTS AND CONTROL At three separated position A, B and C(see Fig.3.3.a), three carbon resistors and a series of chromel versus gold 0.07 at % iron thermocouples(Osaka oxygen Industrial Ltd Bach No 812001--812089)are directly attaced on the tube wall by varnish(G.E 7031). The temperature T_c are measured by one of the resistors (Allen Bradly nominal value 510 ohm 1/8 watt)calibrated against chromel versus gold thermocouple(liquid helium 4.2K as a constant point). The calibrated curve is illustrated in Fig.3.3.b. A simple D.C electric bridge circuit for measuring the resistance thermometry is shown in Fig.3.3.c where lead lines(with method of three wire)are Mn-Ni wire with 0.08mm outer diameter.

Furthermore for obtaining more homogeneous temperature distribution, temperature differences occurred between two separated position are detected by chromel-gold thermocouples at each position. Thermoelectric power caused by temperature difference are monitored by two microvolt-meters(Ohkura Electronic Co). Futhermore they are amplified by D.C amplifiers (Bipolar Power Supply Kikusui Electric Corp,35-1A) Their output voltages are automatically supplied to the respective heaters B and C in such a way that thermoelectric power vanishes A schematic block diagram is shown in Fig.3.3.c.

Thus we could obtain such a near step-functional temperature distribution that the part Δx where the steep temperature change occurs was less than three percents of L. Two reservoirs, a warm and a cold, is inserted into the vacuum

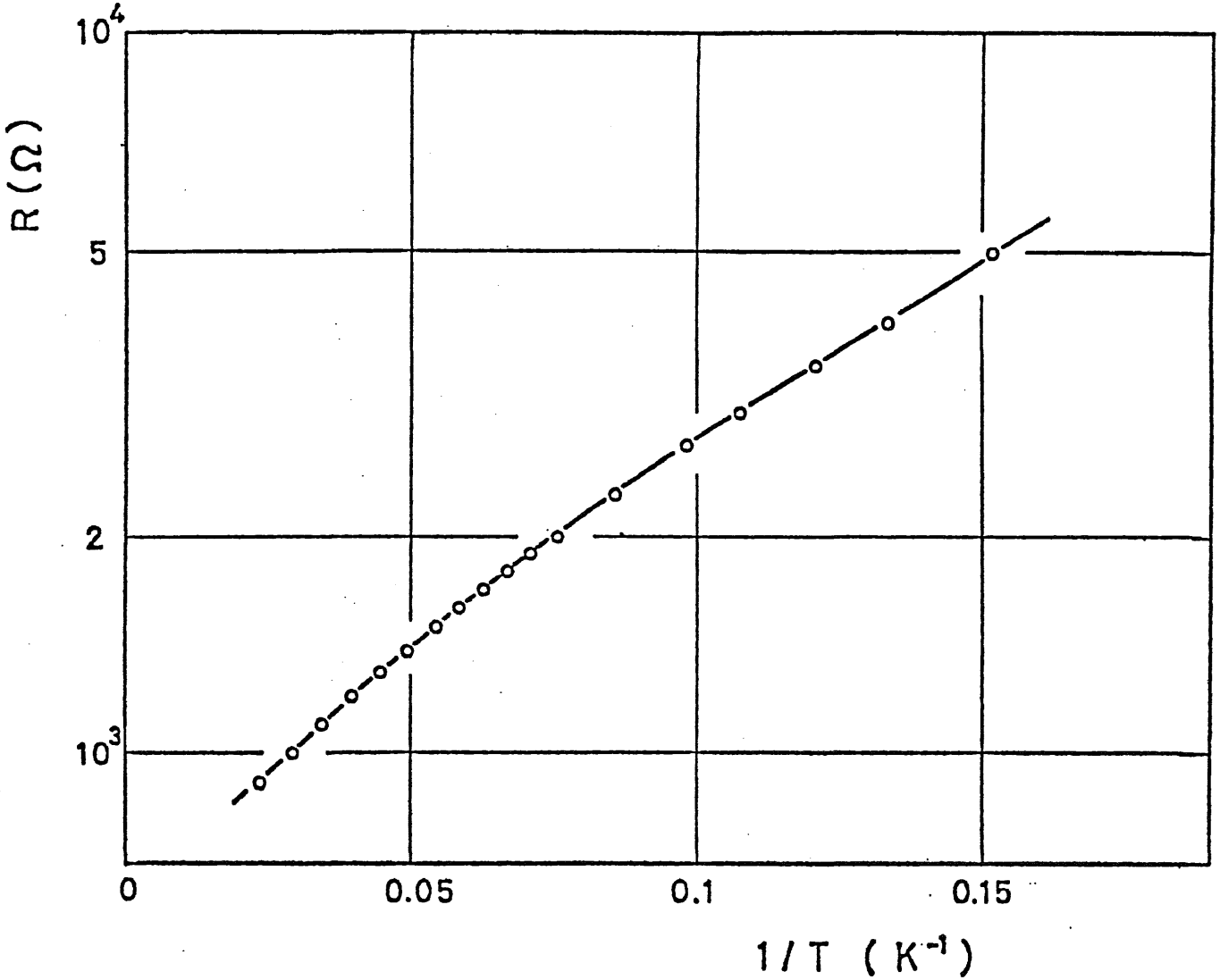

Figure. 3.3 (b) The resistance R of a nominal 510Ω, 1/8 watt Allen Bradly resistor plotted as a function 1/T (calibrated against chromel versus gold 0.07 at % iron thermocouple).

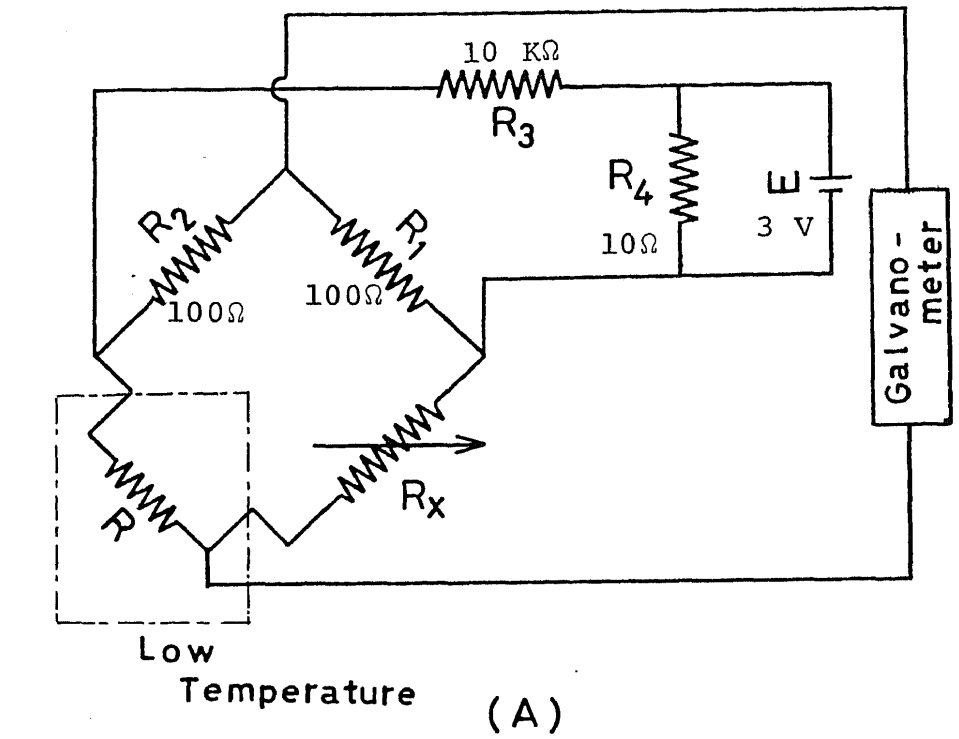

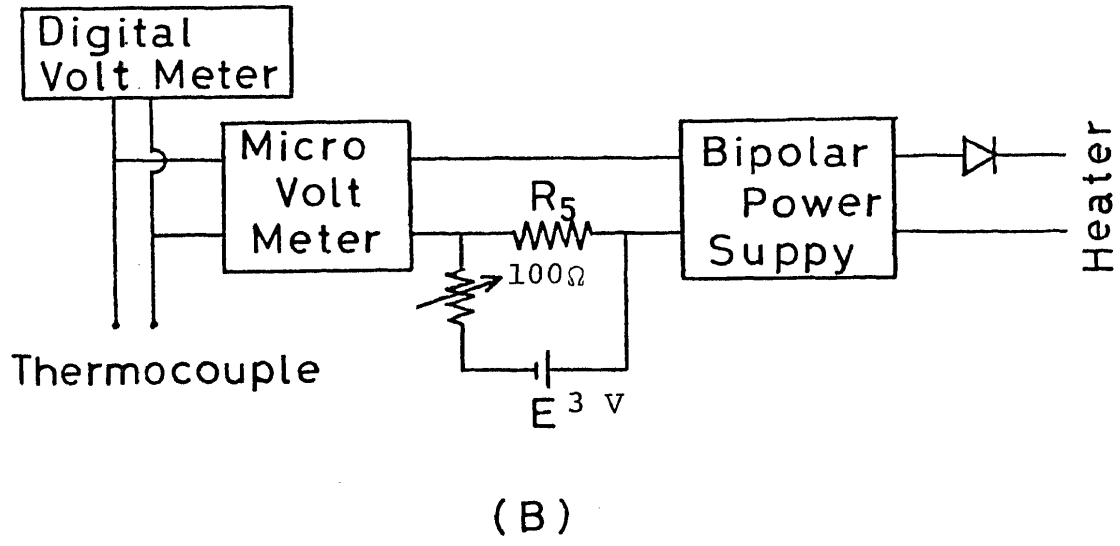

Figure 3.3.(c) (A); A simple D.C bridge circuit for measuring the resistance R of a carbon thermometer up to 10KΩ . (B); A schematic block diagram for establishing the temperature uniformity along the tube axis.

jacket insulated from surrounding liquid helium reservoirs (a stainless steel pipe with 1.5m in wholelength, 50mm outer diameter and 0.5mm wall thickness).

3.4 MEASUREMENTS OF LIQUID HELIUM EVAPORATION RATE

In order to measure a second-order heat flux due to the Taconis oscillations caused by a steep temperature, we employed another apparatus schematically shown in Fig.3.4, which is inserted into the double pyrex-glass dewar subcooled by liquid nitrogen. Thus two reservoirs are directly separated; the cold part is soaked into liquid helium 4.2K and another is immersed into vacuum pump oil maintained at room temperature. The temperature measurements are the same as above. Bellows attached in the vacuum jacket prevents the soldered joint between cold and warm part from being destroyed by thermal contraction.

The evaporation rates of liquid helium is measured instead of the local second order heat flux penetrating into the tube wall. The total heating came from a cold part contributes the evaporation. A helium gas evaporated passes through a calibrated impedance, which is made of a spiral copper tubing (inner radius 4mm and whole length 0.5m). Thus the evaporation rate is estimated by the use of the Poiseuill's law. The pressure difference between an entrance and exit of the impedance is measured by the pressure transducer(Toyoda Ltd 1D101, 0.1F) with D.C amplifier. The calibrated equation of a flow rate was

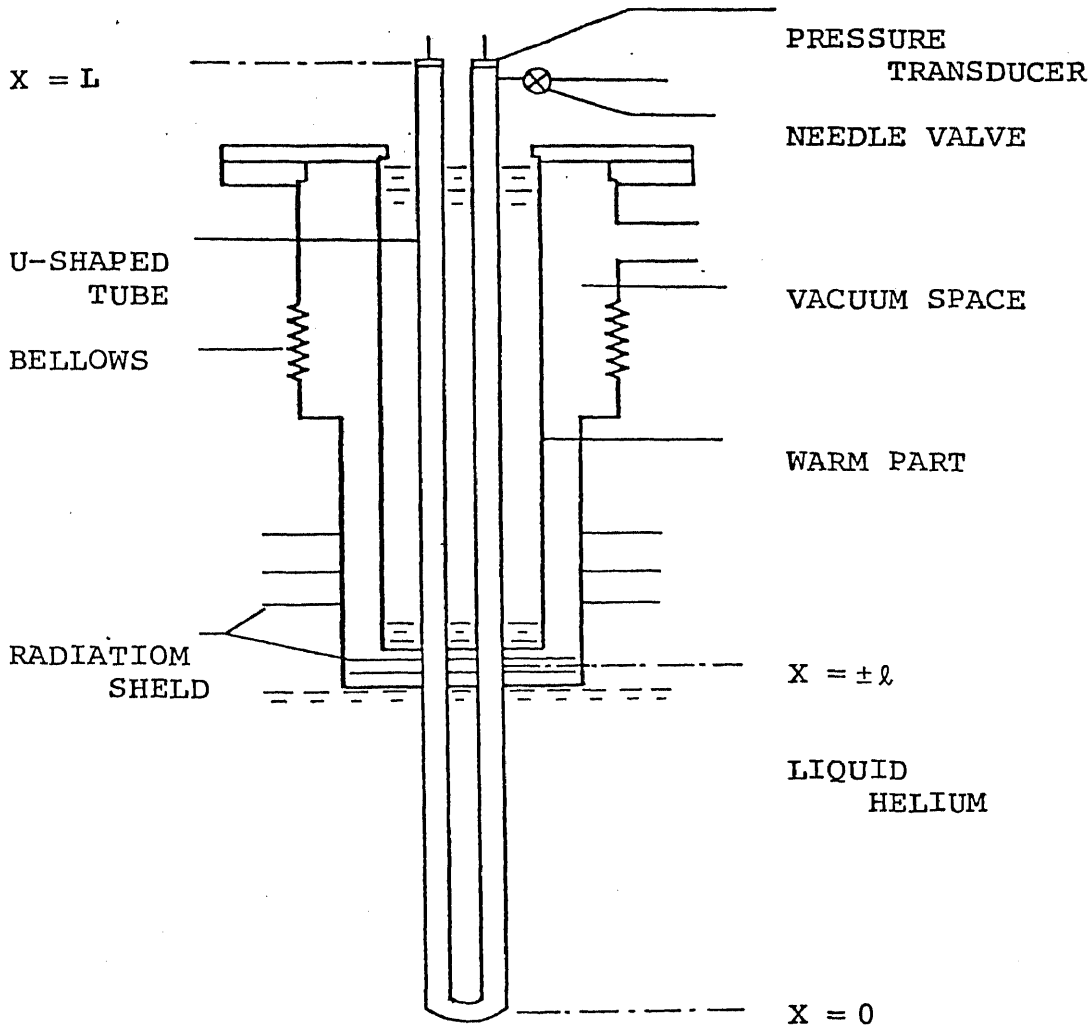

Figure 3.4 The cryostat for measuring the total second-order heat flux produced by Taconis oscillations

$$\dot{n} = 1.30X10^{-5}\ V + 2.0X10^{-4} \qquad \begin{matrix}\dot{n};\ \text{mol/sec} \\ V;\ \text{mm volt}\end{matrix}$$

(V; corresponding to pressure difference between an entrance and exit of the impedance through amplifier(200 times)) which was estimated using the method of least square fiting. The time independent heat current $\dot{Q}_{ex}$ produced by the oscillations is estimated experimentally through a relationship;

$$\dot{Q}_{ex} = L\ (\dot{n} - \dot{n}_o) \qquad (3.4.1)$$

where $\dot{n}$ is flow rate(mol/sec)including the background $\dot{n}_o$ without the oscillations, and L is the heat of vaporization of helium at 4.2K(80 Joul/mol). The quantity $Lx\dot{n}_o$ contains several causes of heat production;

1. radiation heat from the top flange, warm reservoir and liquid nitrogen reservoir.
2. heat conduction transmitted through helium gas in the U-shaped tube and stainless steel tube.

Radiative heating from the top flange is reduced by inserting several thin copper plates.

CHAPTER IV

RESULTS AND DISCUSSIONS

In this chapter we will present the experimental results about, in particular, three subjects: the stability curves and the frequency diagrams of thermally driven acoustic oscillations for gaseous helium, the transition from the fundamentalto the second-harmonic and the thermal effect(second-order heat flux)produced by the oscillations. At first the existences of two branches on the stability curves predicted by Rott et al.(1973-1976)is confirmed in our experiments. For the ratio ξ of the length $(L-\ell)$ to ℓ as a parameter, the stability curves and the frequency diagrams are experimentally determined and quantitatively compared with the theory of Rott and qualitatively explained from the results presented in Chapter II. The optimal conditions for driving the oscillations are also discussed. At the "left-hand branch"for small ξ, we have found the oscillations with higher harmonics(second-harmonic and third harmonic) which have never been observed on previous works. Secondly the classification of the unstable region for the fundamental and the second harmonic is experimentally and numerically performed. Lastly the evaporation of liquid helium accompanied by the oscillations is measured and the effective thermal conductivity of the oscillations is determined from it. Results are compared with the theory of the second-order heat flux introduced in section 2.8.

4.1 STABILITY LIMITS

The first approaches of the stability limits has been performed crudely by Von Hoffman et al.(1973). Their results are shown in fig.4.1, where the excistence of two branches is indirectly suggested by use of tubes closed at one end(half open tubes). However in their experiments it was difficult to say that the stability curves were exactly determined, because there is no continuous variables to approach to the critical point(neutral point). In our case where a U-shaped tube instead of a half open tube was employed, we could confirm not only the existence of two branches but also determine the stability curves.

The relationship between the cold and the warm parts which gives the stability limits of the oscillations is determined from the solutions of eq.(2.9.12)with real
In order to characterize the stability limits, non-dimensional variables

$$\alpha = |\eta_{0c}| / |\eta_{0H}| = T_{H/T_c} \ , \ |\eta_0| = r_0 (\omega/\upsilon)^{\frac{1}{2}} \quad (4.1.1)$$

are employed. These suggest us that instead of the tube radius r_0, we select the boundary layer thickness at the tube wall as a continuous variable. In our tubes the boundary layer thickness is able to be varied continuously.

The only temperature dependent term υ is proportional to $T^{1+\beta}$ ($\mu \propto T^{\beta}$; for helium gas, the best fitting value of β is equal to 0.647: refer to the paper of Keesom). As shown in Appendix III, both of the coefficient of viscosity

and thermal conductivity of gas are independent of the static pressure but dependent of only the temperature. In the analysis of experimental data, we employed,as the values of viscosity for temperatures,the experimental data obtained by previous works, or interporated ones of them.

Determination of the stability limits between oscillations and no-oscillations are experimentally defined as follows. The gas in the cavity becomes unstable and oscillates with finite amplitudes, when, near the left-hand limit(see Fig.4.1), a small quantity of gas is gradually poured into the U-shaped tube through a needle valve(see Fig.3.3.a)under constant temperature ratio; namely the warm and the cold temperatures are kept constant. In the unstable region,when thedensity of gas is reduced, the boundary layer thickness becomes large, then the syste approaches to the stability limit where the oscillations are neutral. Near the other hand limits, under constant temperature ratio, the reverse operations to the above procedures are carried out. Amplitudes of the oscillations near the stability limits are illustrated in Fig.4.1 for typical examples. They have a tendency to increase(left limit, and decrease(right limit)in proportion to $|\eta_{0c}|$. The critical values $|\eta_{0c}|$where the oscillations are neutral may be determined by the extraporation of the line. Practically instead of the extraporation, the values $|\eta_{0c}|$where the acoustic pressure amplitudes are within the range between 27pa(resolution of the pressure transducers including the following electronic systems)and 107pa are employed as the critical points in our experiments. Figure.4.1 shows clearly that the differences

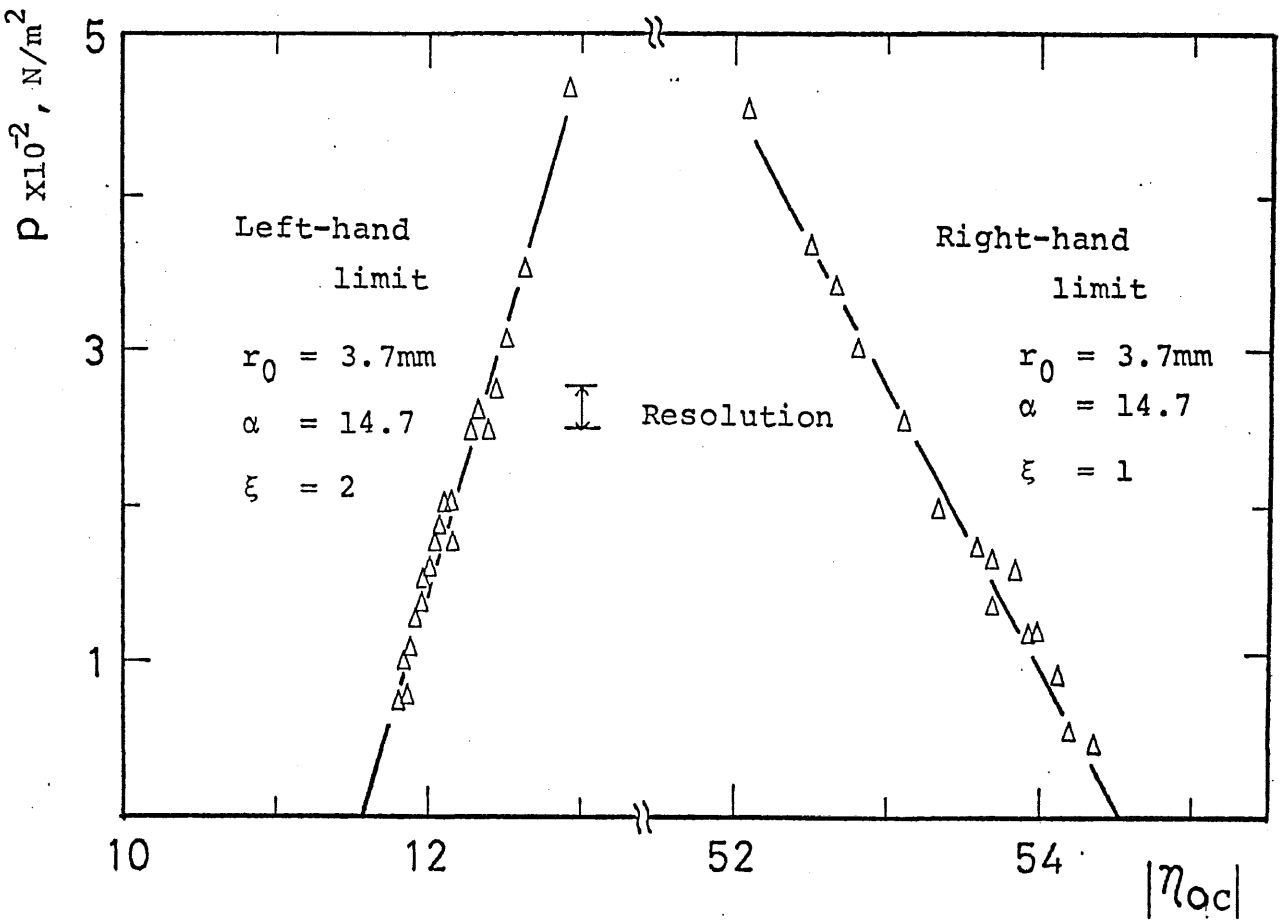

Figure.4.1 Acoustic pressure amplitudes at the closed end(peak to peak values) versus the ratio of the tube radius to the viscous boundary layer thickness in the cold part. Two branches, left and right-hands, predicted by Rott are strikingly confirmed in our experiments.

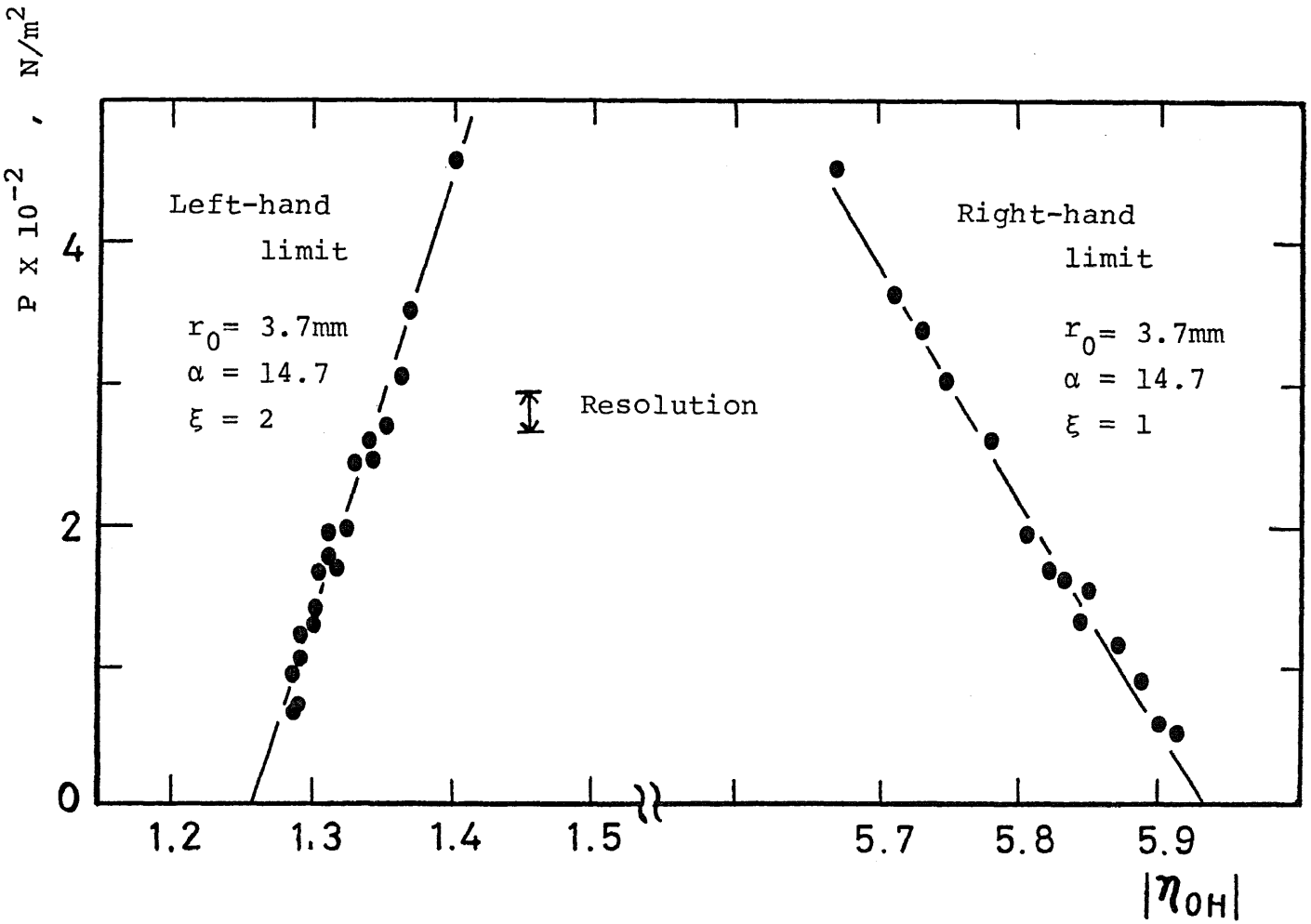

Figure.4.1' Acoustic pressure amplitudes versus the ratio of the tube inner radius to the viscous boundary layer thickness at the warm part.

between them are sufficiently small(less than 5%). In the region around the minimum of the stability curves, where the critical temperature ratio is lowest, that is $\alpha \simeq 6$ for $\xi=1$ (see later section)the critical points of $|\eta_{0c}|$ are determined by slowly changing the temperature in the cold part with heater while the amount of gas in the tube is kept constant. Near the critical points the angular frequency of a harmonic gas motion(relative error is below 2%)is almost independent of the pressure amplitudes. In the following discussion, the quantities $|\eta_0|$, α and λ represent the critical values on the stability curves.

4.2 STABILITY CURVES FOR THERMALLY DRIVEN ACOUSTIC OSCILLATIONS FOR GASEOUS HELIUM.

The stability limits for various temperautre ratios are experimentally determined by the methods described above section(4.1). Under constant ξ we could obtain the stability curves normalized on the plane of the dimensionless variables α versus $|\eta_{0c}|$. The experimental results of the stability curves for helium gas are shown in Fig.4.2.a($\xi=1$, 2, 5 and 10)

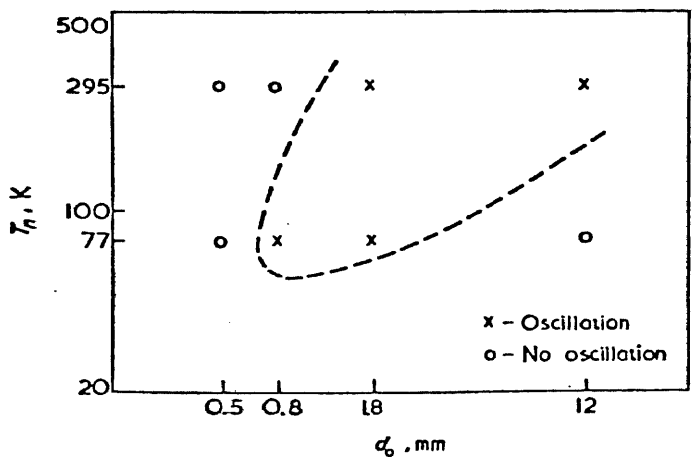

fig.4.1
Oscillations observed with half-open tubes of different diameter for $\xi=1$ [Hoffman et al. 1973]

T_n; warm temperature
d_o; diameter of tube

and Fig. 4.2.b(ξ =1, 0.5, and 0.3)where the temperature ratio T_H/T_c for driving the oscillations is plotted on a logarithmic scale as a function of the ratio of tube inner radius to the viscous boundary layer thickness in the cold part. Cavities with various inner radii(r_0=1.2-4.7mm)are employed according to the viscous boundary layer thickness; that is, narrow enough tubes are utilized near the left-hand branches and wide ones near the right-hand branches, because the mean pressure which can be measured by our pressure transducers is less than about $1.1X10^5$pa. All data shown here are obtained for the case that the warm temperature is room one(297K). For the case that the warm part is at liquid nitrogen temperature(77.3K)we also obtained almost same the stability curve as that in Fig.4.2.a for ξ =1. However not shown here, because these data are unreliable; the warm part is sufficiently immersed in liquid nitrogen on account of the pressure transducers.

Stating the survey of experimental results, each stability curves for various ξ as a parameter is consisted of two branches, "right-hand branch" and "left-hand one". Such two branches join together near the region where the minimum critical temperature ratio is found. Of course, thermally driven acoustic oscillations are induced insides of these curves (unstable region)and not induced outsided(stable region). The lowest critical temperature ratio is found for about $\xi \simeq 1$; near $|\eta_{0c}| \simeq 10$ the stability curve takes a minimum value $\alpha \simeq 5.5$ and $|\eta_{0c}|$ofabout 8 at $\alpha \simeq 7$ is the smallest value for which neutral oscillation can exist(see fig.4.2.a). After the bend,

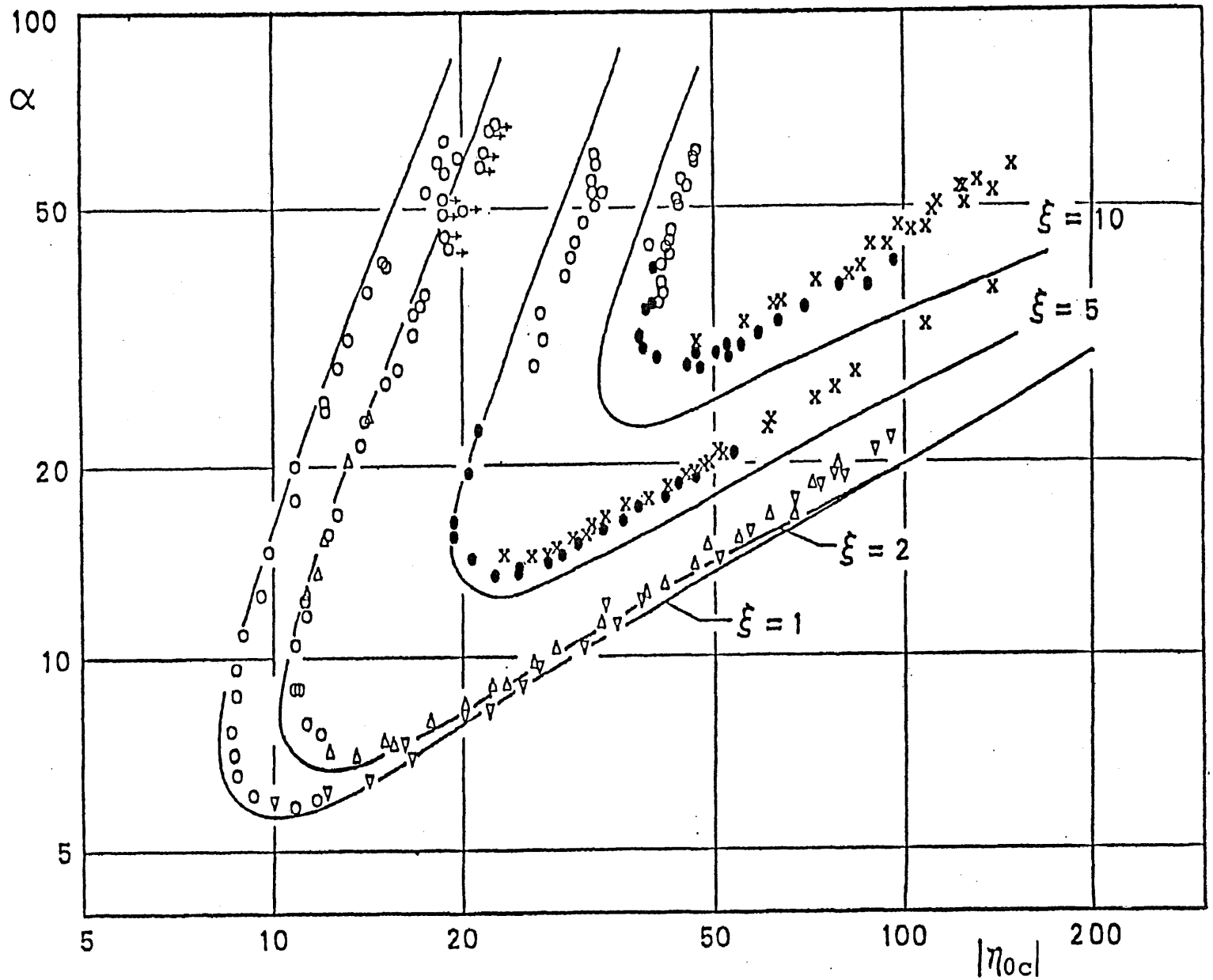

ξ	r_0 (mm)	L (m)	
1	1.2	1	O
1	3.7	1	∇
2	1.2	1.5	O
2	3.7	1.5	Δ
5	1.2	1.8	O
5	2.7	1.8	●
5	4.7	1.8	X
10	1.2	1.65	O
10	2.7	1.65	●
10	4.7	1.65	X

Figure.4.2.a Stability curves for helium gas, critical temperature ratio $\alpha(T_H/T_C)$ versus the ratio of tube inner radius to the boundary layer thickness $|\eta_{0c}|$

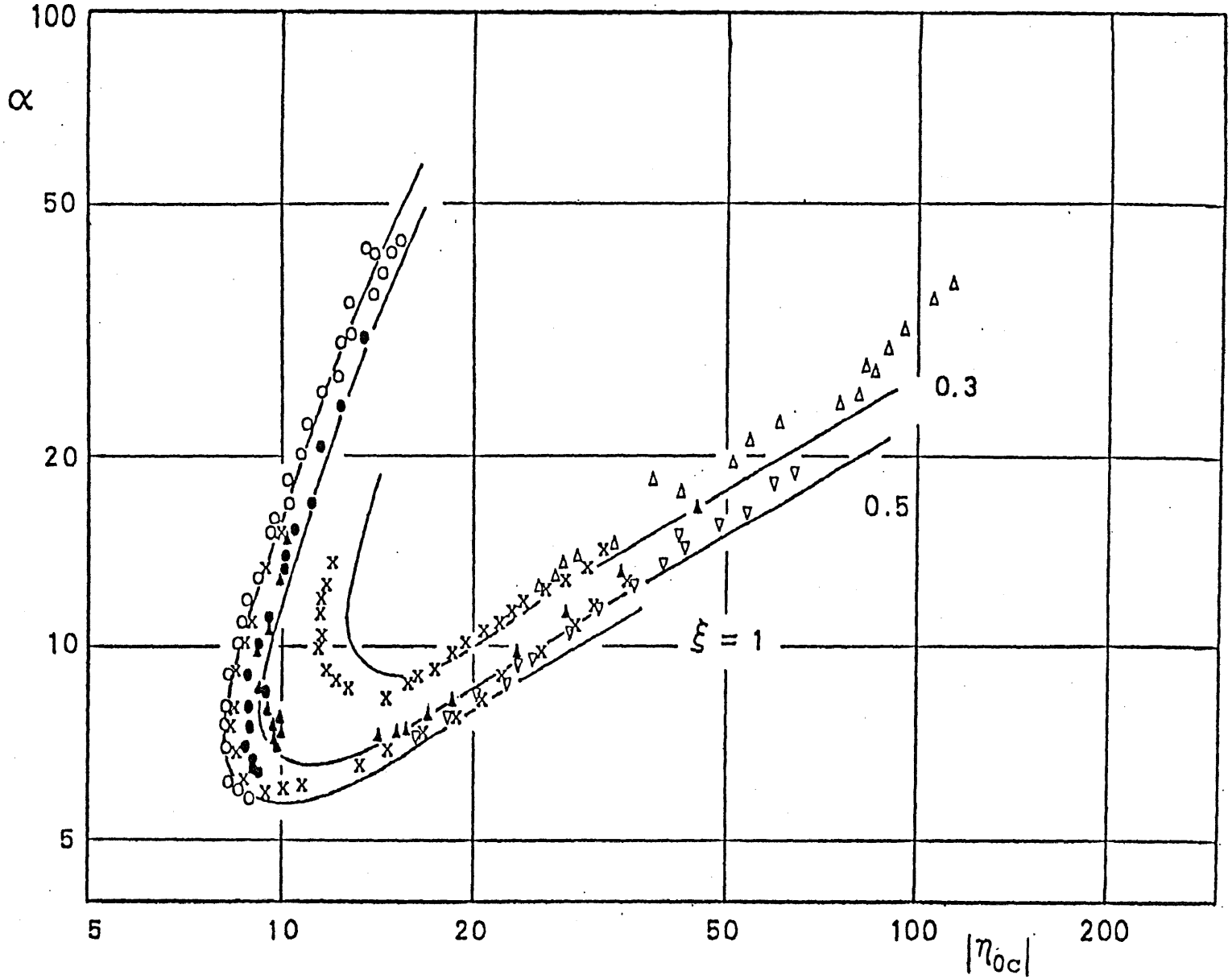

ξ	r_0 (mm)	L (m)	
1	1.2	1	o
1	2.2	1	x
0.5	1.2	0.75	●
0.5	2.2	0.75	▲
0.5	3.7	1.26	▽
0.3	2.2	1.07	x
0.3	3.7	1.07	Δ

Figure.4.2.b Stability curves for helium gas for $\xi \leq 1$.

the stability curves rise sharply; for any given temperature ratio more than 5.5 there is a minimum(left limit)and a maximum(right limit)value for $|\eta_{0c}|$, showing the ends of the interval in which excited oscillations are found. At the cold part the boundary layer thickness is small enough compared with the tube inner radius at all regions.

The solid curves are from the numerical studies by Rott. For convenience his resulting equation determining the stability curves and the frequency is presented here. The key equation(2.9.12)is written as

$$\frac{G_c \cot\lambda_c^*}{\xi\ \lambda_c^*} = \frac{G_H \tan\lambda_H^*}{\lambda_H^*} \qquad (4.2.1)$$

with the notation

$$\lambda_c^* = \omega\ell/a_c^* \ ,\ \lambda_H^* = \omega(L-\ell)/a_H^* \text{ and } \xi = (L-\ell)/\ell \qquad (4.2.2)$$

where the quantity G indicates the effects of the dissipation and it s value takes unity for non-dissipative case($|\eta_0|\to\infty$). For big values of α and moderate ξ , λ_H $(=\frac{(L-\ell)}{a_H})$ is nearly equal to zero, because $\lambda_H = \xi\alpha\sqrt{-1}\lambda_H$, so that in eq.(4.2.1) $\frac{\tan\lambda_H^*}{\lambda_H^*} \simeq 1$. As $|\eta_{0c}|$ is large(more than about 8 as indicated in experiments), the left-hand side of eq.(4.2.1)is expanded into series in term of a $2/\eta_{0c}$. Considering that the angular frequency is real, we obtain readily the following set of equations, after splitting the eq.(4.2.1)into real and imaginary parts;

$$\cot\lambda_c/\lambda_c = \xi(\mathrm{Re}G_H + \mathrm{Im}G_H) \qquad (4.2.3)$$

$$|\eta_{0c}| = \frac{\sqrt{2}}{\xi \mathrm{Im}G_H}\{c[1+\frac{\cot\lambda_c}{\lambda_c}+\lambda_c\cot^2\lambda_c]+\frac{d\cot\lambda_c}{\lambda_c}\} \quad (4.2.4)$$

The coefficients c and d are Kirchhoff and Kramers constant of gases; 0.90825 and 0.0022 for helium gas respectively. From the above two equations the stability curves are, in principle, determined. The experimental results are in qualitative agreements with the theory of Rott.

The stability limits are able to be given on the plane of α versus $|\eta_{0H}|$, which are mathematically equivalent to that on the plane of α versus $|\eta_{0c}|$. Figure.4.2.c shows the stability curves corresponding to Fig.4.2.a, where the temperature ratio is plotted on the logarithmic scale as a function of the ratio of the ratio of r_0 to the boundary layer thickness at the warm part. As discussed later, the plots in Fig.4.2.c may be physically more valuable than that in Fig.4.2.a to characterize the thermally driven acoustic oscillations. In the following we will give the qualitative discussion about the respective branches.

RIGHT_HAND BRANCHES At the right-hand branches, values of viscous(thermal)boundary layer thickness in both cold and warm parts are sufficiently small compared with the tube inner radius; namely the part of the "core"is dominant compared to that of the boundary layer, as shown in Figs.4.2.a, 4.2.b and 4.2.c The results show that, for constant $|\eta_{0c}|$, a very flat minimum of α is found in the region $1 \geqq \xi \geqq 1/2$. The ξ -dependence of the stability curves, in particular for $\xi \leqq 1$, is fitted

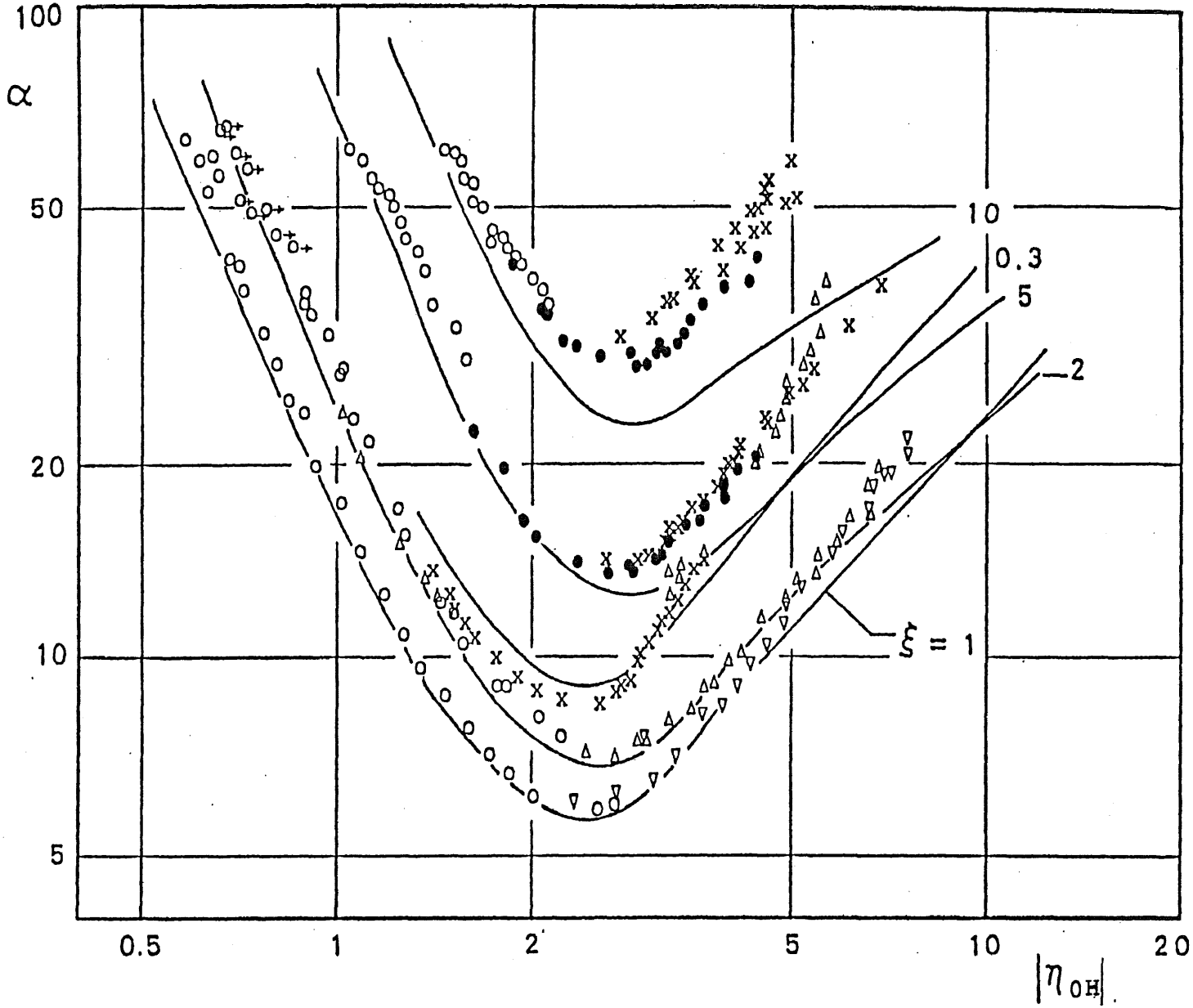

Figure.4.2.c Stability curves, plotted by the temperature ratio α versus the ratio of tube inner radius to the boundary layer thickness in the warm part $|\eta_{0c}|$. Marks are the same as in Figs.4.2.a and 4.2.b.

with the asymptote equation for helium gas;

$$\log \alpha = 0.60[\log|\eta_{0c}| + \log(1+\xi^{-1}+\lambda_c^2\xi)]-0.22$$

where $\xi = \frac{\cot\lambda_c}{\lambda_c}$ as will be discussed in the next section.

The above behavior can be explained by the use of the energyconsideration discussed in section 2.7. The driving term $\Delta\bar{Q}_1$ in eq.(2.7.4) is proportional to the term, imaginary part of F*, which characterizes the effect of the thermal conductivity of the gas. Figure 2.5 indicates that when the boundary layer(consider the thermal layer here)becomes thin compared with the tube inner radius, imaginary part of F* gradually decreases, so that the oscillations should become unfavorable. The gradual slope of the stability curves in this branch is on account of such gradual decrease of the driving term. Consequently, roughly speaking, the right hand branch may be characterized as follows; the thermal boundary layer thickness $\sqrt{\nu/\omega\sigma}$ becomes small, so that the oscillations are not able to be sustained because of the lack of sufficient heating and cooling from the tube wall. The effects of the thermal conductivity plays an important role to maintain the oscillations.

The driving term is also proportional to the derivative of the square of the acoustic pressure amplitudes. As shown in Fig.2.7.a, the derivative takes maximum in the middle location of the half open tube(wide tube). Therefore the maximum driving of the oscillations occurs when the gradient of mean temperatures is established in the middle location

of the tube. This qualitatively agrees with the experimental results stated above.

LEFT HAND BRANCHES On the other hand, at the left hand--branch the boundary layer thickness at the cold part is still small compared with tube inner radius, but the boundary layer thickness is not small in the warm part, as understood from Fig.4.2.c. Thus the damping of the oscillations in the warm part is dominant compared with that in the cold part. The damping at the left-hand limit is not due to the effect of the thermal conductivity, but that of the shear viscosity of gas. When we take into account only the effect of viscosity instead of thermal conductivity, the driving term $\Delta\bar{Q}_1$ is never positive in the case that the closed end is at warm and the open end is at cold, so that the effect of the viscosity does not contribute to the driving but contribute to the damping of the oscillations.

Let's consider the driving term $\Delta\bar{Q}_1$ including both effects of viscosity and thermal conductivity, which is proportional to imaginary parts of $F^*-F/1-\sigma$ shown in Fig.2.7.b. When only the effect of thermal conductivity is taken into account, the oscillations are favorable independent of the thickness of the boundary layer. However comparing Fig.2.5 with Fig.2.7.b, we shall understand that the effect of viscosity restricts the unstable region; namely at about $|\eta_0| \simeq 2.8$, the sign of $\Delta\bar{Q}_1$ drastically varies from positive to negative value, so that below $|\eta_0| \simeq 2.8$ only the damping is possible along the tube

in spite of a steep temperature gradient. The steeper slope of the stability curves at the left-hand branch compared with that at the right-hand branch may be caused by such a drastic change of the sign of the driving term. Thus the viscous boundary layer thickness instead of the thermal one plays an important role to characterize the damping of the oscillations in the left branch; qualitatively because the viscous layer fills up the tube in the warm part and near the location with temperature gradient, the oscillations are unfavourable.

The ξ -dependence of the stability curves at this branch is qualitatively same as that at right hand branch; near $\xi = 1$ the oscillation are easy to be induced. This comes from the gradient of the acoustic pressure amplitudes.

OPTIMUM CONDITION TO EXCITE THE OSCILLATIONS The oscillations are very powerful, for example under suitable conditions in the unstable region, especially in helium gas--filled pipe coexisted with liquid helium under atmospheric pressure, the acoustic pressure amplitudes sometimes run up to a few hundred torr. Some experimental studies on the amplitudes up to now have been described and suggested qualitatively that the amplitudes take a maximum when the inner diameter of a cylindrical cavity is about 3-5mm($L \simeq 1m$). Self--sustained oscillation with such large amplitudes may be applied, in future, to an engine. The optimum condition, where the pressure amplitudes take maximum, will be important as a point of the operation of the engine.

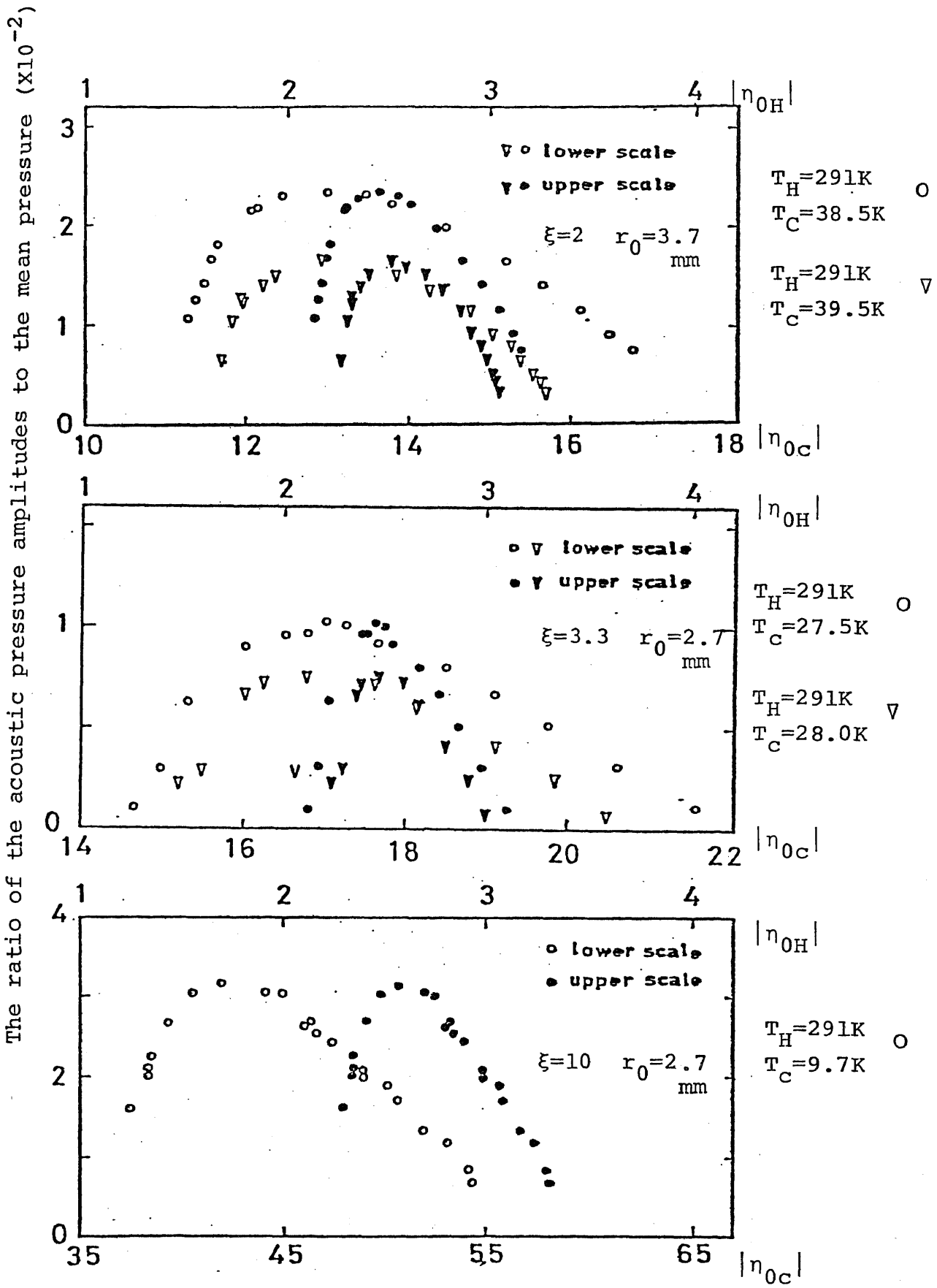

Figure.4.2.d Normalized acoustic pressure amplitudes as a function of $|\eta_{0c}|$ and $|\eta_{0H}|$ for different temperature ratio and different the ratio of the length at warm part to that at cold part.

The acoustic pressure amplitudes(rms)normalized by the mean pressure are plotted as a function of $|\eta_{0c}|$ and $|\eta_{0H}|$ under constant temperature ratio as a parameter. The results are shown in Fig.4.2.d. Since the experiments were performed in the neighborhood of the stability curves, the amplitudes are two or three orders of magnitudes smaller than mean pressure. The left and the right limits in Fig.4.2.d correspond to two branches stated previously. The normalized pressure takes a maximum between two limits. Figure 4.2.d suggests that the optimum condition is determined at the warm part rather than at the cold part. The condition occurs when the value $|\eta_{oH}|$ is near 2.5. This is also understood from Fig.4.2.c where the stability curves take a minimum at $|\eta_{0H}|=2.5$ independent of ξ . Therefore when thermally driven acoustic oscillations are induced in helium gas coexisted with liquid helium under one atomospheric pressure, in order to obtain the maximum amplitudes, the optimum condition is

$$\log r_0 = -1/2 \log \omega + 10g2.68$$

since ν_H is equal to $0.15 cm^2 s^{-1}$ at room temperature. Since angular frequency normally varies from about 250 to 350 rad/sec near liquid helium surface($L \simeq 1m$), we may select the tube with inner radius between 1.4mmand 1.7mm. These tubes are usually employed as the level indicator of liquid helium as indicated by Clement and Gaffney(1955)or Gaffney and Clement(1956). Rott (1976)calculated the power function for helium gas in the case of constant cross section tube and predicted that the oscill-

ations take a maximum when $|\eta_{0H}|$ is equal to about 2.2 for various values of parameter T_H/T_c.

DISCREPANCY BETWEEN EXPERIMENTAL RESULTS AND THEORERICAL

The experimental results were compared with the theory of Rott by solid curves in Figs.4.2.a, b and c, where as temperature distribution, the step functional one is employed(discontinuous model). The numerical studies have been carried out at the right hand branch under continuous model taking into account a finite temperature gradient. The steepness of the mean temperature at $x=\ell$ is characterized by

$$S = \frac{2\ \ell}{T_H - T_c} \left[dT_m/dx\right]_{x=\ell}$$

and $S=\infty$ corresponds to the discontinuous model. The numerical data calculated by Rott using a computer show that if S is enough large, the stability curves are not so different from those in the discontinuous ones. But with the reduction of S, the discrepancy between them becomes large. It is probably attributed to the decrease of S that the experimental data deviate from the theoretical curves to more inside; in our experiments S is more than about 40, 24 and 12 for ξ =1, 5 and 10 respectively.

At the left-hand branches for small ξ (=0.5 and 0.3), we have discovered the acoustic waves with higher harmonic frequency modes(second and third)which have a velocity node at x=0. Such a higher harmonic has never been found in the

previous works. More detailed studies will be discussed in the section 4.4.

The stability curves given here will be important, in future, when we will manufacture a cryostat at low temperature experiments avoiding such oscillating instability. Therefore we present here in this paper the experimental data(Table.4.2.1) relating with the stability curves.

T_c(K)	P_{st}(x10^{3}Pa)	τ (msec)	η_c	η_H	λ_c(rad)	α
4.9	10.5	19.0	19.8	0.647	1.260	60.2
5.2	10.4	18.5	18.9	0.652	1.265	56.7
7.2	10.7	16.5	15.2	0.701	1.206	40.9
7.9	10.9	16.0	14.3	0.721	1.187	37.3
9.3	12.1	15.5	13.3	0.770	1.129	31.7
10.3	12.9	15.0	12.8	0.808	1.109	28.6
11.6	14.1	15.0	12.1	0.845	1.045	25.4
14.7	16.2	14.0	10.9	0.937	0.994	20.0
20.0	20.0	13.0	9.8	1.080	0.918	14.7
27.2	25.7	12.0	8.9	1.274	0.853	10.8
23.3	22.5	12.0	9.5	1.193	0.921	12.6
4.6	8.62	19.5	18.8	0.579	1.276	64.1
5.0	9.14	18.5	18.4	0.612	1.290	59.0
5.5	9.45	18.0	17.4	0.630	1.264	53.6
7.1	10.4	17.0	14.9	0.682	1.178	41.5
12.2	14.3	14.0	12.0	0.879	1.092	24.1
16.6	18.1	13.0	10.8	1.027	1.008	17.7
30.6	28.1	11.5	8.7	1.361	0.839	9.6
33.9	31.9	11.0	8.7	1.482	0.833	8.7
37.8	36.8	10.7	8.6	1.610	0.807	7.8
41.6	42.6	10.7	8.6	1.734	0.770	7.1
44.5	48.1	10.5	8.7	1.865	0.762	6.6
48.1	61.1	10.5	9.2	2.100	0.733	6.1
48.9	106	10.9	11.8	2.708	0.697	6.0
50.2	91.5	10.5	10.8	2.540	0.701	5.8
			(r_0=1.2mm,L=1m, ξ=1)			
15.5	114	16.7	78.8	7.03	0.812	19.0
15.3	119	16.8	80.9	7.13	0.812	19.2
14.1	139	17.5	91.8	7.56	0.812	20.9
13.3	142	17.9	96.6	7.57	0.818	22.1
18.7	76.6	15.3	57.6	6.00	0.807	15.7
23.2	52.8	14.0	41.8	5.21	0.792	12.7
16.0	104	16.3	74.2	6.79	0.819	18.4
20.6	69.4	14.6	51.8	5.85	0.805	14.3
26.2	44.2	13.3	35.5	4.89	0.784	11.2
30.6	32.2	12.4	26.6	4.32	0.778	9.6
39.4	15.0	11.3	16.0	3.09	0.752	7.4
47.3	10.7	10.5	12.1	2.70	0.739	6.2
47.6	10.7	10.5	12.1	2.71	0.737	6.2
49.3	7.79	10.4	10.0	2.32	0.731	5.9
24.3	45.7	13.7	33.8	4.90	0.790	12.1

T_c(K)	P_{st}(x10^{3}Pa)	τ(msec)	η_c	η_H	λ_c(rad)	α
36.3	21.6	11.6	20.3	3.66	0.764	8.1
17.2	95.3	15.7	67.9	6.61	0.820	17.1
28.4	37.9	12.7	31.5	4.63	0.789	10.3
32.8	28.3	11.9	24.9	4.14	0.783	8.9
35.2	24.5	11.6	22.2	3.90	0.776	8.3
42.1	16.8	10.8	16.4	3.35	0.762	7.0
45.6	13.9	10.5	14.2	3.09	0.753	6.4
19.9	73.2	14.9	54.2	5.94	0.803	14.7
			(r_0=3.7mm,L=1m, ξ=1)			
5.9	16.4	20.6	20.1	0.77	1.067	50.0
6.5	17.2	20.6	18.9	0.79	1.016	45.3
8.3	20.1	18.9	17.1	0.89	0.980	35.5
8.6	20.4	18.7	16.8	0.91	0.973	34.3
10.9	23.8	17.6	15.3	1.01	0.918	27.0
13.6	27.4	16.9	13.8	1.11	0.856	21.7
25.1	46.3	15.4	11.3	1.51	0.692	11.7
4.5	13.3	23.1	22.1	0.66	1.089	65.5
5.7	14.1	21.6	18.8	0.70	1.035	51.7
6.0	15.0	21.1	18.6	0.73	1.033	49.1
12.6	25.9	17.3	14.2	1.06	0.869	23.5
17.3	33.4	16.3	12.7	1.24	0.787	17.0
18.8	35.6	16.2	12.3	1.29	0.760	15.6
24.3	43.7	15.5	11.3	1.46	0.698	12.1
27.6	49.8	15.2	10.9	1.57	0.668	10.6
4.4	13.7	22.9	22.8	0.67	1.111	67.0
4.8	14.3	22.3	21.9	0.69	1.092	61.4
5.1	15.1	21.7	21.4	0.72	1.089	57.8
6.8	18.6	19.6	19.3	0.84	1.044	43.4
7.9	19.8	19.0	17.7	0.89	0.999	37.3
9.2	22.5	18.2	16.9	0.96	0.967	32.0
10.5	24.0	17.6	15.9	1.01	0.936	28.1
32.5	61.2	14.7	10.7	1.77	0.637	9.0
32.9	63.9	14.7	10.9	1.81	0.633	8.9
36.7	81.8	14.7	11.2	2.05	0.600	8.0
38.5	96.7	14.7	11.8	2.23	0.585	7.6
			(r_0=1.2mm,L=1.5m, ξ=2)			
14.9	143	22.1	79.2	6.84	0.625	19.8
17.7	108	20.6	61.7	6.14	0.616	16.6
20.0	81.9	19.5	49.8	5.50	0.612	14.7
23.5	62.3	18.3	39.3	4.95	0.602	12.5
30.0	37.2	16.5	26.1	4.03	0.590	9.8

T_c(K)	P_{st}(x10^{3}Pa)	τ(msec)	η_c	η_H	λ_c(rad)	α
33.0	29.9	15.9	22.3	3.71	0.584	8.9
36.9	22.5	15.2	17.9	3.27	0.578	8.0
16.0	131	21.3	72.7	6.66	0.626	18.4
19.3	96.5	19.9	55.1	5.90	0.610	15.2
26.0	50.2	17.5	33.2	4.54	0.598	11.3
35.1	27.1	15.4	20.3	3.56	0.585	8.4
39.5	18.6	14.6	15.7	3.03	0.582	7.4
41.6	14.4	14.2	13.4	2.70	0.583	7.1
40.9	12.0	14.3	12.3	2.46	0.583	7.2
39.8	17.2	14.5	15.0	2.92	0.583	7.4
17.5	128	20.4	68.2	6.72	0.625	16.8
21.5	78.4	18.7	46.9	5.49	0.615	13.7
22.5	67.6	18.3	42.4	5.15	0.615	13.1
28.7	41.1	16.7	28.3	4.20	0.596	10.2
14.2	2.68	16.1	13.2	1.09	0.880	20.7
32.2	32.8	16.0	23.5	3.84	0.588	9.1
23.9	4.23	14.7	11.2	1.43	0.743	12.3
12.2	2.52	16.8	14.2	1.04	0.910	24.1
18.9	3.49	15.2	12.2	1.28	0.808	15.6
21.5	3.90	14.8	11.8	1.37	0.778	13.7
19.9	3.51	15.1	11.8	1.29	0.792	14.7
		(r_0=3.7mm,L=1.5m, ξ=2)				
7.8	108	26.6	139	6.89	0.430	37.5
20.5	10.3	17.6	23.2	2.61	0.401	14.2
11.4	48.6	22.6	72.8	4.99	0.419	25.7
12.7	40.1	21.6	61.5	4.64	0.415	23.0
14.4	30.6	20.9	49.2	4.12	0.403	20.3
14.6	30.1	20.8	48.3	4.10	0.402	20.0
15.2	27.6	20.4	45.2	3.96	0.402	19.2
15.8	25.7	20.1	42.5	3.86	0.400	18.5
16.5	22.9	19.7	39.1	3.67	0.399	17.7
18.0	18.9	19.0	33.7	3.40	0.397	16.2
18.4	18.3	18.9	32.6	3.36	0.394	15.9
18.7	17.3	18.7	31.5	3.28	0.395	15.6
19.3	15.9	18.1	29.8	3.19	0.401	15.1
19.9	14.9	18.0	28.3	3.10	0.398	14.7
20.1	14.4	18.0	27.5	3.05	0.396	14.5
20.7	12.6	17.0	25.8	2.93	0.413	14.1
21.3	10.9	17.0				
12.4	38.3	21.5	61.6	4.55	0.422	23.6
14.0	31.3	20.8	51.0	4.18	0.411	20.9
11.0	54.8	23.1	78.8	5.25	0.417	26.6

T_c(K)	P_{st}(x10^{3}Pa)	τ(msec)	η_c	η_H	λ_c(rad)	α
14.9	28.7	24.0	46.8	4.04	0.406	19.6
9.0	83.1	25.2	110	6.19	0.423	32.5
10.5	60.0	23.5	85.0	5.44	0.420	27.9
11.4	49.4	22.6	73.4	5.04	0.419	25.7
13.9	30.5	20.6	51.0	4.15	0.416	21.0
17.0	20.1	19.2	36.2	3.49	0.404	17.2
16.4	21.6	19.4	38.5	3.59	0.407	17.8
18.3	17.3	18.7	32.0	3.27	0.400	16.0
			(r_0=4.7mm,L=1.8m, ξ=5)			
15.7	84.7	20.4	44.2	3.99	0.395	18.6
17.0	70.5	19.7	38.4	3.71	0.393	17.1
18.3	59.4	19.2	33.3	3.45	0.389	15.9
19.2	51.4	18.7	30.4	3.25	0.390	15.2
21.1	37.8	17.9	24.7	2.85	0.389	13.8
21.4	31.3	17.5	22.4	2.62	0.395	13.6
14.2	110	21.1	53.9	4.47	0.402	20.5
15.3	93.0	20.5	47.3	4.18	0.399	19.0
16.4	81.9	20.0	42.4	3.97	0.395	17.8
17.8	66.8	19.3	36.3	3.65	0.393	16.4
20.2	49.7	18.5	28.8	3.21	0.384	14.4
20.6	45.3	18.2	27.3	3.09	0.387	14.1
21.4	38.3	17.8	24.6	2.88	0.388	13.6
20.4	24.8	17.4	20.8	2.34	0.407	14.3
18.7	18.2	17.1	19.4	2.02	0.432	15.6
17.7	17.0	17.2	19.5	1.95	0.442	16.5
15.3	14.7	17.3	20.6	1.82	0.472	19.0
13.1	12.4	17.7	21.2	1.64	0.499	22.3
			(r_0=2.7mm,L=1.8m, ξ=5)			
4.7	31.0	21.7	33.2	1.04	0.680	61.7
5.2	35.1	21.2	32.5	1.12	0.662	55.7
5.4	37.3	20.9	32.6	1.16	0.658	53.7
5.4	38.8	20.6	33.5	1.19	0.668	53.7
5.7	41.1	21.0	32.6	1.23	0.638	50.8
6.1	42.4	20.8	31.2	1.24	0.623	47.5
6.5	45.1	20.8	30.4	1.28	0.603	44.6
6.9	47.3	20.1	30.0	1.33	0.606	42.0
7.3	51.0	20.6	29.3	1.37	0.575	39.7
9.1	60.6	19.5	27.0	1.53	0.544	31.8
10.0	65.7	19.5	25.9	1.60	0.519	29.0
4.9	34.7	22.1	33.4	1.09	0.654	59.1
8.3	49.9	19.3	26.7	1.40	0.575	34.9
			(r_0=1.2mm,L=1.8m, ξ=5)			

T_c(K)	P_{st}(x10^{3}Pa)	τ(msec)	η_c	η_H	λ(rad)	α
5.6	48.1	21.4	139	5.11	0.316	52.1
7.7	20.1	18.3	73.0	3.57	0.315	37.9
8.3	16.0	17.6	62.1	3.25	0.315	35.1
5.0	48.2	22.4	150	5.00	0.319	58.4
5.6	36.9	20.0	125	4.63	0.338	52.1
5.8	34.9	20.6	117	4.44	0.322	50.3
5.9	32.8	20.4	112	4.32	0.333	49.5
6.3	28.0	19.7	99.2	4.06	0.323	46.3
8.1	16.4	17.8	64.0	3.28	0.315	36.0
5.3	39.5	21.5	132	4.62	0.323	55.1
5.5	36.7	20.9	125	4.52	0.326	53.1
6.7	24.5	18.9	89.6	3.88	0.327	43.5
7.5	19.1	18.1	73.2	3.50	0.322	38.9
8.7	13.6	16.9	55.9	3.05	0.321	33.5
9.2	10.2	16.1	47.4	2.71	0.327	31.7
5.8	42.2	20.5	128	4.89	0.324	50.3
6.3	34.9	19.6	111	4.55	0.325	46.3
6.4	31.8	19.3	105	4.38	0.327	45.6
6.8	29.1	19.1	95.9	4.20	0.321	42.9
7.2	24.6	18.4	85.5	3.94	0.324	40.5
			(r_0=4.7mm,L=1.65m, ξ=10)			
7.1	104	20.0	98.1	4.47	0.300	41.1
7.8	78.9	18.9	80.7	4.00	0.303	37.4
8.3	65.1	18.4	70.4	3.69	0.301	35.1
8.8	58.0	17.9	64.2	3.54	0.301	33.1
9.5	44.8	17.6	53.1	3.13	0.295	30.7
9.8	36.0	17.0	47.1	2.85	0.300	29.8
7.7	94.3	19.3	88.4	4.33	0.298	37.9
9.3	54.8	17.6	59.7	3.46	0.298	31.4
9.6	51.1	17.4	56.4	3.36	0.296	30.4
9.8	46.7	17.2	53.3	3.23	0.297	29.8
9.9	43.0	17.0	51.1	3.12	0.299	29.5
10.2	40.2	16.9	48.3	3.02	0.296	28.6
10.3	37.7	16.8	46.5	2.93	0.296	28.3
8.5	19.1	16.2	39.9	2.13	0.338	34.3
9.6	23.2	16.3	39.3	2.34	0.316	30.4
9.9	27.6	16.4	41.6	2.54	0.310	29.5
9.2	20.8	16.3	38.6	2.21	0.323	31.7
8.2	18.4	16.1	40.5	2.09	0.347	35.6
7.1	14.7	16.3	40.8	1.86	0.368	41.1
			(r_0=2.7mm,L=1.65m, ξ=10)			

T_C(K)	P_{st}(x10^{3}Pa)	τ(msec)	η_C	η_H	λ_C(rad)	α
4.7	55.1	19.1	47.2	1.47	0.386	61.7
4.8	56.8	19 1	46.9	1.50	0.382	60.4
4.9	58.8	18.9	47.0	1.53	0.382	59.1
5.2	59.8	18.9	45.0	1.55	0.371	55.7
5.3	63.9	18.7	45.9	1.61	0.371	54.7
5.6	65.0	18.6	44.2	1.62	0.363	51.7
5.7	67.5	18.5	44.5	1.66	0.362	50.8
6.6	70.9	18.4	39.9	1.71	0.338	43.9
6.2	73.8	18.2	43.3	1.75	0.353	46.7
6.4	77.3	18.2	43.1	1.79	0.347	45.3
6.6	79.3	18.1	42.6	1.82	0.344	43.9
6.8	84.9	18.1	42.9	1.88	0.339	42.6
7.1	86.2	17.9	41.9	1.91	0.335	40.8
7.5	95.1	18.0	41.7	2.00	0.324	38.6
7.8	96.1	17.8	40.8	2.02	0.321	37.1
7.8	102	17.8	42.1	2.08	0.321	37.1
8.2	107	17.8	41.2	2.13	0.314	35.3
			(r_0=1.2mm,L=1.65m, ξ=10)			
40.2	19.9	14.2	16.2	3.17	0.996	7.2
37.3	23.6	14.6	18.5	3.41	1.006	7.7
34.9	27.9	15.0	20.9	3.66	1.012	8.3
33.0	31.3	15.4	22.9	3.82	1.014	8.7
31.1	29.5	15.8	23.1	3.67	1.018	9.3
29.8	23.9	16.1	24.9	3.82	1.020	9.7
27.2	39.0	16.9	28.7	4.07	1.017	10.6
24.6	42.4	17.4	32.0	4.18	1.039	11.7
22.6	49.0	18.2	36.1	4.40	1.036	12.8
21.0	56.8	19.1	40.3	4.63	1.024	13.8
19.9	61.6	19.5	43.4	4.77	1.031	14.6
18.1	72.3	20.5	49.6	5.04	1.028	16.0
16.0	89.5	21.2	60.1	5.51	1.057	18.1
15.2	96.5	21.7	64.5	5.65	1.060	19.0
19.1	53.2	19.5	41.8	4.43	1.052	15.1
			(r_0=3.7mm,L=1.26m, ξ=0.5)			
37.8	12.0	8.84	9.99	1.86	0.982	7.8
36.8	10.4	8.91	9.49	1.73	0.988	8.0
34.1	8.91	9.04	9.26	1.58	1.011	8.6
33.3	9.63	8.96	9.85	1.65	1.032	8.8
29.9	7.44	9.37	9.26	1.42	1.042	9.8

T_c(K)	P_{st}(x10^{3}Pa)	τ(msec)	η_c	η_H	λ_c(rad)	α
26.9	6.82	9.50	9.61	1.35	1.083	10.9
22.8	5.89	10.0	9.95	1.22	1.115	12.9
19.8	5.06	10.3	10.24	1.12	1.165	14.9
39.0	11.4	8.48	9.71	1.86	1.008	7.5
39.8	12.2	8.44	9.87	1.92	1.003	7.4
40.7	12.3	8.41	9.76	1.93	0.995	7.2
41.8	12.9	8.40	9.79	1.98	0.983	7.0
40.7	28.5	8.76	14.5	2.88	0.955	7.2
39.8	30.4	8.86	15.2	2.96	0.955	7.4
39.1	32.0	8.97	15.7	3.02	0.952	7.5
37.5	36.0	9.13	17.1	3.17	0.955	7.8
35.4	40.4	9.40	18.7	3.31	0.954	8.3
29.9	52.8	10.1	23.6	3.64	0.959	9.8
25.8	62.5	10.9	28.0	3.82	0.963	11.4
22.2	76.1	11.6	33.9	4.09	0.974	13.2
17.6	103	13.3	44.9	4.46	0.957	16.7
		(r_0=2.2mm,L=0.75m, ξ=0.5)				
46.3	46.1	8.44	9.2	2.03	0.929	6.3
45.2	42.6	8.48	9.0	1.95	0.936	6.5
43.8	40.0	8.44	9.0	1.89	0.956	6.7
41.8	36.0	8.52	8.8	1.79	0.969	7.0
39.1	32.6	8.61	8.8	1.69	0.991	7.5
36.8	30.3	8.73	8.9	1.62	1.008	8.0
32.5	26.0	9.08	8.9	1.47	1.031	9.0
29.4	24.1	9.29	9.2	1.40	1.060	10.0
26.8	22.4	9.48	9.5	1.33	1.088	11.0
22.4	19.8	9.99	10.1	1.22	1.129	13.1
19.4	17.9	10.4	10.6	1.14	1.160	15.2
17.2	16.7	10.8	11.1	1.07	1.184	17.1
34.8	31.1	8.83	9.4	1.63	1.025	8.4
21.2	18.9	10.1	10.3	1.19	1.146	13.9
14.1	14.1	11.5	11.6	0.96	1.229	20.9
9.5	10.8	13.6	13.2	0.77	1.274	31.0
12.0	12.8	12.2	12.3	0.88	1.250	24.5
		(r_0=1.2mm,L=0.75m, ξ=0.5)				

T_c(K)	P_{st}(X10^{3}Pa)	τ(msec)	η_c	η_H	λ_c(rad)	α	
20.3	31.0	16.6	33.1	3.66	1.203	14.6	
16.6	39.7	18.3	42.2	3.95	1.210	17.9	
15.0	52.7	19.3	51.7	4.43	1.208	19.9	
13.3	62.4	20.1	61.1	4.73	1.233	22.5	
10.9	71.9	21.6	75.2	4.89	1.269	27.5	
9.9	92.4	23.0	89.1	5.37	1.245	30.1	
9.3	96.1	23.6	95.0	5.41	1.253	32.0	
8.25	102.1	25.1	105.5	5.41	1.255	36.4	
23.6	23.0	15.7	25.8	3.25	1.181	12.6	
22.6	24.6	16.0	27.5	3.33	1.184	13.1	
21.9	23.9	16.1	27.8	3.27	1.198	13.6	
21.2	25.4	16.5	29.0	3.33	1.186	14.0	
16.2	38.3	18.8	42.1	3.83	1.196	18.5	
14.1	55.2	20.0	54.8	4.45	1.202	21.2	
12.4	68.0	21.0	66.3	4.82	1.222	24.1	
11.8	70.1	21.0	70.2	4.90	1.254	25.4	
10.5	84.1	22.1	82.3	5.23	1.258	28.3	
7.7	117.0	26.1	117.5	5.68	1.246	38.8	
		(r_0=0.37mm, L=1.07m, ξ=0.3)					
34.3	24.7	13.0	12.7	2.20	1.120	8.6	
33.2	21.0	13.0	12.0	2.02	1.131	8.8	
31.5	18.7	13.3	11.8	1.89	1.141	9.3	
29.6	16.4	13.6	11.4	1.75	1.150	9.9	
27.6	14.8	13.9	11.4	1.65	1.163	10.6	
24.7	13.3	14.5	11.6	1.52	1.177	11.9	
23.6	12.8	14.8	11.7	1.48	1.184	12.5	
21.4	11.7	15.2	11.9	1.39	1.206	13.7	
4.85	2.68	9.2	26.6	0.86	4.210	60.8	**
5.05	2.83	9.2	26.5	0.88	4.125	58.4	**
34.9	33.7	13.2	14.6	2.55	1.093	8.4	
33.7	37.6	13.3	15.7	2.68	1.098	8.7	
32.5	39.8	13.6	16.5	2.73	1.094	9.0	
31.5	43.2	13.9	17.5	2.82	1.093	9.3	
30.0	46.3	14.3	18.6	2.88	1.089	9.8	
29.2	48.5	14.4	19.3	2.92	1.090	10.1	
27.8	53.5	14.8	20.9	3.03	1.091	10.6	
26.8	57.5	15.1	22.1	3.11	1.089	11.0	
26.0	60.0	15.2	23.0	3.16	1.094	11.3	
25.3	64.1	15.5	24.1	3.24	1.089	11.6	
23.9	69.4	16.0	25.9	3.32	1.089	12.4	
22.6	75.3	16.4	28.0	3.42	1.094	13.0	
21.6	83.3	16.6	30.3	3.57	1.102	13.6	
20.6	88.4	16.9	32.2	3.64	1.106	14.3	
25.6	13.8	14.4	11.5	1.57	1.169	11.5	

T_C(K)	P_{st}(X10^{3}Pa)	τ (msec)	η_C	η_H	λ_C(rad)	α	
5.0	2.81	9.2	26.4	0.88	4.128	59.0	**
5.2	2.91	9.2	26.0	0.90	4.065	56.7	**
15.8	6.86	8.4	15.8	1.44	2.539	18.6	*
		(r_0=0.22mm, L=1.07m, ξ=0.3)					
35.6	59.8	12.7	10.6	1.88	1.078	8.2	
34.7	58.1	12.8	10.6	1.85	1.085	8.4	
34.3	56.1	12.9	10.5	1.81	1.083	8.5	
33.1	52.3	13.0	10.5	1.76	1.099	8.8	
31.7	50.3	13.2	10.5	1.69	1.100	9.2	
30.5	48.2	13.4	10.5	1.65	1.106	9.6	
29.2	45.5	13.6	10.5	1.59	1.116	10.0	
27.4	43.1	13.9	10.7	1.52	1.128	10.7	
26.4	41.3	14.1	10.7	1.49	1.132	11.1	
25.3	39.4	14.2	10.8	1.44	1.146	11.5	
23.9	37.3	14.6	10.9	1.39	1.152	12.2	
22.4	35.4	14.9	11.0	1.34	1.164	13.0	
21.2	34.0	15.2	11.2	1.30	1.174	13.8	
20.3	33.1	15.4	11.4	1.27	1.178	14.4	
19.3	31.1	15.7	11.4	1.22	1.189	15.1	
18.5	29.2	8.32	15.7	1.63	2.297	15.8	*
17.8	28.0	8.46	15.8	1.58	2.303	16.4	*
17.2	24.8	8.45	15.3	1.49	2.345	17.0	*
16.2	24.1	8.67	15.7	1.45	2.355	18.0	*
15.0	21.9	8.93	15.7	1.36	2.376	19.5	*
13.7	19.7	9.21	15.8	1.27	2.411	21.3	*
12.2	18.2	9.59	16.4	1.20	2.453	24.0	*
10.6	15.9	10.12	16.9	1.09	2.495	27.6	*
7.8	13.0	11.25	18.9	0.93	2.616	37.5	*
5.1	10.1	13.55	22.2	0.75	2.686	57.4	*
5.4	10.0	13.2	21.3	0.75	2.679	54.2	*
5.65	10.4	12.8	21.1	0.78	2.701	51.8	*
6.2	10.9	12.3	20.2	0.81	2.668	47.2	*
7.0	11.4	11.9	18.9	0.85	2.597	41.8	*
7.5	12.2	11.4	18.8	0.90	2.628	39.0	*
17.8	26.3	8.34	15.4	1.54	2.336	16.4	*
19.3	27.0	7.99	14.9	1.60	2.341	15.1	*
35.0	63.8	12.84	11.0	1.94	1.082	8.4	
34.3	61.9	12.88	11.0	1.90	1.089	8.6	
32.8	57.5	13.03	11.0	1.83	1.101	9.0	

T_c(K)	P_{st}(X10^3Pa)	τ (msec)	η_c	η_H	λ_c(rad)	α
32.0	55.5	13.1	11.1	1.78	1.104	9.2
29.8	50.8	13.4	11.0	1.69	1.120	9.9
27.9	46.0	13.7	10.9	1.59	1.133	10.6
26.7	44.3	13.9	11.0	1.55	1.140	11.0
24.7	41.3	14.4	11.2	1.47	1.149	11.9
22.4	37.2	14.7	11.4	1.38	1.179	13.2
8.4	12.7	10.7	17.9	0.94	2.645	35.2 *
9.0	13.0	10.5	17.2	0.96	2.599	32.8 *

(r_0=1.2mm, L=1.0m, ξ=0.3)

no mark	the fundamental
*	the second harmonic
**	the third harmonic
T_c	temperature at the cold part
P_{st}	mean pressure
τ	period of the oscillations
η_c	$\lvert\eta_{0c}\rvert$
η_H	$\lvert\eta_{0H}\rvert$
λ_c	$\omega\ell/a_c$
α	temperature ratio T_H/T_c

4.3 FREQUENCY OF THE ACOUSTIC OSCILLATIONS

The frequency of the oscillation corresponding to every point on the stability curves is discussed in this section. The dimensionless numbers λ_c and $|\eta_{0c}|\bar{\lambda}_c^{1/2}$ are employed as variables characterizing the acoustic oscillations instead of the angular frequency ω :

$$\lambda_c = \omega \ell / a_c \quad \text{and} \quad \bar{\lambda}_c^{1/2} |\eta_{0c}| = \sqrt{a_c / \ell \nu_c}\, r_0 \qquad (4.3.1)$$

The value λ_c means the phase* of the amplitudes of the acoustic pressure at the location $x = \ell$ (λ_c at $x=0$ is equal to zero, where the pressure node exists). The relationship between the stability curves and the frequency diagram is schematically illustrated in Fig.4.3.a. One point in unstable region corresponds to the one state(frequency)in the frequency diagram.

The experimental results are shown in Fig.4.3.b, where the frequency parameter λ_c is plotted as a function of the variable $|\eta_{0c}|\bar{\lambda}_c^{1/2}$, because the frequency is initially not known.

---

* The important feature of the stational wave is that the x and t variables are separated as

$$p = f(x)\ \exp(i\,\omega t) \qquad (1)$$

This is the characteristic of standing wave. The quantity f(x) is the amplitudes of the standing wave at the location x and written as

$$f(x) = A_1 \sin \hat{k}_c x / a_c \Big/ \sin \hat{k}_c \ell / a_c$$

for wide tubes. The expression $(i\omega t \pm i\hat{k}x)$ no longer appear and eq.(1) does not represent a traveling wave.

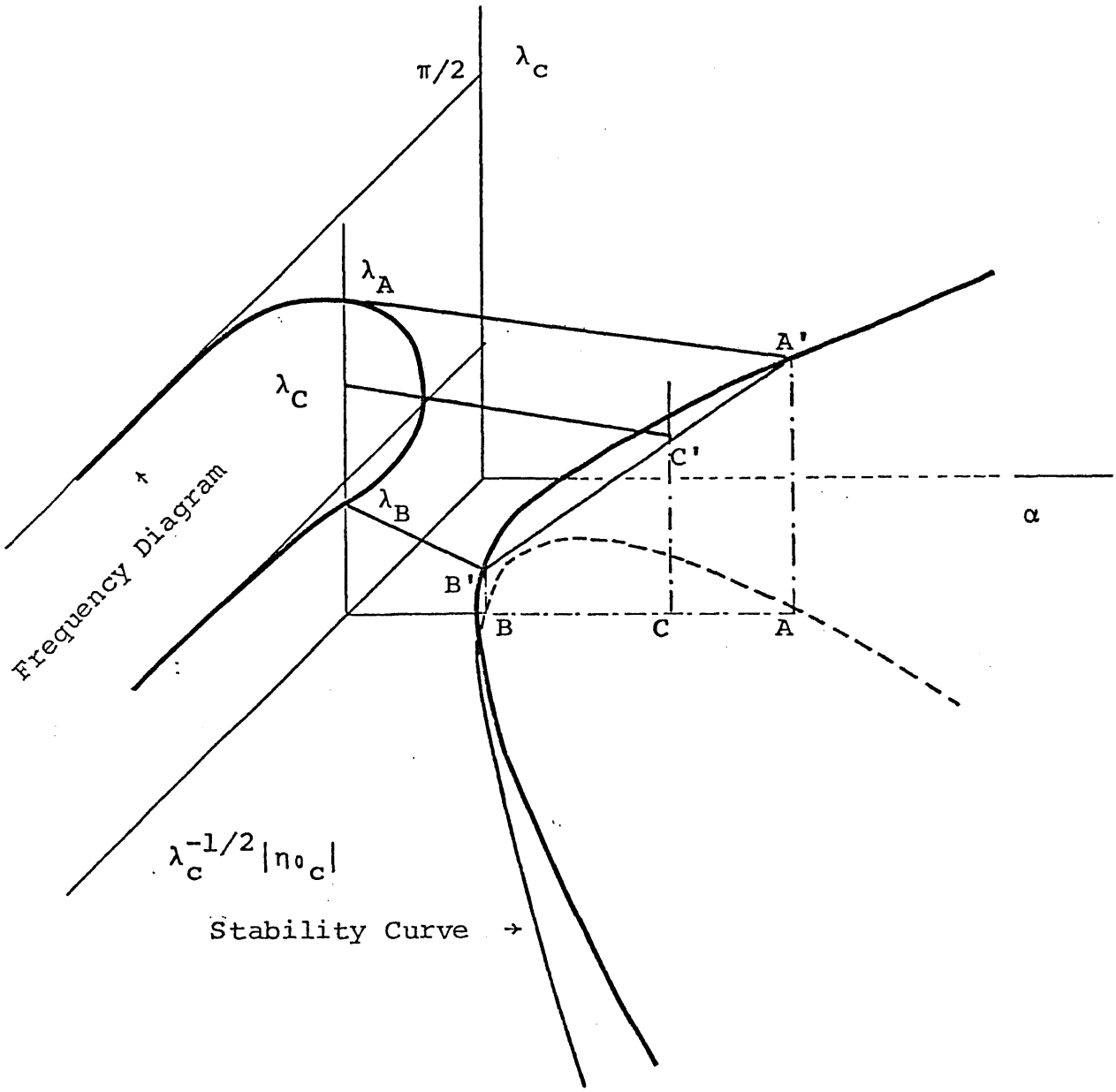

Figure.4.3.a The relationship between the stability curve and the frequency diagram for the fundamental

Thus the frequency of the oscillations near the stability curves is able to be determined using Fig.4.3.b, since $|\eta_{oc}|\lambda_c^{-1/2}$ is independent of the angular frequency. The solid curves show the numerical results derived by Rott from important equation(4.2.1), which determines not only the stability limits but also the frequency of the oscillations. The agreements between the experimental and the theoretical results are satisfactory. The behavior of the frequency is able to be classified by three separated regions;the lower branches, the upper branches($\lambda_c = \pi/2$)and the region between such two branches. We are going to give a qualitative explanation of these results in the following discussion.

At first let's consider the lower asymptotes of the frequency diagrams for each ξ . These limits correspond to the right-hand branches(or asymptotes)in Figs.4.2.a and 4.2.b. The boundary layer thickness is sufficiently small compared with tubes inner radii at both cold and warm parts so that both viscosity and thermal conductivity should not influence on the frequency of the oscillation everywhere. The key equation for non-dissipative($|\eta_0| \to \infty$)case which gives the frequency is

$$\frac{\cot \lambda_c}{\lambda_c} = \xi \frac{\tan \lambda_H}{\lambda_H} \qquad (4.3.2)$$

Since both G_c and G_H take unity as shown in Fig.4.3.c where the quantity G is plotted as a function of$2/|\eta_0|$(refer [16]). Equation (4.3.2) shows that the velocity at $x=\ell$ is essentially continuous. For large temperature ratio λ_H is nearly equal

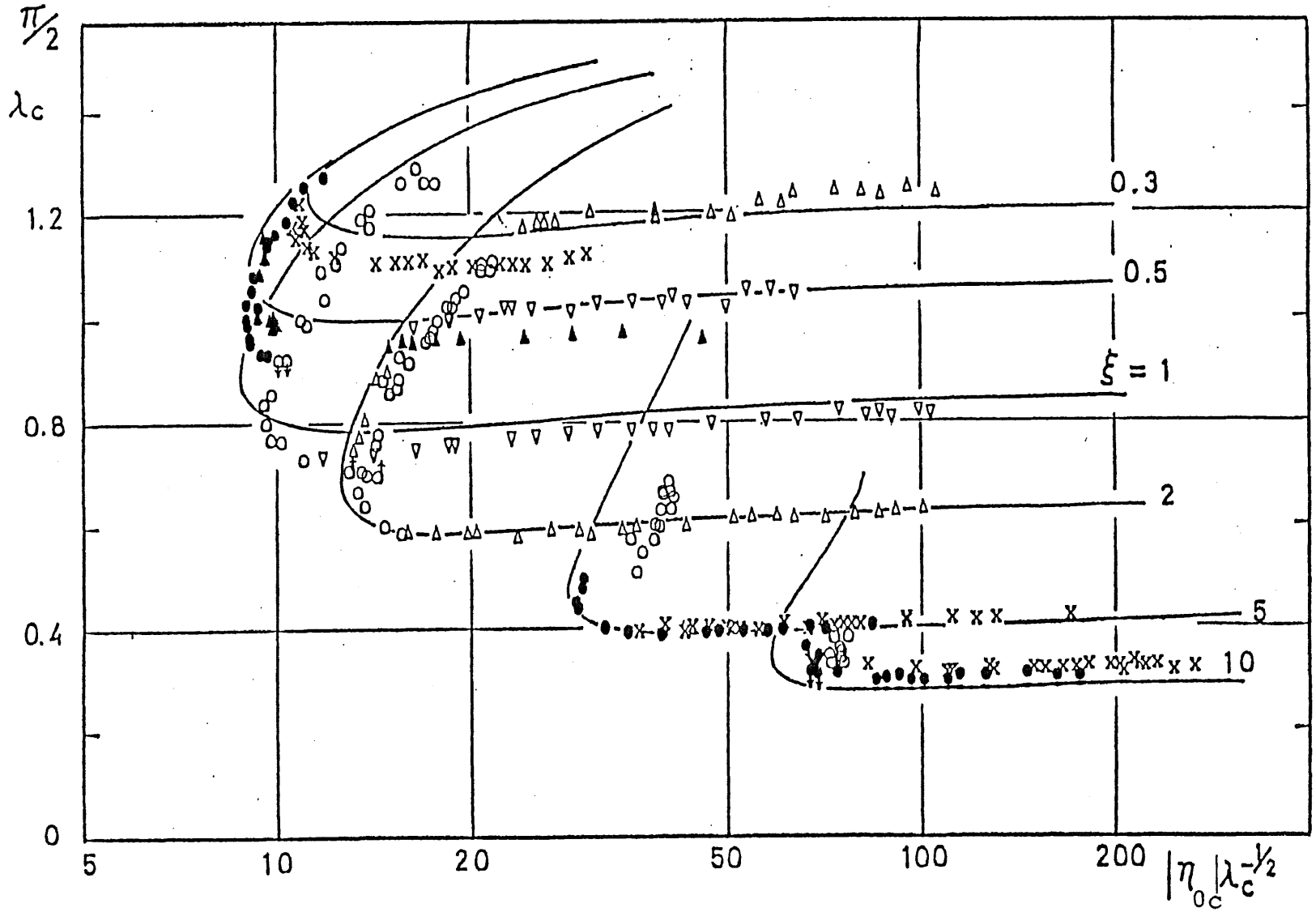

Figure.4.3.b The frequency diagram for helium gas, the dimensionless number $\lambda_c=\omega\ell/a_c$ versus $\bar{\lambda}_c^{1/2}|\eta_{0c}|=(a_c/\nu_c\ell)^{1/2}r_0$. Marks are the same as in Figs.4.2.a and 4.2.b.

to zero, so that eq.(4.3.2) is equal to eq.(4.2.3) where the real parts of G_c and G_H are reduced to unity but the imaginary parts of them are equal to zero; namely

$$\cot \lambda_c / \lambda_c \simeq \xi \qquad (4.3.3)$$

This equation shows a good correspondence with our experimental results at the lower branches of Fig.4.3.b. The solutions of eq.(4.3.3), for the fundamental mode, take 1.07, 0.86, 0.65 and 0.43 for $\xi = 0.5$, 1, 2 and 5 respectively. These values are excellently agreed with the experimental data. Thus at lower branches the equation for non-dissipative case is suitable. The sound velocity at the warm and cold parts is equal to the adiabatic velocity, a_c and a_H respectively because in the dispersion relation(2.9.2), the effective sound velocity $a[\frac{1 - F}{1+(1-\gamma)F^*}]$ becomes adiabatic one for large $|\eta_0|$ ($F=F^*=0$ for $|\eta_0| \to \infty$).

Secondly we consider the other hand branch(upper) of the frequency diagram. At upper limits, which correspond to the left-hand branches of the stability curves, the boundary layer fills the whole tube at the warm part but at the cold part, the boundary layer thickness is still small compared with tube inner radius. Quantitatively since both imaginary part and real part of G_H approach to nearly zero for large $|\eta_0|^{-1}$ as shown in Fig.4.3.c, eq.(4.3.2)becomes

$$\cot \lambda_c / \lambda_c = 0 \qquad (4.3.4)$$

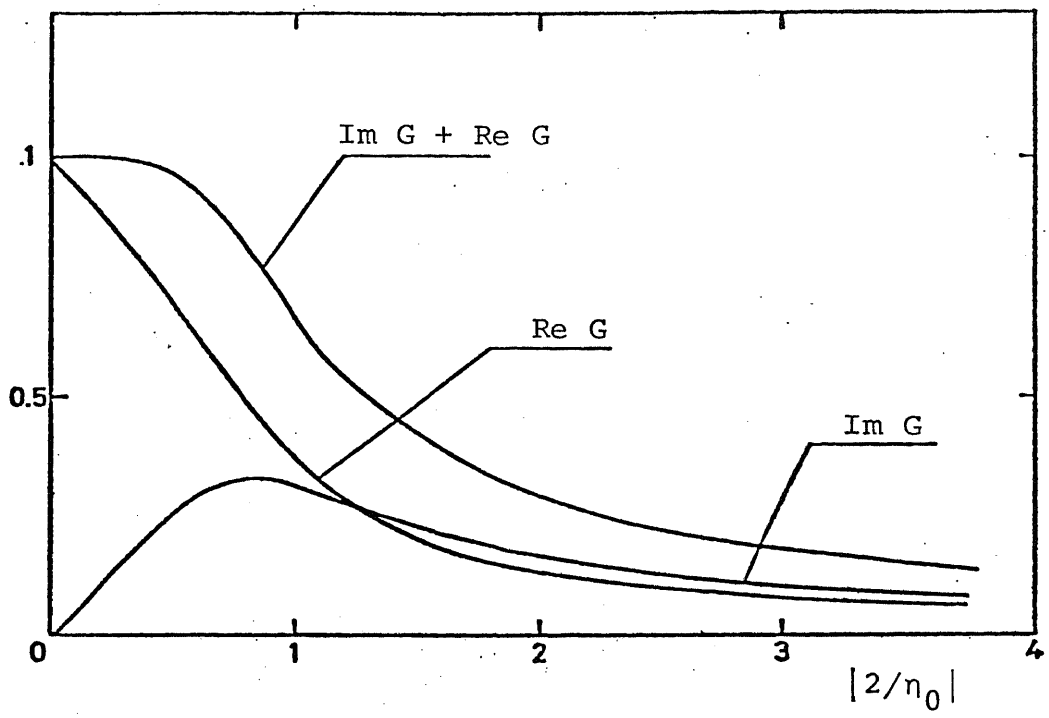

(C)

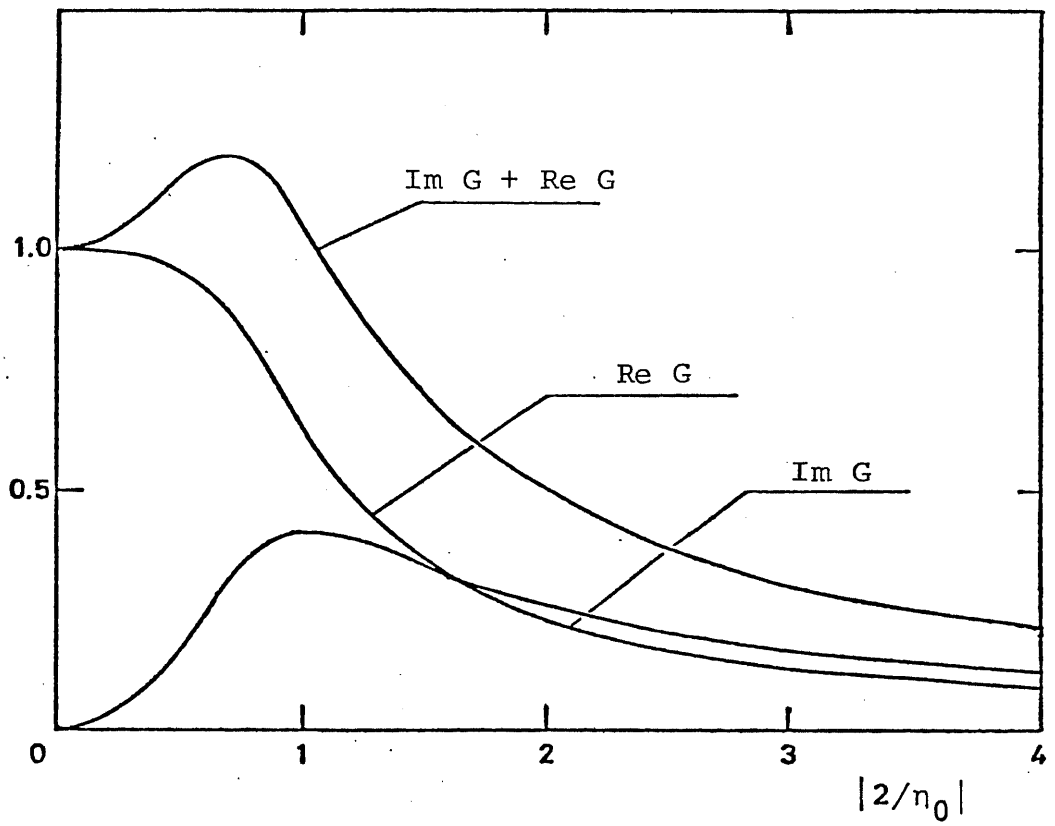

(C')

Figure.4.3.c The G-function for helium gas neglecting the the term $[1+(\gamma-1)F^*]$.

Figure.4.3.c' The G-function calculated by Rott including the term $[1+(\gamma-1)F^*]$.

where G_c takes still unity. The solution of eq.(4.3.4)is nearly equal to $\pi/2$ independent of ξ . This means that the location at a sudden temperature change behaves like a closed end(of course exact boundary condition at closed end corresponds to $\lambda_c = \pi/2$)because the fluid in the warm part can not move on account of large viscous and thermal boundary layer thickness. There may be no variation(x-dependence)of the acoustic pressure amplitudes in the warm part and the pressure in the cold part occupies most of the variation of the amplitudes. Practically such a limit is difficult to be confirmed by experiments because of the large temperature ratio. Our experimental data, however, show a tendency to approach to $\pi/2$.

Lastly in the region corresponding to near minimum of the stability curves, where the dissipative effects in the warm part are moderate. It is interesting that the frequency parameter λ_c does not directly tend from the non-dissipative solution to $\pi/2$, but takes values less than the solutions derived from eq.(4.3.3). In order to express the minimum, Figure.4.3.d rather than Fig.4.3.b is convenient where the quantity $\frac{\cot\lambda_c}{\lambda_c}$ is plotted as a function of $|\eta_{0c}|$. The minimum in Fig.4.3.b corresponds to the maximum in Fig.4.3.d. The position of the maximum is situated at $|\eta_{0c}|\simeq 2.5$ independent of ξ . It is understood from eq.(4.2.3)that such a maximum comes from that of the addition of imaginary part of G_H and the real part of G_H. Let's imagine the qualitative meaning of such a maximum. The maximum comes from the term of F* in the quantity$[1+(\gamma-1)F^*]$. The addition of ImG

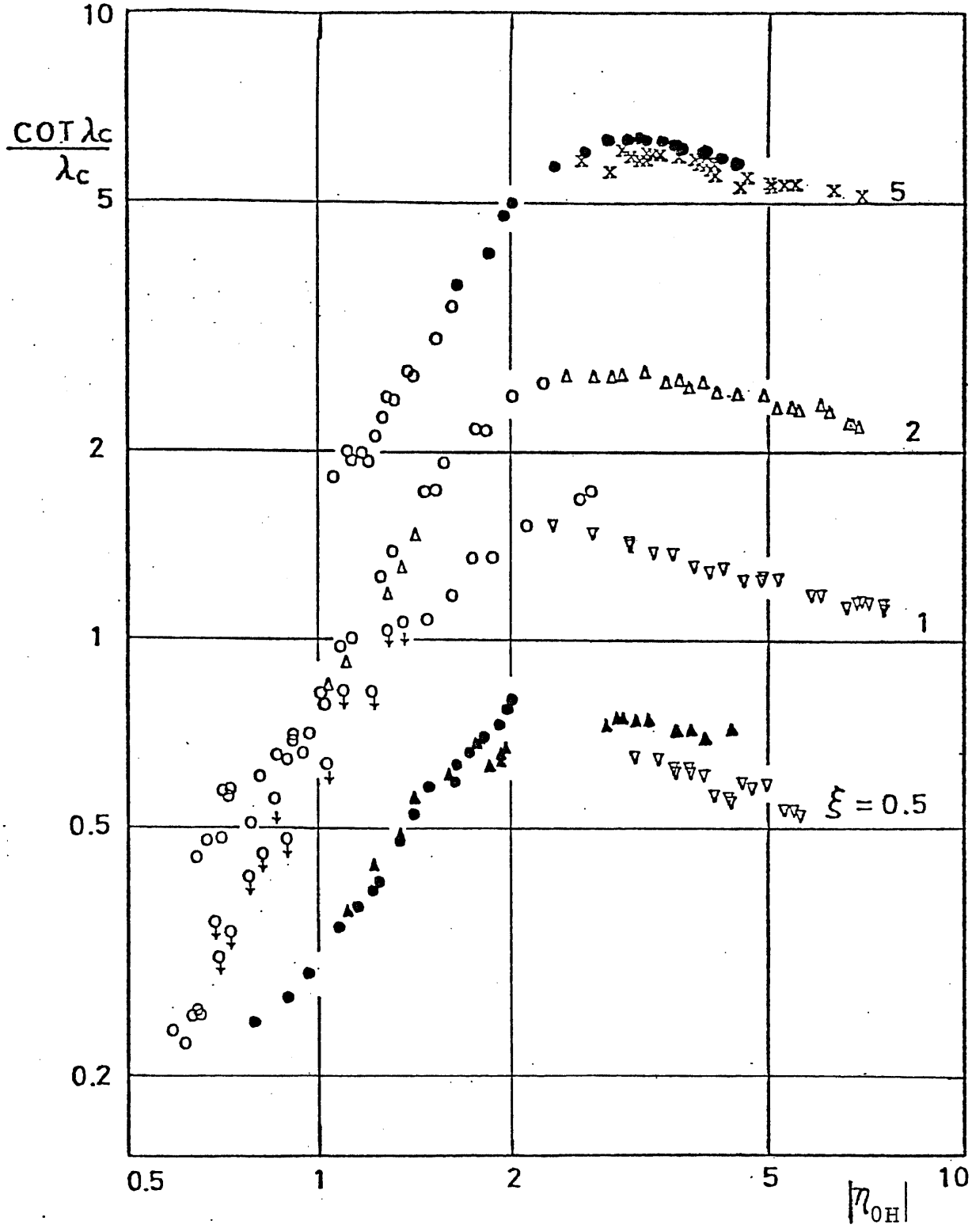

Figure.4.3.d The diagram corresponding to the frequency diagram in Fig.4.3.b. The maximum occurs at $|\eta_{0H}|=2.5$ independent of ξ.

and ImG excluding the term F* is shown in Fig.4.3.c' where any peak does not exist. Therefore the maximum in Fig.4.3.d is due to the effect of thermal conductivity. Another reason is as following. As discussed in section 2.9 previously, the effective sound velocity is written as

$$a_{eff} = a^* = a\left[\frac{1 - F}{1+(\gamma-1)F^*}\right]^{1/2}$$

where F* shown the effect of thermal conductivity. We again consider the effective sound velocity(practically the real part of a_{eff}). Neglecting the viscous effect(F=0), when the thermal boundary layer gradually becomes thick, the sound velocity approaches from adiabatic to the isothermal ones. At the warm part, such an effect of the sound velocity should be remarkable, since $|\eta_{0H}|$ varies from large value to the small. The value of λ_H^* varies from $\omega \ell'/a_H$ to $\frac{\gamma\omega\ell'}{a_H}^*$, when $|\eta_{0H}|$ changes from infinity to zero. Therefore the right hand side of eq. (4.3.2)' takes the value more than ξ because $\frac{\tan\lambda_H^*}{\lambda_H^*}$ becomes larger than unity as shown in fig.4.3. Thus the minimum in Fig.4.3.b comes from the thermal effect in the warm part. After taking the minimum, the frequency diagram approaches to constant value $\pi/2$ on account of stronger dissipative effects at the warm part. The sound velocity at the cold part is still adiabatic one.

fig.4.3.

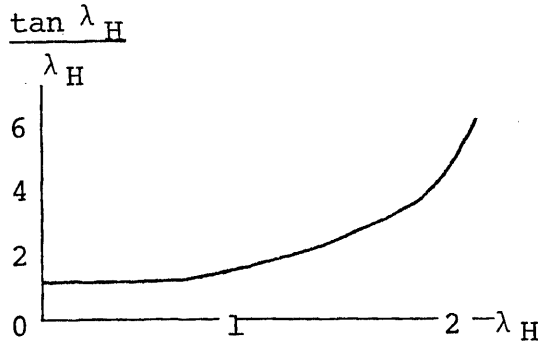

* ℓ' ; (L-ℓ)

4.4 STABILITY LIMITS FOR TUBES WITH VARIABLE CROSS SECTION

Spontaneous oscillations of a gas column with temperature stratification were first investigated experimentally by Sondhauss(1850). His paper is quated in the text book by Rayleigh and the device employed by him is called a "sondhauss Tube". The earlier experiments were as follows: when a glass-bulb attached to a pice of narrow tube as a flask is heated by a burner, as glass-blowers sometimes experience, audible sounds(a air gas oscillation)are spontaneously produced. Estimating from the melting temperature of glass, the temperature ratio between the warm part and cold part is considered as about 3 or less. As studies in previous section, the minimum critical temperature ratio for helium gas is about 5.5 for exciting the oscillations. Although the gas is not helium but air, in such a device corresponding to the tube with variable cross-section, the critical temperature ratio is reduced. The part with constant temperature distribution contributes only to the damping of the oscillations, so that the enlarging of inner radius, in particular, of the warm part where the kinematic viscosity is high may contribute to widen the unstable region. In order to confirm this, the stability curves were experimentally determined for the tube with configuration as shown in Fig.4.4.a; tubes have inner radii r_H=1.7mm and r_c=0.8mm or r_H=4.7mm and r_c=2.2mm for ξ=1 with whole length 1m. The steep change of mean temperature was established near x=L/2 within $\delta x/L \simeq 3\%$. The warm part

is immersed into the reservoir at room temperature and the temperature at the cold part varies from about 70K to 5.5K. The results for helium gas are shown in Fig.4.4.b where the left-hand branch of the stability curve shifts towards the left and the right branch towards the right, and the critical temperature is reduced compared with that of constant cross-section tube. Thus the experiments of Sondhauss were quantitatively confirmed by our experiments.

Mathematical approaches have been investigated by Rott and Zouzoulas(1976). Taking into account the x-dependence of the tube inner radius, we obtain the differential equation (wave equation) for the acoustic pressure corresponding to eq.(2.9.1);

$$r_w^2[1+(\gamma-1)F^*]p_1+\frac{d}{dx}[r_w^2\frac{a^2}{\omega^2}(1-F)\frac{dp_1}{dx}]-r_w^2\frac{a^2}{\omega^2}\frac{F^*-F}{1-\sigma}\theta\frac{dp_1}{dx}=0$$

$r_w(x)$; tube inner radius

where the notation is the same as before. Using the same procedure as section 2.9, the key equation is obtained. The solid curve in Fig.4.4.b is the stability curve calculated by Rott and Zouzoulas for $\xi=1$ and $r_H/r_c=2$. The agreement between theory and experiment is satisfactory.

The optimum configuration of a tube for driving the oscillations is schematically shown in Fig.4.4.c; namely as only the damping is possible at both warm and cold parts, the optimum configuration is that both inner radii r_c and r_H are large as possible(in particular r_H), but the tube inner radius with temperature gradient must be suitably so narrow

that the driving is effective. According to the discussion in section 2.7, the optimum value of $|\eta_0|$ is about 3 (refer to Fig.2.7.b).

The frequency at lower branch are determined from the equation for non-dissipative case[eq.(4.3.3)], where has to be redefined as the volume ratio V_H/V_c,($V_H = \pi r_H^2(L-\ell)$ and $V_c = \pi r_c^2 \ell$), and that at other branch approaches to constant $\pi/2$. The experimental results, not shown here, satisfactorily agree with such qualitative discussions.

By the way it is considered that when the tube inner radius is sufficiently small compared with the thickness of the boundary layer, the quantities F* or F is also small, so that the damping energy is reduced. However, in such a case, the driving energy is also reduced because the gradient of the square of the acoustic pressure is small on account of $\lambda_c \to \pi/2$. Thus only enlarging the tube inner radius is favorable for lowering the minimum critical temperature ratio.

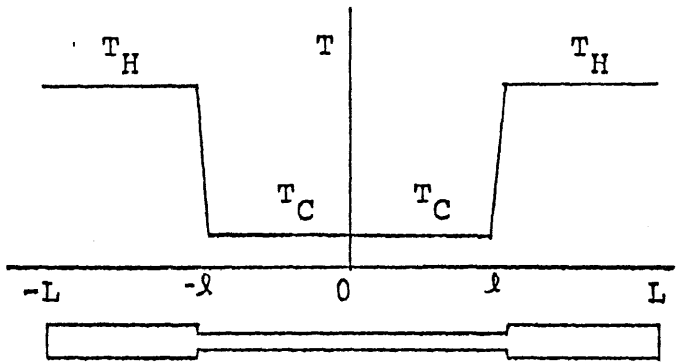

Figure.4.4.a Mean temperature distribution along a U-shaped tube with variable cross-section. Inner tube radius steeply varies at the temperature stratification.

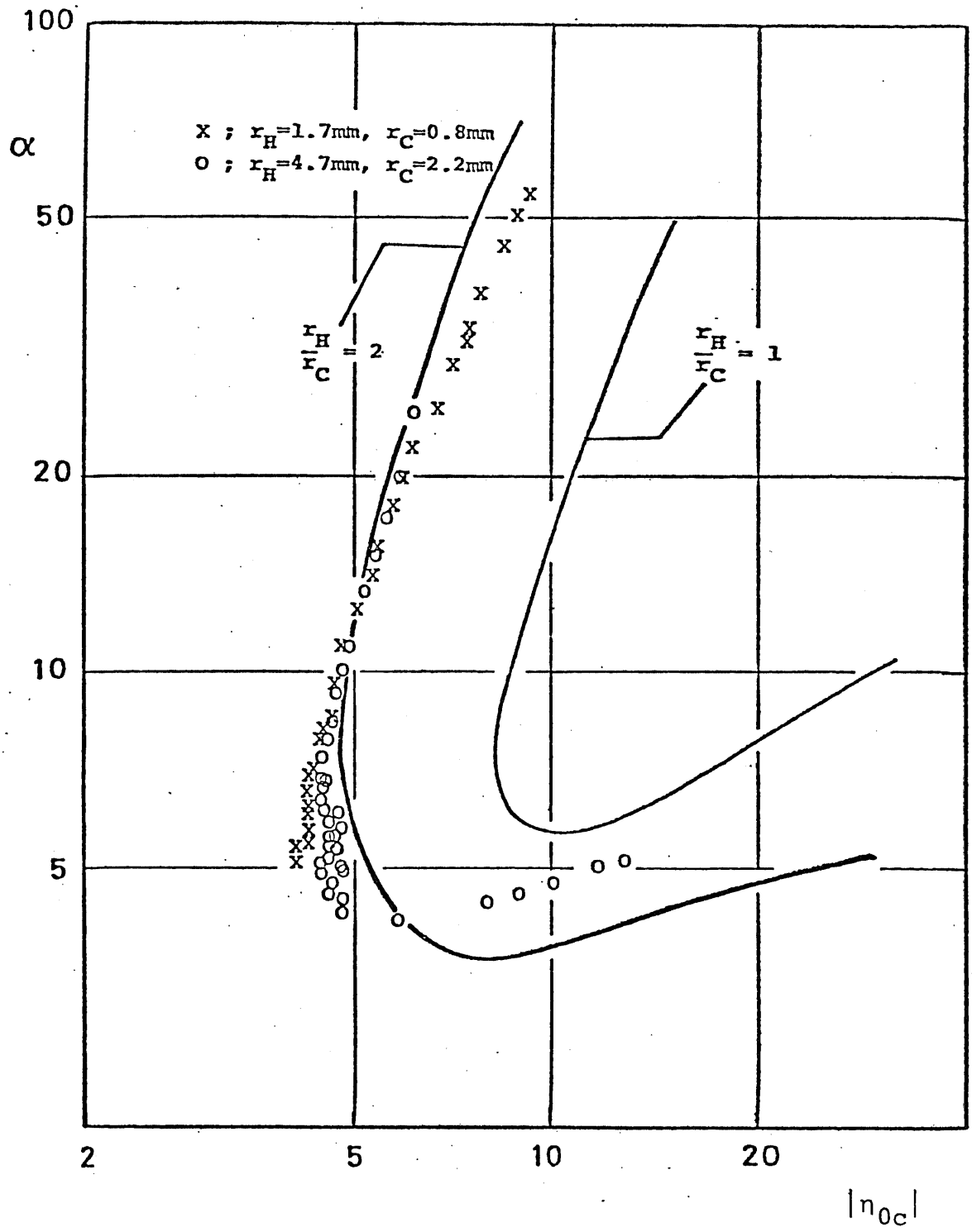

Figure.4.4.b The stability curve for the tube with variable cross-section. The solid curve is due to the theoretical one by Rott and Zouzoulas(1976).

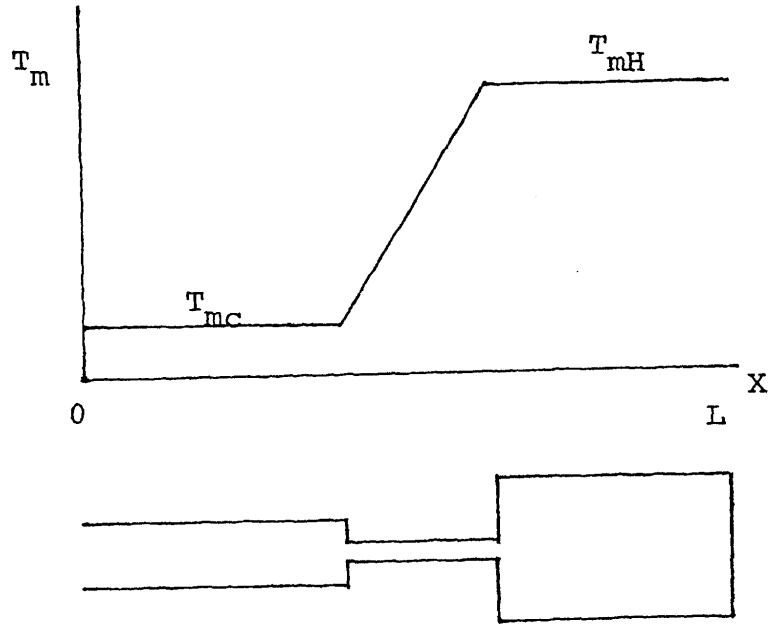

Figure.4.4.c Optimum configuration of tubes for driving thermally oscillations.

4.5 SECOND-HARMONIC

The experimental results for the fundamental were quantitatively interpreted by the linearized theory of Rott. For small ξ (0.3 and 0.5), we found a new phenomenon, which is the second-harmonic spontaneously induced in a U-shaped tube. The second-harmonic with small amplitudes was generated independent of the fundamental in this system. In experiments up to present, the second-harmonic as treated here has not been found, but only the fundamental has been observed. We experimentally determined the stability curve of the second-harmonic. It was concluded from experiments that the unstable region is classified into three regions, where the fundamental, the second-harmonic and the superposition of them are induced. We will also suggest that the results for the second-harmonic are supported by expansion of the linearized theory of Rott.

When we draw up the stability curves of the fundamental for $\xi = 0.3$, we found a higher harmonic at the left-hand limits. As shown in Fig.4.5.a, the stability curve suddenly shifts to the more inside stability curve at about 15 of temperature ratio(T_H=300K and T_C=20K). From the wave-forms monitored by an oscilloscope and the value measured by the frequency counter, it was confirmed that the new oscillations were second-harmonic. Of course the phase difference between x=L and x=-L for pressure fluctuations is not 180 degree but zero(in phase) for the second-harmonic.

The important variables which characterize the stability

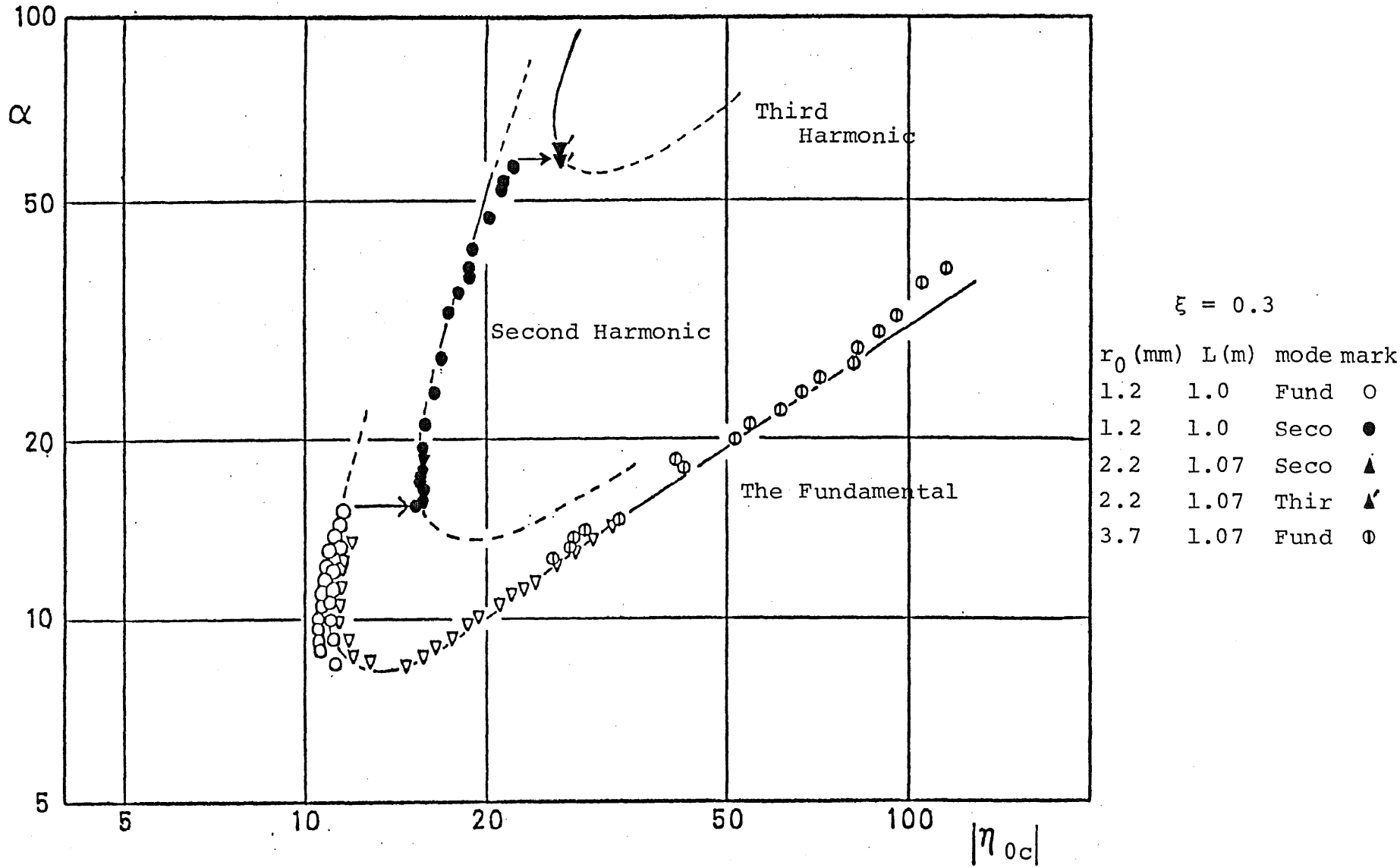

Figure.4.5.a The stability curves for the fundamental, second-harmonic and third-harmonic. At left-hand branch, the transitions occur.

curve are, already studied here, the temperature ratio between the warm and the cold parts and the ratio of tube inner radius to the Stokes boundary layer thickness. However, the ratio of $|\eta_{0c}|$ to the square root of the frequency parameter $\lambda_c = \omega\ell/a_c$ is employed here instead of $|\eta_{0c}|$ in order to obtain the variable independent of the frequency.

In Fig.4.5.b, the stability curve corresponding to Fig.4.5.a is rearranged on the plane α-$|\eta_{0c}|\lambda_c^{-1/2}$. The neutral points for the second-harmonic and the fundamental are marked by the symbols [▲ and ●] and [⊕, O and Δ] respectively. The experimental results are given in Table.4.2.1.

The second-harmonic is observed only at the left-hand branch of the stability curve and at the right-hand branch only the fundamental is observed, so that the respective stability curves may be extraporated as shown in Fig.4.5.b (dashed curves). The stability curves of the second-harmonic intersects with that of the fundamental at the left-hand branch near $\alpha = 15$. Thus if higher harmonic more than third, which is induced by bigger temperature ratio, are not taken into consideration, the unstable region is classified into three regions I, II , III.

In the region I, only the fundamental is induced, and typical wave-forms of the pressure fluctuations observed at the closed ends of the pipe are shown in Fig.4.5.c(a) where α , λ_c and $|\eta_{0c}|\lambda_c^{-1/2}$ are 13.0, 1.16 and 10.6 respectively. In the region II , only the second-harmonic is induced and the wave-forms are shown in Fig.4.5.c(b) where α , λ_c and $|\eta_{0c}|\lambda_c^{-1/2}$ are

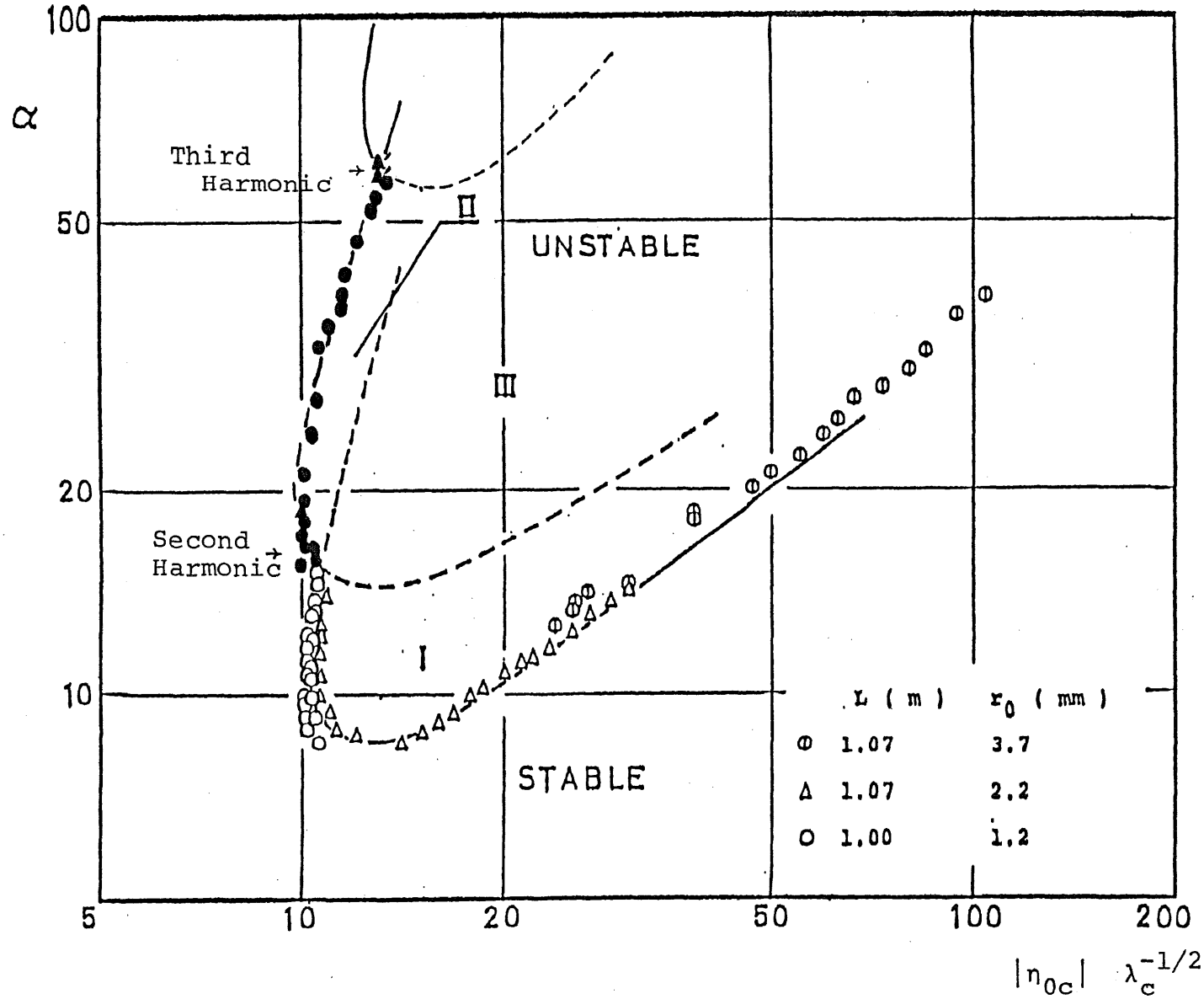

Figure.4.5.b The stability curves of the fundamental and the second-harmonic (solid marks) for helium gas. Two solid marks show the third harmonic (▲) near $\alpha \simeq 60$.

a)

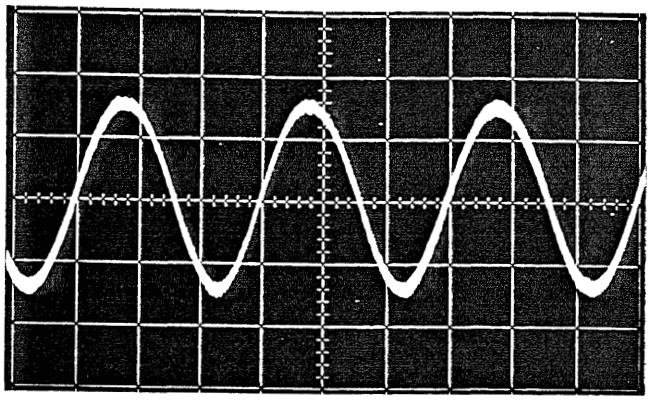

b)

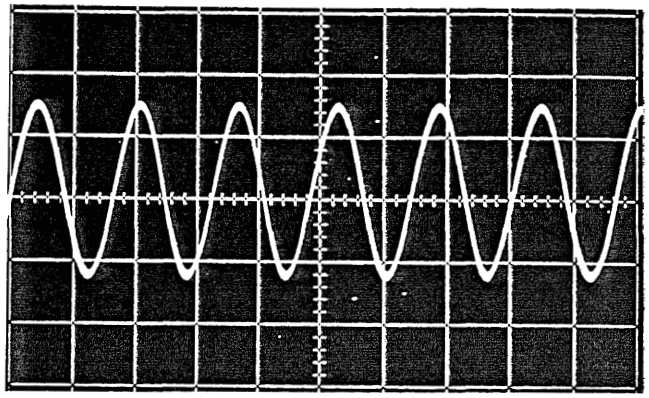

c)

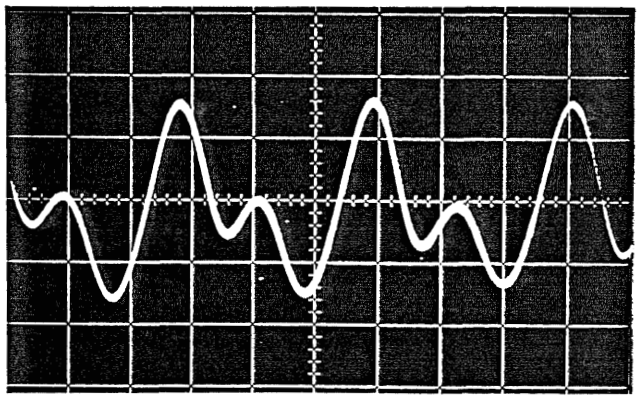

Figure.4.5.c Pressure fluctuations observed at the closed end of the pipe. a); the fundamental b); the second-harmonic and c); the superposition of them.

15.2, 2.34 and 10.0 respectively. In the region III, the wave-forms are expected to be the superposition of them. In fact as shown in Fig.4.5.c(c) the wave-forms are the superposition of the fundamental and the second-harmonic. These photographs are taken using the storage-oscilloscope(National Co., LTD VP-5701A). Thus the second-harmonic is excited on account of the intersection between the stability curves of the fundamental and the second-harmonic. Under constant temperature ratio more than 15, when a helium gas is poured into the U-shaped tube, which is initially vacuum, at first only the second harmonic is excited, then the superposition of the wave-forms between the fundamental and the second-harmonic will be observed and lastly only the fundamental is favorable to oscillate. It is interesting to see that the higher harmonic are able to be induced before the fundamental.

The frequency parameter λ_c lies between π and $\pi/2$. Therefore one pressure node exists between x=0 and x= ℓ .

Such a higher mode was not observed for $\xi \geqq 1$ below $\alpha \leqq 70$. It is expected that such a mode is set up at the left-hand branch for small ξ , where the dissipative layer is so thick that it fills up the whole tube at the warm part. The stability curve for the second harmonic is numerically derived from the suitable boundary conditions below.

The boundary condition corresponding to the second-harmonic is

$$\frac{dp_1}{dx} = 0 \quad \text{at } x=0 \text{ and } x=L$$

$$p_1(\ell+0) = p_1(\ell-0) \tag{4.5.1}$$

Step change of the temperature exists at $x=\ell$. The following expression for the pressure account for eq.(4.5.1)

$$P_H = A \frac{\cos \hat{k}_H(L-x)}{\cos \hat{k}_H(L-\ell)} \qquad \ell \leqq x \leqq L$$

$$P_C = A \frac{\cos \hat{k}_C x}{\cos \hat{k}_C \ell} \qquad -\ell \leqq x \leqq \ell \qquad (4.5.2)$$

$$P_{-H} = A \cos \hat{k}_H(L+x)/\cos \hat{k}_H(L-\ell) \qquad -\ell \geqq x \geqq -L$$

where A is the pressure at $x=\ell$. Equation.(4.5.2) shows that the phase difference of the pressure fluctuation between x=L and x=-L should be in phase for the second-harmonic. From the other condition corresponding to eq.(2.9.10), the key equation for the second harmonic is given

$$-\frac{G_C \tan \lambda_C^*}{\xi \lambda_C^*} = \frac{G_H \tan \lambda_H^*}{\lambda_H^*} \qquad (4.5.3)$$

As already pointed out, simplifications are performed for big values of α and small or moderate ξ ; then $\lambda_H \simeq 0$ and the right-hand side of eq.(4.5.3) is G_H. We obtain the following pair equation;

$$\frac{\tan\lambda_C}{\lambda_C} = -\xi(\mathrm{Im}G_H + \mathrm{Re}G_H)$$

$$|\eta_{0C}| = \frac{\sqrt{2}}{\xi \mathrm{Im}G_H}\{c[1+\tan^2\lambda_C - \frac{\tan\lambda}{\lambda_C}c] - \frac{d\tan\lambda_C}{\lambda_C}\} \qquad (4.5.4)$$

c; kramers constant, d; kirffihoff constant

The stability curves determined from eq.(4.5.4) certainly intersects with that for the fundamental at the left-hand branch for $\xi=0.3$, so that the linearized theory supported that the second-harmonic is induced independent of the fundamental as shown in Fig.4.5.d.

The excitation of higher harmonic is qualitatively able to be understood from eq.(2.7.6). Figure.2.7.b shows that

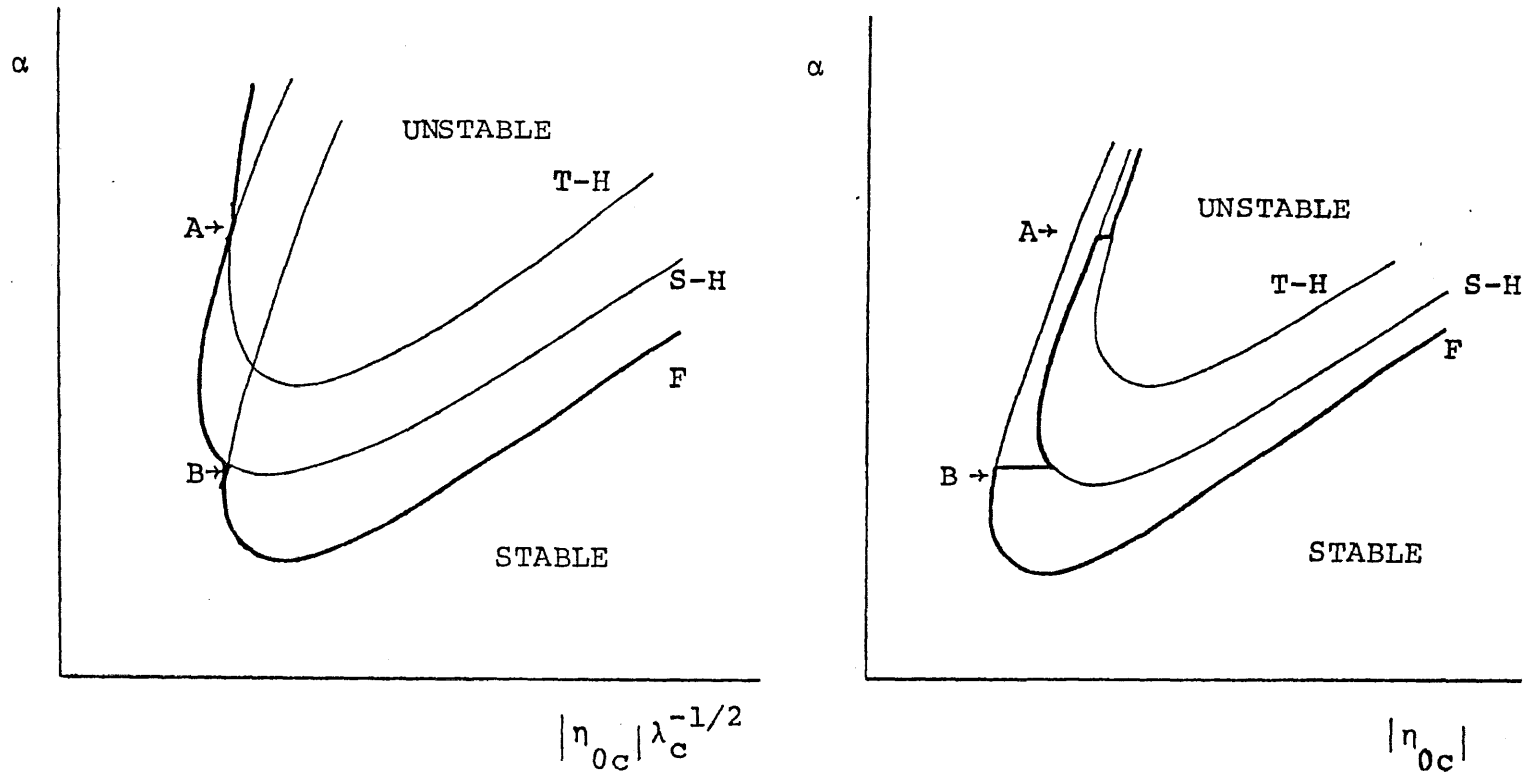

Figure.4.5.d The stability curves numerically derived from the key equations for the fundamental(F), the second-harmonic(S-H)and the third harmonic(T-H)for helium gas. At the location A and B the transition occur.

below $|\eta_0| \simeq 2.3$ only damping is possible through tube length, and the driving is not possible. The value $|\eta_0|$ of the second harmonic is larger than that of the fundamental because the former frequency is about twice larger than the latter. Therefore at the left-hand branch there exist some regions where the second-harmonic is favorable but the fundamental is not favorable. It is concluded that the excitation of higher harmonic is due to the viscosity of gas.

The stability curve for a second harmonic excited in a U-shaped tube is equivalent that for the fundamental induced in a closed tube at x=0 and x=L. Therefore the spontaneous oscillations should be expected in such a closed tube. Sergeev et al.(1979) shows that the oscillations were not able to be observed in such a tube. The cause of no oscillations may be due to the fact that the location of the temperature stratification is not suitable. The positive gradient of the square of the pressure amplitudes lies between $x=\ell$ and x=L for the wide tube with constant temperature, so that recalling eq.(2.7.6), we find that the oscillations will be possible to oscillate for smaller ξ than unity. We confirmed that the oscillations were able to be produced for $\xi = 0.3$ in a closed tube and the stability curve for such a tube agrees with that for the second-harmonic.

We observed a third harmonic at left-hand branch for $\xi = 0.3$. At about $\alpha \simeq 60$, the transition from the second-harmonic to the third harmonic occurs, as shown in Fig.4.5.a.

It is also considered that this is on account of the intersection, on the plane of α versus $|h_{0c}|\ \lambda_c^{-1/2}$, of the stability curves between the second-harmonic and the third-harmonic. The stability curve for the third harmonic is obtained from the key equation.(2.9.12). The relationship of the stability curves among them is given in Fig.4.5.d, which is calculated by use of data of G-function derived by Rott. The transition occurs at the left-hand branch near $\alpha \simeq 60$.

4.6 SECOND-ORDER HEAT FLUX

When "Taconis oscillations"are sustained in cryogenic systems; liquid helium transfer line, pumping lines from low temperature to room temperature system and the lines to measure the pressure, they are usually accompanied by a large amount of the evaporation of liquid helium. The attainable evaporation rates are emperically three orders of magnitudes larger than those without the oscillations. However there is very little quantitative data on the heat flux produced by the oscillation under a established temperature distribution.

Experiments are performed by the apparatus shown in Fig.3.4, where the warm part is immersed into the reservoir at room temperature and the cold part is immersed into the reservoir at liquid helium(4.2K). The heat produced by thermally driven acoustic oscillations is estimated from the evaporation of the liquid helium. Measurements are performed near the left-hand branch for ξ=2 and 3, where the boundary layer in the warm part fills up the whole tube. As shown in Fig.4.6.a, when helium gas is gradually poured into the pipe through a needle valve under constant temperature ratio α=70.5(T_{mH}=296K and T_{mc}=4.2K), the oscillation with small amplitudes are generated at a certain mean density. For example its critical values,$|\eta_{0c}|$ for ξ =2 is 22.6 for r_0=1.2mm or 22.4 for r_0=2.2mm in our experiments, which is in good agreements with theoretical value: the frequency and the critical mean density are 273 rad/sec and 91.8 torr for r_0=1.2mm and 273 rad/sec and 27.0torr for r_0=2.2mm. When$|\eta_{0c}|$increases,

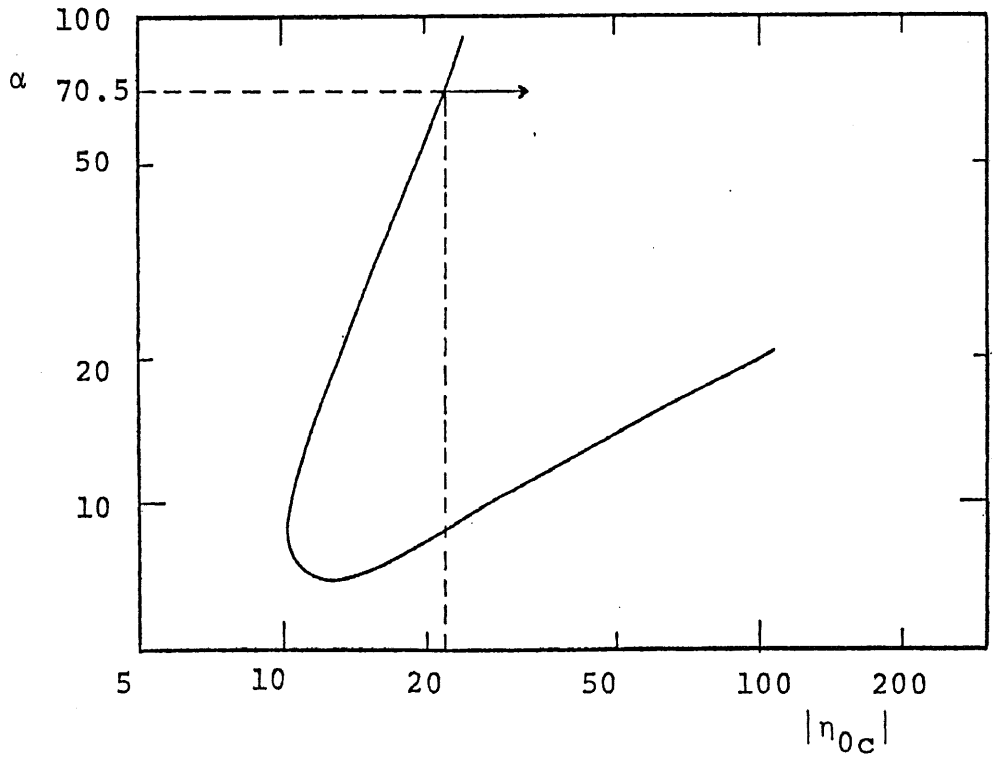

Figure. 4.6.a The stability curves for $\xi=4$ predicted by Rott(1973) Under constant temperature ratio $\alpha=70.5$($T_{mH}=296K$ and $T_{mc}=4.2K$) the experiments are performed.. Experimental value of critical value of $|\eta_{0c}|$ is equal to 22.4.

the acoustic pressure amplitude rapidly increase, and the evaporation of liquid helium is strongly dependent of the pressure amplitudes. The heat due to the oscillations $\dot{Q}_{ex}$ is plotted as a function of the square of the real pressure($\hat{p}_1$) amplitudes(a half of peak to peak value)at x=L as shown in Fig.4.6.b. The heat is proportional to $\hat{p}_1^2$ independent of and r_0. According to the section 2.8, $\hat{p}_1$ is proportional to the displacement of particles at $x=\ell$. The experiments by Banister(1966) show that $\dot{Q}_{ex}$ is proportional to the product of the pressure amplitudes and the frequency. However in his experiments, an important parameter, temperature distribution along the tube(half open type)was not sufficiently established. The experiments* using a half open tube, along which the temperature distribution is not established, confirm the $\hat{p}_1^2$ - dependence obtained in the U-tube(refer to [25]).

As discussed in section 2.8, the heat flux penetrating into the tube wall should come from the second-order heat flux derived by Merkli and Thomann(1975). In particular, it is expected that such a considerable heat flux produced in the tube with a steep temperature gradient may be caused by the second term in eq.(2.8.6), $\bar{E}_2^2$ given by Rott. Thus we will rearrange the experimental data given above comparing to the second-order theory.

The total heat flux penetrating into the tube wall in the cold part, which contributes to the evaporation is from eq.(2.8.2)

$$2\pi r_0 \int_{\text{cold part}} q_2 \, dx \simeq A k_{eff} dT_m/dx|_{x\simeq\ell} \tag{4.6.1}$$

* our experiments

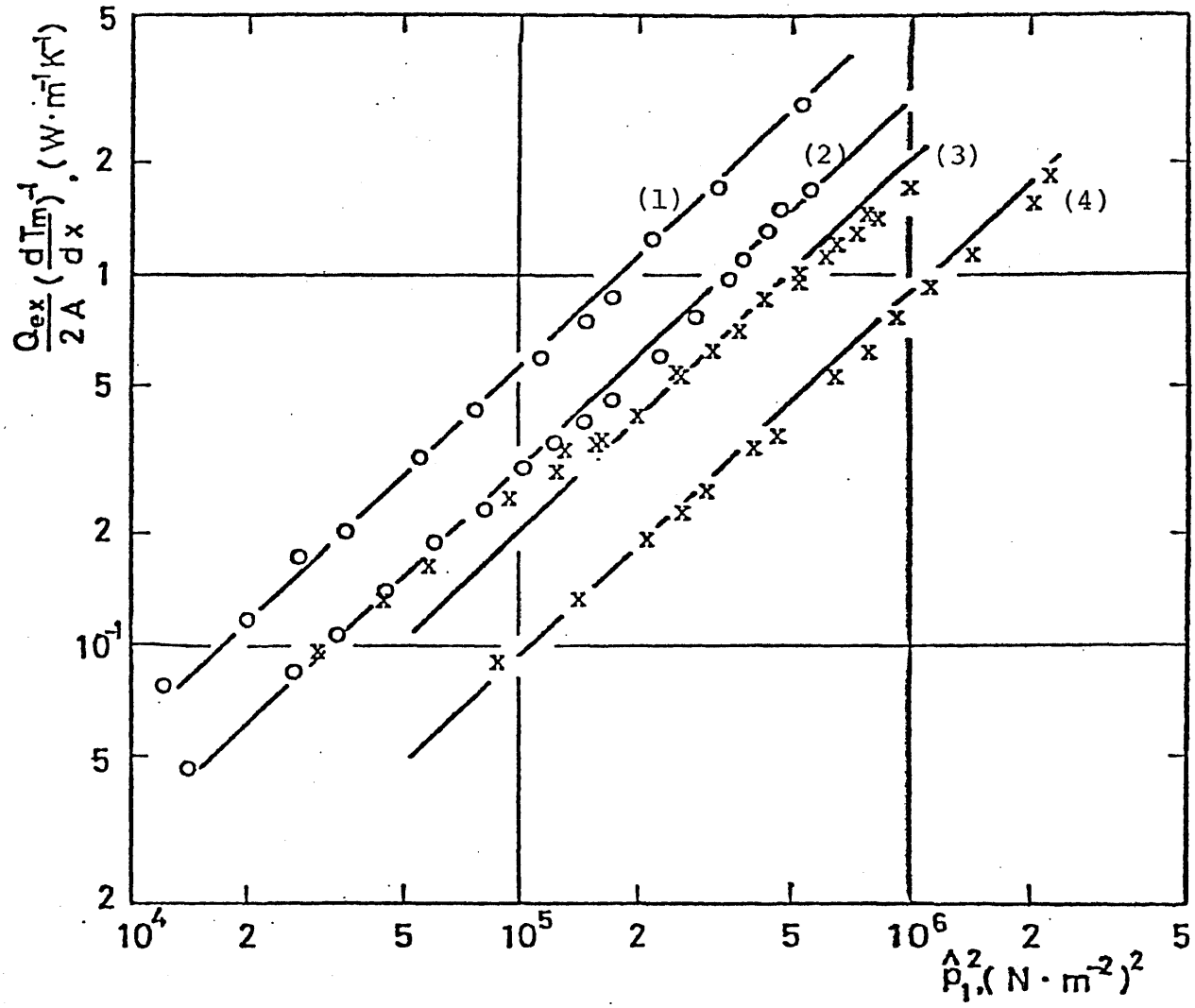

Figure.4.6.b The effective thermal conductivity of the oscillations versus the square of the pressure amplitudes at x=L. O(1); ξ=3, r_0=2.2mm and L=1.33m O(2); ξ=2, r_0=2.2mm and L=1.5m. X(3); ξ=3, r_0=1.2mm and L=1.33m. X(4); ξ=2, r_0=1.2mm and L=1.5m.

since a temperature gradient is vanished everywhere except near the position $x=\ell$. Here A is inner cross-sectional area of the tube and k_{eff} is, as given in eq.(2.8.11), formally the mean effective thermal conductivity due to thermally driven acoustic oscillations.

If the evaporation is dominantly based on the second-order heat flux, we can obtained the following equation, from eqs.(4.6.1)and(3.4.1),

$$\dot{Q}_{ex} = 2A\, k_{eff}\, dT_m/dx|_{x=\ell} \qquad (4.6.2)$$

$$k_{eff} = \frac{k|u_{1c}|^2}{2\omega\nu}\, Im\left(\frac{\sigma^2 F - \sigma F^*}{1-\sigma^2}\right) \qquad (4.6.3)$$

where the factor 2 means the contribution from $x=\pm\ell$. Oue data is arranged by eq.(4.6.2). In order to perform this, we are obliged to make several assumptions as following:

[1] the temperature gradient dT_m/dx is replaced by the mean value $(T_{mH}-T_{mc})/\Delta x$.

[2] the mean value of viscosity, thermal conductivity without oscillations and mean density are substituted by those at the mean temperature($\simeq$ 150K).

[3] in order to estimate the velocity of the core at $x=\ell$ the acoustic pressure variation is neglected at the warm part, so that from

$$p_1 = \frac{i\gamma p_m}{\omega}\,\frac{du_{1c}}{dx} \qquad (4.6.4)$$

the velocity of the core at $x=\ell$ is given by

$$|u_{1c}|^2_{x=\ell} = \frac{\omega^2}{\gamma^2 p_m^2}\,(L-\ell)^2\,\hat{p}_1^2 \qquad (4.6.5)$$

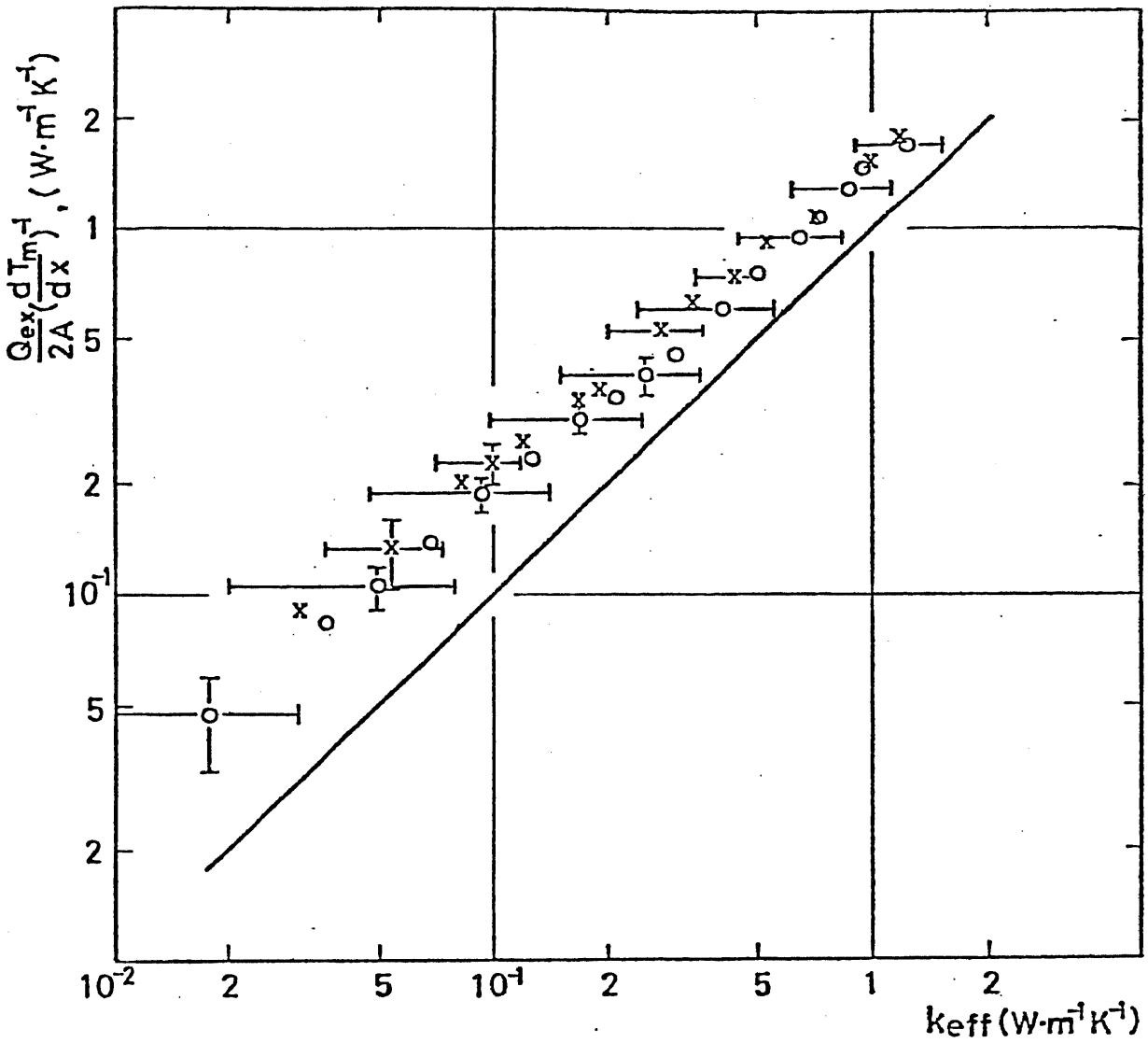

Figure.4.6.c The effective thermal conductivity obtained by experiments $[Q_{ex}/2A\cdot(dT_m/dx)^{-1}]$ versus that derived by the theory of the second-order heat flux for $\xi = 2$ Marks are the same as that in Fig.4.6.b.

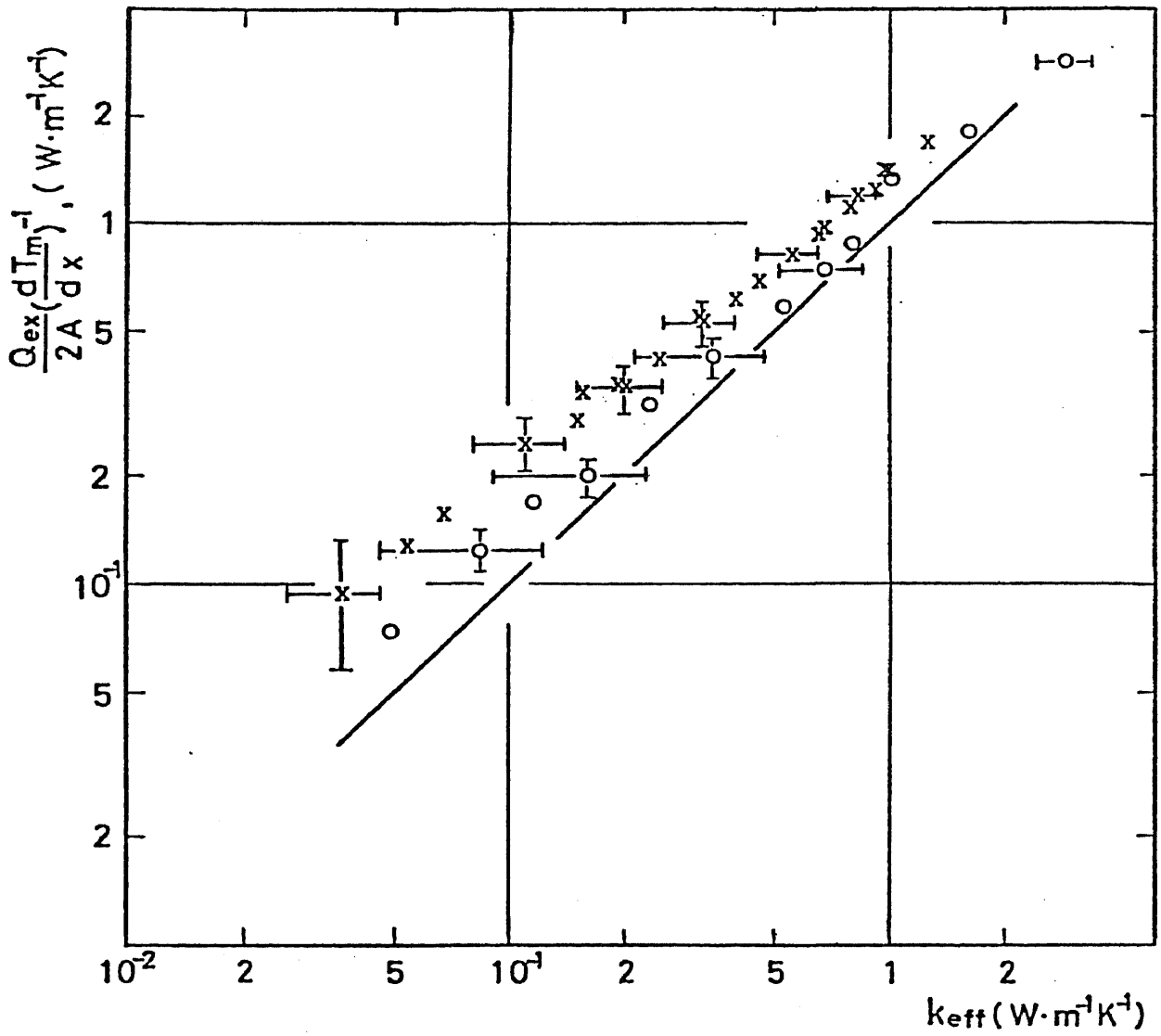

Figure.4.6.d The effective thermal conductivity obtained by experiments $[Q_{ex}/2A \cdot (dT_m/dx)^{-1}]$ versus that derived by the theory of the second-order heat flux k_{eff} for $\xi = 3$. Marks are the same as that in Fig.4.6.b.

where $\hat{p}_1$ is real pressure amplitudes at x=L and is experimentally observable.

Thus we can numerically determine k_{eff} from the measurements of the pressure amplitudes at the closed end, the mean pressure in the cavity and the frequency of the oscillations.

The effective heat conductivity is proportional to the square of the pressure amplitudes as indicated by eq.(4.6.3). As pressure amplitudes near the stability curves increase abruptly, it is dominant term compared with others in k_{eff}. Thus the results in Fig.4.6.b is explained by second-order heat flux qualitatively.

Quantitative comparison between theory and experiments are shown in Fig.4.6.c and Fig.4.6.d. The order of magnitude agreement between them is satisfactory.Thus majority of the evaporation of the helium under the oscillations is dominantly due to the second-order heat flux contributed from the part with a large temperature gradient. An excess in $\dot{Q}_{ex}$ may be attributed to the higher order heat flux or a large temperature gradient compared with an averaged value assumed here.

The effective heat conductivity becomes an order of magnitude larger than that of gas without any disturbances even near the stability limit($k_m=0.9X10^{-1}$watt.$m^{-1}K^{-1}$ at 150K). In more inside region of the stability curve where the oscillation are so vigorous that it is difficult to maintain the temperature constant in the warm part, the pressure amplitudes becomes more than an order of magnitude larger than those achieved here. Thus it is expected from Fig.4.6.b that the

effective thermal conductivity may be the order of 10^2(watt.m^{-1} K^{-1}), which is the same order as that of a metal(aluminium alloy at 150K). Such a high conductivity will enable us, in future, to apply for precooling a large cryogenic systems.

Appendix 1

Fundamental Equation Governing the Oscillatory Motion

The basic equations governing the motion of viscous and compressible fluid are, as well-known, the mass conservation, the axial and the radial momentum equations, the energy equation and the equation of state. In cylindrical co-ordinates, these are

$$\frac{\partial \rho}{\partial t} + u\frac{\partial \rho}{\partial x} + v\frac{\partial \rho}{\partial r} + \rho\left[\frac{1}{r}\frac{\partial}{\partial r}(vr) + \frac{\partial u}{\partial x}\right] = 0$$

$$\rho\left[\frac{\partial u}{\partial t} + u\frac{\partial u}{\partial x} + v\frac{\partial u}{\partial r}\right] = -\frac{\partial p}{\partial x} + \frac{\mu}{3}\frac{1}{r}\frac{\partial}{\partial r}\left(r\frac{\partial v}{\partial x}\right) + \frac{4\mu}{3}\frac{\partial^2 u}{\partial x^2} + \frac{\mu}{r}\frac{\partial}{\partial r}\left(r\frac{\partial u}{\partial r}\right)$$

$$\rho\left[\frac{\partial v}{\partial t} + u\frac{\partial v}{\partial x} + v\frac{\partial v}{\partial r}\right] = -\frac{\partial p}{\partial r} + \frac{4}{3}\mu\left[\frac{1}{r}\frac{\partial}{\partial r}\left(r\frac{\partial v}{\partial r}\right) - \frac{v}{r^2}\right] + \frac{\mu}{3}\frac{\partial^2 u}{\partial x \partial r} + \mu\frac{\partial^2 v}{\partial x^2}$$

$$\rho c_p\left[\frac{\partial T}{\partial t} + u\frac{\partial T}{\partial x} + v\frac{\partial T}{\partial r}\right] = \frac{\partial p}{\partial t} + v\frac{\partial p}{\partial r} + u\frac{\partial p}{\partial x} + \frac{k}{r}\frac{\partial}{\partial r}\left(r\frac{\partial T}{\partial r}\right) + k\frac{\partial^2 T}{\partial x^2}$$
$$+\frac{4}{3}\mu\left[\left(\frac{\partial v}{\partial r}\right)^2 + \left(\frac{\partial u}{\partial x}\right)^2 + \left(\frac{v}{r}\right)^2 - \frac{v}{r}\frac{\partial v}{\partial r} - \frac{\partial u}{\partial r}\frac{\partial v}{\partial x} - \frac{v}{r}\frac{\partial u}{\partial x}\right] + 2\mu\frac{\partial v}{\partial x}\frac{\partial u}{\partial r} + \mu\left(\frac{\partial v}{\partial x}\right)^2$$

$$p = \rho R' T \quad , \quad R' = \frac{R}{M}$$

If we accept the several assumption(long tube approximation) given in section 2.2, the above set of equations, as given by Rott(1969) for non-uniformed temperature distribution,

the continuity equation

$$i\omega\rho_1 + \rho_m\frac{\partial u}{\partial x} + u\frac{\partial \rho_m}{\partial x} + \rho_m\frac{\partial (rv)}{r\,\partial r} = 0 \qquad \text{(A.1.1)}$$

the radial momentum equation

$$\frac{\partial p_1}{\partial r} = 0 \qquad \text{(A.1.2)}$$

the axial momentum equation

$$i\omega u + \frac{1}{\rho_m}\frac{dp_1}{dx} = \nu\frac{\partial}{r\,\partial r}\left(r\frac{\partial u}{\partial r}\right) \qquad \text{(A.1.3)}$$

the energy equation

$$i\rho_m C_p \omega \left(T_1 - \frac{p_1}{\rho_m C_p} \right) + \rho_m C_p u \frac{\partial T_m}{\partial x} = k \frac{\partial}{r \partial r}\left(r \frac{\partial T_1}{\partial r} \right) \qquad \text{(A.1.4)}$$

the equation of state for ideal gas

$$\frac{p_1}{p_m} = \frac{\rho_1}{\rho_m} + \frac{T_1}{T_m} \qquad \text{(A.1.5)}$$

where thermal conductivity k is equal to be $\mu C_p/\sigma$.

The boundary conditions are, at the tube wall,

$$\begin{aligned} T_1 &= 0 \\ u &= 0 \\ v &= 0 \end{aligned} \qquad \text{(A.1.6)}$$

When the wall substance has large heat capacity or is good thermal conductor compared with a oscillating gas, the influ ence of the wall temperature fluctuation is negligible in most cases. The second and third boundary conditions are due to finite viscosity of gas and shows unmovable wall. In principle, the five equations(A.1.1)-(A.1.5) determines the five unknown variables T_1, p_1, ρ_1, u and v. The solution of eq.(A.1.3) determining the distribution of radial velocity is given by, using eq.(A.1.6)

$$u = \frac{i}{\rho_m \omega} \frac{\partial p_1}{\partial x} \left\{ 1 - \frac{J_0(i\eta)}{J_0(i\eta_0)} \right\} \qquad \text{(A.1.7)}$$

where J_0 is the Bessel function of the first kind in term of the complex variables

$$\eta \equiv r\sqrt{\frac{i\omega}{\nu}} \qquad \text{and} \qquad \eta_0 \equiv r_0\sqrt{\frac{i\omega}{\nu}} \qquad \text{(A.1.8)}$$

The variable η_0 is concerned with the complex viscous boundary

layer thickness given in the next Appendix 2. The first order temperature solution is derived from eq.(A.1.4), using eq. (A.1.7);

$$\rho_m C_p T_1 = \left[P_1 - \frac{\theta}{(\gamma-1)(1-\sigma)} \frac{a^2 dP_1}{\omega^2 dx}\right]\left\{1 - \frac{J_0(i\sqrt{\sigma}\eta)}{J_0(i\sqrt{\sigma}\eta_0)}\right\} + \frac{\sigma\theta}{(\gamma-1)(1-\sigma)} \frac{a^2 dP_1}{\omega^2 dx}\left\{1 - \frac{J_0(\eta)}{J_0(\eta_0)}\right\} \quad \text{(A.1.9)}$$

where the notation $\theta = \frac{1}{T_m}\frac{dT_m}{dx}$ shows the steepness of the mean temperature. The value $\sqrt{\sigma}\eta_0$ is associated with the thermal boundary layer thickness treated in next Appendix. From eqs. (A.1.7) and (A.1.9), the gradients of temperature fluctuation and the velocity at the wall are determined as

$$\mu\left(\frac{\partial u}{\partial r}\right)_{r=r_0} = \frac{r_0}{2} F \frac{\partial P_1}{\partial x} \quad \text{(A.1.10)}$$

which physically means the tangential force per unit area acting on the wall surface, and

$$R\left(\frac{\partial T_1}{\partial x}\right)_{r=r_0} = \frac{r_0}{2}\left\{-i\omega F^* P_1 + \frac{i}{\omega}\frac{F^*-F}{1-\sigma} C_p \frac{\partial T_m}{\partial x}\frac{dP_1}{dx}\right\} \quad \text{(A.1.11)}$$

which is the heat flux to the tube wall per unit area. In eqs.(A.1.10)and(A.1.11), F and F* are determined by

$$F = \left\langle \frac{J_0(i\eta)}{J_0(i\eta_0)} \right\rangle \quad \text{(A.1.12)}$$

$$F^* = \left\langle \frac{J_0(i\sqrt{\sigma}\eta)}{J_0(i\sqrt{\sigma}\eta_0)} \right\rangle \quad \text{(A.1.13)}$$

which express effects of the viscosity and thermal conductivity of gas respectively, and vanish in the non-dissipative case. The next step consists of the reduction to one-dimensional differential equations of (A.1.1)-(A.1.5).

Let these equations be multiplied by the factor $2\pi r dr$ and

integrated from zero to the tube inner radius r_0 with notation (2.1.3). The results are, using the boundary conditions

$$i\omega \langle \rho_1 \rangle + \rho_m \frac{\partial \langle u \rangle}{\partial x} + \langle u \rangle \frac{\partial \rho_m}{\partial x} = 0 \qquad \text{(A.1.1')}$$

$$i\omega \rho_m \langle u \rangle + \frac{d P_1}{d x} = \frac{2\mu}{r_0} \left(\frac{\partial u}{\partial r} \right)_{r=r_0} \qquad \text{(A.1.3')}$$

$$i\omega (\rho_m C_p \langle T_1 \rangle - P) + \rho_m C_p T_m \theta \langle u \rangle = \frac{2k}{r_0} \left(\frac{\partial T_1}{\partial r} \right)_{r=r_0} \qquad \text{(A.1.4')}$$

$$\frac{P}{P_m} = \frac{\langle \rho_1 \rangle}{\rho_m} + \frac{\langle T_1 \rangle}{T_m} \qquad \text{(A.1.5')}$$

where the assumptions in section 2.2 again are employed here. A combination of eq.(A.1.2') and (A.1.10) leads to

$$i\omega \rho_m \langle u \rangle + (1 - F) \frac{d P_1}{d x} = 0 \qquad \text{(A.1.14)}$$

and also from eqs.(A.1.4') and (A.1.13) we obtain an equation

$$i\omega \left\{ \rho_m C_p \langle T_1 \rangle - (1 - F^*) P_1 \right\} + \rho_m C_p T_m \theta \langle u \rangle = \frac{i (F^* - F)}{\omega (1 - \sigma)} C_p T_m \theta \frac{d P_1}{d x} \qquad \text{(A.1.15)}$$

From eqs.(A.1.15), (A.1.1') and (A.1.5') we have an equation of $\frac{\partial \langle u \rangle}{\partial x}$ expressed by p_1 and $\frac{\partial p_1}{\partial x}$;

$$\frac{\partial \langle u \rangle}{\partial x} = -i\omega \frac{1 + (\gamma - 1) F^*}{\gamma \rho_m} P_1 + \frac{i (F^* - F)}{\omega (1 - \sigma)} \frac{1}{\rho_m T_m} \frac{d T_m}{d x} \frac{d P_1}{d x} \qquad \text{(A.1.16)}$$

Our final purpose is to calculate the eq.(2.1.5). The time averaged product of the pressure fluctuation and the radial averaged gradient of u becomes, from eq.(A.1.16)

$$P_1 \frac{\partial \langle u \rangle}{\partial x} = \frac{\omega |P_1|^2}{2\gamma \rho_m} (\gamma - 1) I_m F^* - \frac{R}{2\omega M \rho_m} \frac{d T_m}{d x} \tilde{\rho} \frac{d P}{d x} I_m \frac{F^* - F}{1 - \sigma} \qquad \text{(A.1.17)}$$

Similarly the product of $\langle u \rangle$ and dp_1/dx is

$$\langle u \rangle \frac{d P_1}{d x} = \frac{\omega \rho_m}{2} \left| \frac{\langle u \rangle}{1 - F} \right|^2 I_m F \qquad \text{(A.1.18)}$$

We employ that the time average of the product of complex quantities A and B is the real part of a half the product of a complex conjugate of A and complex conjugate of A and complex expression B.

By the way, we present here the differential equation for the acoustic pressure(the wave equation)in order to derive the stability limits of the oscillations;

$$[1+(\gamma-1)F^*]P_1+\frac{d}{dx}\left[\frac{a^2}{\omega^2}(1-F)\frac{dP_1}{dx}\right]-\frac{a^2}{\omega^2}\frac{F^*-F}{1-\sigma}\theta\frac{dP_1}{dx}=0 \qquad \text{(A.1.19)}$$

which is obtained by elimination of <u> from eqs.(A.1.15), (A.1.14)and (A.1.16). Such a generalization of the wave equation appling to the case of a variable wall temperature have been performed by Rott(1969).

Appendix 2

Viscous and Thermal Boundary Layer

In order to understand thermal and viscous boundary layer formed at the wall, oscillating flow in the plane instead of in the cylindrical pipe will be discussed below. When a solid body immersed in a viscous fluid oscillates, the flow thereby set up has a number of characteristic properties. As a simple but typical example, let's imagine that an incompressible fluid is bound by an infinite plane surface which executes a simple harmonic oscillation in its own plane, with frequency ω . We take the solid surface as the yz-plane, and the fluid occupies the region $x > 0$; the y-axis is taken in the direction of the oscillations. The velocity of the oscillating surface is a function of time, of the form

$$U = U_0 \exp(-i\omega t) \qquad \text{(A.2.1)}$$

The fluid velocity must satisfy the boundary condition $u_x = u_z = 0$ and $u_y = u$ for $x = 0$. It is further evident from symmetry that the velocity is everywhere in the y-direction. Therefore from the simplified Navie-Stokes equation for one dimentional incompressible viscous fluid, we obtain, for $v_y = v$

$$\frac{\partial v}{\partial t} = \nu \frac{\partial^2 v}{\partial x^2} \qquad (\nu = \mu/\rho_m) \qquad \text{(A.2.2)}$$

which is equivalent to one dimensional heat conduction equation. If the solution of this equation is periodic in x and t of the form

$$V = U_0 \exp\{i(\hat{k}x - \omega t)\}$$

We find $i\omega=\nu\hat{k}^2$, where $\hat{k}=\sqrt{\frac{i\omega}{\nu}}=\frac{1}{\sqrt{2}}\sqrt{\frac{\omega}{\nu}}(1+i)$, so that the velocity is

$$V = U_0 e^{-\sqrt{\frac{\omega}{2\nu}}x} e^{i\left(\sqrt{\frac{\omega}{2\nu}}x - \omega t\right)} \qquad (A.2.3)$$

We have taken $\hat{k}$ to have a positive imaginary part, since the velocity would increase without limit in the interior of the fluid, which is physically impossible. The solution obtained represents a transverse wave; namely the transverse wave can occur in a viscous fluid, but they are rapidly damped in the interior of the fluid, so that practically the character of them does not appear(over a distance of one wavelength the amplitude diminishes by a factor 540).

At the solid surface x=0, when the temperature is executed a harmonic oscillation $T=T_0e^{-i\omega t}$, the distribution of them at x is determined by the equation of one dimensional heat conduction corresponding to eq.(A.2.2);

$$\frac{\partial T_1}{\partial t} = \hat{\chi}\frac{\partial^2 T_1}{\partial x^2} \qquad (A.2.4)$$

$\hat{\chi}$; thermal diffusivity

The solution of eq.(A.2.4) is

$$T_1 = T_0 \exp\left[-x\sqrt{\frac{\omega}{2\hat{\chi}}}\right] \exp\left\{i\left[x\sqrt{\frac{\omega}{2\hat{\chi}}} - \omega t\right]\right\} \qquad (A.2.5)$$

The most important property of both waves of velocity and temperature is that the amplitude decreases exponentially as the distance x from the solid surface increase.

The distance δ over which the amplitude falls by a factor

e is called the viscous δ_v and the thermal boundary layer δ_T thickness; thus

$$\delta_v = \sqrt{\frac{2\nu}{\omega}} \quad \text{and} \quad \delta_T = \sqrt{\frac{2\chi}{\omega}} \qquad \chi \equiv \frac{k}{c_p \rho_m} \qquad \text{(A.2.6)}$$

The factor $\sqrt{2}$ is neglected in this paper. The ratio of the thermal boundary layer thickness to the viscous one is

$$\frac{\delta_T}{\delta_v} = \sqrt{\frac{\chi}{\nu}} = \frac{1}{\sqrt{\sigma}} > 1 \qquad \text{(A.2.7)}$$

$\sigma = 2/3$ for helium gas

where σ $(= \frac{c_p \mu}{k})$ is Plandtl number; $\sigma = 0$ for $k \to \infty$ or $\mu = 0$ and $\sigma \to \infty$ for $k = 0$. For real gases the Plandtl number σ ranges usually from 1/3 to 1 depending on the kinds of gases, so that the thermal boundary layer is ordinarily thicker than the viscous boundary layer. This is important to excite the acoustic oscillation thermally, because when σ is more than unity, the oscillation is not excited as understood in section 2.7.

In the oscillating flow (Poiseuille flow) in cylindrical pipe, as illustrated in several textbooks (Imai, 1977), when $\delta/r_0 >> 1$, the radial distribution of the axial velocity must be parabola , and when $\delta/r_0 \ll 1$, Poiseuille flow consists of two parts; the uniform flow in the "core" and the boundary layer covered over the wall.

Appendix III The Transport Coefficients of Gaseous Helium

I briefly introduce the temperature and pressure dependences of viscosity and thermal conductivity for helium gas refering to the experimental results up to present.

The phenomena of diffusion, viscosity and thermal conductivity are all physically similar in the sense that they involve the transport of some physical property through the gas; for example viscosity is the transport of momentum....

A detailed classical treatments of rigorous kinetic theory of dilute monoatomic gases and mixtures has been early investigated by Chapman and Enskog. According to rigorous theory for rigidsphere molecules, the shear viscosity coefficient and the thermal conductivity can be written as following expressions;

$$\mu = 2.6693 \times 10^{-5} \sqrt{mT}/d^2 \quad g/cm \cdot sec$$

$$k = 1.9891 \times 10^{-4} \sqrt{mT}/d^2 \quad cal/cm\ deg\ sec$$

where m = molecular weight

d = molecular diameter in Å

T = temperature in K

In the first approximation the coefficients of viscosity and thermal conductivity are both indepensent of the pressure and increase with the square of the temperature. The above equation would be correctly suitable to those propertis if the molecules actually were rigid sphere. As stated later, these

results give only the approximate pressure and temperature dependence must include the effect of the interactions which take place between real molecules.

At low temperature several authors experimentally investigated the temperature effect of viscosity. A complete discussion of experimental results obtained prior to 1942 was given by Keesom. These results can be represented emprically by the straight-line relation in log-log co-ordinates, according to Keesom,

$$\mu = 5.023\ T^{0.647} \quad \text{micro poise}$$

with a deviation of less than $\pm$ 1 %, so that we should employ the value 0.647 as the best fitting value of β for analysing our experimental data. This experimental value is slightly different from that due to the classical theory as stated above.

The pressure effect was measured by Kestin and Pilarczk in the range 1-124 atm at room temperature. Their experimental results indicates that the effect of the pressure is negligible. This is accorded with the kinetic theory.

REFERENCES

[1]. Bannister, J. D. (1966). Spontaneous pressure oscillations in tubes connecting liquid helium reservoirs to 300K environments. Bull. Intern. Inst. Refrigeration. 5, 127.

[2] Betchov, R. (1958) Nonlinear Oscillations of a column of gas. Phys. Fluids. 1, 205.

[3] Bergh, H., and Tijdeman, H. (1965). Theoretical and experimental results for the dynamic response of pressure measuring experiments. Rep. NLR-TRF. 238.

[4] Clement, J. R., and Gaffney, J. (1954). Thermal oscillations in low temperatrue apparatus. Advance in Cryogenic Engineering. 1 302.

[5] Gaffney, J., and Clement, J. R. Liquid helium level--finder. Rev. Sci. Instr. 26, 620.

[6] Imai, I. (1978). Ryutairikigaku(in japanese). Shōkabō.

[7] Itoh, T. (1979). Onkyo-kogaku(in japanese). Denkishoin.

[8] Kramers, H. A. (1949). Vibrations of a gas column. Physica, 15, 971.

[9] Kohashi, U. (1976). Oto to onpa(in japanese). Shōkabō.

[10] Keesom, W. H. (1942). Helium. Elsevior, 302.

[11] Landau, L. D., and Lifshitz. (1959). Course of theoretical Physics 6 Fluid Mechanics. Pergamon Press.

[12] Merkli, H. A., and Thomann, H. (1975). Thermoacoustic effects in a resonance tube. J. Fluid Mech. 70, 161.

[13] Narahara, Y., Yazaki, T., and Tominaga, A. (1980). Nagare. 12, No.3 24.

[14] Rayleigh, J. W. S. Lord. (1896) Theory of Sound. 2nd ed.,

Vol. II (reprinted at Macmillan, London, 1944).

[15] Rott, N. (1969). Damped and thermally driven acoustic oscillations in wide and narrow tubes. Z. Angew. Math Phys. 20, 203.

[16] Rott, N. (1973) Thermally driven acoustic oscillations. Part II. Stability limits for helium. Z. Angew.Math Phys. 24, 54.

[17] Rott, N. (1975). Thermally driven acoustic oscillations. Part III. Second-order heat flux. Z. Angew. Math Phys. 26, 43.

[18] Rott, N., and Zouzoulas, G. (1976). Thermally driven acoustic oscillations. Part IV. Tubes with variable cross-section. Z. Angew. Math Phys. 27, 197.

[19] Rott, N. (1980). Thermoacoustics. Advance in Applied Mechanics. 20, 135.

[20] Sergeev, S. I., Popov, O. M., and Vishnev, I. P. (1977) Thermally induced oscillations of helium in cryogenic apparatus. Inzhenerno-Fizicheskii Zhurnal. 32, 691.

[21] Sondhauss, C. (1850). Ann. Phys. Chem. 79, 1.

[22] Taconis, K. W., Beenakker, J. J., Nier, A. O. C., and Aldrich, L. T. Physica. 15, footnote on p. 738.

[23] Temkin, S. (1968). Nonlinear gas oscillations in a resonant tube. Phys. Fluids. 11, 960.

[24] Temkin, S. (1969). Propagating and standing sawtooth waves. J. Acous. Soc. Amer. 45, 224.

[25] Tominaga, A., Yazaki, T., and Narahara, Y. (1979). Stability limit for thermally driven acoustic oscillation

Cryogenic Engineering. 14, 3.

[26] Von Hoffman, T., Lienert, U., and Quack, H. (1973). Experiments on thermally driven gas oscillations. Cryogenics. 19, 490.

[27] Yazaki, T., Tominaga, A., and Narahara, Y. (1979). Stability limit for thermally driven acoustic oscillations. Cryogenics. 19, 393.

[28] Yazaki, T., Tominaga, A., and Narahara, Y. (1980). Experiments on thermally driven acoustic oscillations of gaseous helium. J. Low Temp. Phys. 41, 1/2 45.

[29] Yazaki, T., Tominaga, A., and Narahara, Y. (1980). Thermally driven acoustic oscillations: Second-harmonic. Phys. Letters A. 79A, Nos 5,6 407.

[30] Yazaki, T., Tominaga, A., and Narahara, Y. (1980) Effective thermal conductivity of thermally driven acoustic oscillations. (to be submitted).

[31] Zouzoulas, G., and Rott, N. (1976). Thermally driven acoustic oscillations. Z. Angew. Math Phys. 27, 325.

SUMMARY AND CONCLUSIONS

We have experimentally studied following properties of spontaneous oscillations of a gas columns generated in a tube with steep temperature gradients;

1. determination of the boundaries between unstable and stable regions, and the frequency of the oscillations.
2. transition from the fundamental to the second-harmonic and from the second to the third harmonic.
3. rough estimate of the effective thermal conductivity of the oscillating instability.

In experiments U-shaped tube was employed, which was separately immersed into two reservoirs, cold(temperature T_C)and warm(T_H) ones.

The stability curves and frequency diagrams for helium gas were determined under established temperature distribution for several ξ (=0.3, 0.5, 1, 2, 5, 10; the ratio of the length of warm part to that of cold)as a parameter. The experimental results were compared with the theory of Rott. The agreements between them are satisfactory, and the existences of two branches on the stability curves were confirmed. Two types of the boundary layer formed on the tube wall, viscous and thermal, play an important role to characterize the stability of the oscillations.

For small ξ(=0.3), higher harmonics(second and third) were observed at one-hand branch. The transitions from the

fundamental to the second-harmonic occur near $T_H/T_c=15$, and that from the second to the third harmonic near $T_H/T_C=60$. These take place on account of a finite viscosity of gas, and are theoretically explained from the intersections between the stability curves.

A effective thermal conductivity of the oscillations was estimated from the evaporation rate of liquid helium under given boundary layer thickness. Under suitable conditions, the conductivity is more than three orders of magnitude larger than the normal one of gas. Such a high conductivity was able to be interpreted from the theory of the second-order heat flux.

PERSONAL HISTORY

Name in Full: Taichi Yazaki

Date of Birth: September 24th, 1951

Family Relation: First son of Hiroyuki Yazaki

Permanent Domicile: 392, No.6330, Shiga, Suwa City, Nagano Prefecture

Present Adress: 112, No.3-13, 3-chome, Sekiguchi, Bunkyō-ku, Tokyo

Education:

Entered Suwa Junior High School in April in 1964, completing the whole course March 1967.

Entered Okaya-minami Senior High School in April of the same year. Graduated from the same in March 1970.

Admitted through examination to the Department of Physics in Gakushūin University in April in 1971. Graduated from the same in March 1976.

Entered Postgraduate course of the University of Tsukuba(Institute of Physics)in May in 1976.

Reward and Punishment: None

I hereby certify the above statement to be true and correct in every detail.

December 1st, 1980.

Taichi Yazaki

ACKNOWLEDGMENTS

First I would like to express my sincere gratitude to Prof. Y. Narahara for his continuous guidance during the course of the investigation. Next I am particulary grateful to Dr. A. Tominaga for his helpful discussions and suggestions throughout this study. I wish to express deepest appreciation to them for making this study possible and for their kind advice in the preparation of this dissertation.

I want to thank Prof. N. Rott in the Institut fur Aerodynamik der ETH for his valuable discussions, advice and his many papers. I also thank Professors K. Sawada, M. Nakamura and E. Matsuura for their valuable criticisms, discussions, and suggestions.

I am grateful to Dr. T. Kobayashi for his numerical calculation using a computer, and would like to thank Dr. H. Doi for his advice and encouragement.

I am indebted to Professers D. ter haar in Oxford University and T. Takahashi in Tokyo Metropolitan University for introducing some interesting references to me.

Particular thanks are due to Mr. Y. Abe, Mr. K. Kuroiwa, Mr. N. Takagi and Mr. T. Miyairi who cooperated with me and performed qualitative experiments on Taconis Oscillation.

I also thank Mr. M. Saito and Mr. T. Fujii for their assistance during experiments on the stability limit of the oscillations.

In experiments on the second-order heat flux, I wish to express my gratitute to Mr. K. Ichikawa for his assistance and discussions.

I would like to thank the members(Mr. F. Haruyama and Mr. T. Ikeda)of the cryogenic center and the central work shop of the University of Tsukuba.